UC Irvine

UC Irvine Electronic Theses and Dissertations

Title

Improvements to and applications of remotely sensed evapotranspiration

Permalink

https://escholarship.org/uc/item/2bv5f38x

Author

Purdy, Adam Jacob

Publication Date

2018

Copyright Information

Peer reviewed|Thesis/dissertation

UNIVERSITY OF CALIFORNIA,
IRVINE

Improvements to and applications of remotely sensed evapotranspiration

DISSERTATION

submitted in partial satisfaction of the requirements
for the degree of

DOCTOR OF PHILOSOPHY

in Earth System Science

by

Adam Jacob Purdy

Dissertation Committee:
Professor James S. Famiglietti, Co-Chair
Professor Michael L. Goulden, Co-Chair
Professor James T. Randerson

2018

DEDICATION

To

Mom, and Dad
For your love, guidance and emphasizing the importance education

&

Katherine
Your love, patience, and support made this possible

TABLE OF CONTENTS

LIST OF FIGURES

v

LIST OF TABLES

ACKNOWLEDGMENTS

I would like to first thank my committee chair, Professor James Famiglietti. Over 5 years ago Jay took a chance on me to join his lab at Irvine. Over the years he has provided continued support, instilled confidence to take on big challenges, and set an example of what it takes to be a pioneer in hydrology and have impactful and relevant research. His guidance and motivation to communicate science will resonate with me beyond the work presented below.

I would like to thank Dr. Joshua Fisher. Josh took on an advising role midway through this process and has been integral in developing my proposal writing acumen and motivating superior work. His quest to fill gaps in science contributed to the success of this dissertation.

I would like to thank my committee members, Professor Michael Goulden and Professor Jim Randerson, who provided candid feedback and direction to help shape this dissertation. Their expertise tackling global studies from the ground to space and breadth of knowledge have provided a great resource to support my work.

In addition, I would like to thank the countless friends I have met along this journey. Their camaraderie made this a great experience. I would also like to thank the Department of Earth System Science for stability throughout this process. The department and the School of Physical Sciences at UC Irvine provides a great foundation to succeed in science.

CURRICULUM VITAE

A.J. Purdy

Education

PhD, University of California, Irvine	2018

Earth System Science, Advisor: James Famiglietti

Master in Science University of California, Irvine	2014

Earth System Science, Advisor: James Famiglietti

Master in Science California State University of Monterey Bay	2010

Coastal Watershed Science and Policy, Advisors: Fred Watson & Forrest Melton

Bachelor of Arts & Bachelor of Science University of San Diego	2008

Industrial and Systems Engineering

Awards & Fellowships

2017	Jet Propulsion Laboratory Visiting Student Research Program participant
2016-2018	NASA Earth System Science Fellowship: Water vs Carbon: An evaluation of SMAP soil moisture and OCO-2 Fluorescence to characterize global plant stress.
2015	NASA summer grant to examine SMAP soil moisture to support evapotranspiration
2014	University of California, Irvine Public Impact Honorable Mention Fellow
2014	Earth System Science Graduate Student Representative
2008	Tau Beta Pi, Engineering Honor Society
2007	Academic excellence for Industrial and Systems Engineering, University of San Diego
2007	Outstanding service award for Engineering, University of San Diego

Publications

2018	**Purdy, A.J.**, Fisher, J.B., Sun, Y., Goulden, M., Randerson, J., Famiglietti, J. (in prep) *Carbon vs. Water: Characterizing vegetation stress from space* with OCO-2 and SMAP
2018	Massoud, E.C., **Purdy, A.J.**, Miro, M., Famiglietti, J.S. (in prep) *A data fusion approach to model and project groundwater storage changes in California's Central Valley.*
2017	Massoud, E.C., Christoffersen, B.O., **Purdy, A.J.**, Xu, C. (in review) *Bayesian inference of hydraulic properties in and around a Douglas White Fir using a process based ecohydrologic model* Environmental Modelling & Software.
2017	**Purdy, A.J.**, Fisher, J.B., Goulden, M.L., Colliander, A., Halverson, G., Tu, K., Famiglietti, J.S., (in review), *SMAP to improve global evapotranspiration*. Remote Sensing of Environment
2017	Talsma, C., Good, S.P., Jimenez, C., Martens, B., Fisher, J.B., Miralles, D., McCabe, M., **Purdy, A.**J. (in review) *Partitioning of Evapotranspiration in Remote Sensing-based Models.* Agricultural and Forest Meteorology.
2017	Joshua B. Fisher, Elizabeth Middleton, Forrest Melton, Martha Anderson, Simon Hook, Christopher Hain, Richard Allen, Matthew McCabe, Jean-Pierre Lagouarde, Kevin Tu, Dennis Baldocchi, Philip A. Townsend, Ayse Kilic, Johan Perret, Diego Miralles, Duane Waliser, **A.J. Purdy**, Andrew French, David Schimel, James S. Famiglietti, Graeme Stephens, Eric F. Wood, *The Future of Evapotranspiration: Global requirements for ecosystem functioning,*

carbon and climate feedbacks, agricultural management, and water resources. Water Resour. Res., 53, 2618–2626, doi:10.1002/2016WR020175.

2016 **Purdy, A.J**., Fisher, J.B., Goulden, M., Famiglietti,J.S., (2016), *Ground heat flux: An analytical review of 6 models evaluated at 88 sites and globally.* JGR Biogeosciences 10.1002/2016JG003591

2016 Castle, S., Thomas, B., Reager, J.T., **Purdy, A.J.,** Lo, M., Famiglietti, J.S., (2016), *Remote detection of water management impacts on evapotranspiration in the Colorado River Basin.* Geophysical Research Letters.

2011 Melton, F.S., Johnson, L.F., Lund, C.P., Pierce, L.L., Michaelis, A.R., Hiatt, S.H., Guzman, A., Adhikari, D.D., **Purdy, A.J**., Rosevelt, C., Votava, P., Trout, T.J., Temesgen, B., Frame, K., Sheffner, E.J., Nemani, R.R., (2011*), Satellite irrigation management support with the terrestrial observation and prediction system: a framework for integration of satellite and surface observations to support improvements in agricultural water resource management.* IEEE Journal of Selected Topics in Applied Earth Observation and Remote Sensing 5(6): 1709-1721

Conference Presentations

2017 **Purdy, A.J.,** Fisher, J., Goulden, M.L., Randerson, J.S., Famiglietti, J.S., Water vs. Carbon: An evaluation of SMAP soil moisture, evapotranspiration, & OCO-2 solar induced fluorescence to characterize global plant stress. Poster Presentation AGU Fall 2017

2016 **Purdy, A.J.,** Fisher, J., Famiglietti, J.S., Potential for SMAP soil moisture observations to improve remote sensing of evapotranspiration algorithms. *Oral Presentation AGU Fall 2016*

2015 **Purdy, A.J.**, Fisher, J., Famiglietti, J.S., Ground Heat Flux: What's the best approach. *Oral Presentation AGU Fall 2015*

2014 Castle, S., Reager, J.T., Thomas, B.F., **Purdy, A.J.**, Lo, M. H., Rodell, M., Famiglietti, J.S., Assessing the impacts of water management on evapotranspiration in the Colorado River Basin. H34D-06 *AGU Fall 2014*

2013 **Purdy, A.J**., Famiglietti, J.S. Remote sensing and modeling evapotranspiration: A high-resolution multi-method comparison at point and basin scales in California. *Oral Presentation AGU Fall 2013*

2012 Melton, F.S. Lund, C., Johnson, L., Michaelis, A., Pierce, L., Guzman, A., Hiat, S., **Purdy, A**., Rosevelt, C., Brandt, W., Votava, P., Nemani, R., Satellite Mapping of Agricultural Water Requirements in California with the Terrestrial Observation and Prediction System. H21H-1272 *AGU Fall 2012*

2011 **Purdy, A.J**., Lund, C.P., Pierce, L., Melton, F.S., Guzman, A., Harlen, I., Holloway, R., Johnson, L., Lee, C., Nemani, R.. Applications of wireless sensor networks, soil water balance modeling, and satellite data for crop evapotranspiration monitoring and irrigation management support. H21F-120: *Poster AGU Fall 2011*

2011 Melton, F., Johnson, L., Lund, C., Michaelis, A., Pierce, L., Guzman, A., Hiat, S., **Purdy, A.J.**, Lee, C., Rosevelt, C., Fletcher, N., Votava, P., Milesi, C., Hashimoto, H., Wang, W., Scheffner, E.J., Nemani, R., Satellite Monitoring and Management Support in California with the Terrestrial Observation and Prediction System H21F-1227 *AGU Fall 2011*

Journal Reviewer

Journal of Hydrometeorology | Geoscientific Model Development | Remote Sensing | Applied Water Science

Field Experience

2016	FLUXCOURSE: Boulder, CO. Two-week workshop focused on theory, measurement, and modeling of leaf and canopy scale gas and energy exchange
2015	SMAP-Ex 5 2015: Soil Moisture Active Passive Calibration & Validation. Murrumbidgee River, Australia
2010-2012	TOP-SIMS: Satellite irrigation management support project. Central Valley and Salinas Valley, California. Installed and maintained wireless meteorological and soil moisture sensor networks to calculate field scale water budgets. Installed surface renewal flux towers to measure Latent Heat in agricultural fields. Processed soil moisture data. Attended meetings with agricultural growers and field managers to communicate how potential evapotranspiration and soil moisture data can assist irrigation management.

Teaching Experience

2017	CUAHSI: Invited instructor, Workshop on NASA remote sensing and hydrology. Boston, MA
2016	CUAHSI: Invited instructor, Workshop on NASA remote sensing and hydrology. Tucson, AZ
2016	Terrestrial Hydrology: Teaching Assistant University California, Irvine
2015	Data Analysis: Teaching Assistant University California, Irvine
2014	On Thin Ice: An introduction to cryosphere science: Teaching Assistant UCI
2014	Local and Regional Environmental Issues: Teaching Assistant UCI
2013	Fundamental Processes in Earth and Environmental Studies: Teaching Assistant UCI
2012	Fundamental Processes in Earth and Environmental Studies: Teaching Assistant UCI
2010-2011	Physics II: Lab Instructor CSUMB
2010-2011	Physics I: Teaching Assistant CSUMB

ABSTRACT OF THE DISSERTATION

Improvements to and applications of remotely sensed evapotranspiration

By

Adam Jacob Purdy

Doctor of Philosophy in Earth System Science

University of California, Irvine, 2018

Professor James S. Famiglietti, Co-Chair
Professor Michael L. Goulden, Co-Chair

Evapotranspiration is one of the largest fluxes in the terrestrial water cycle, and also impacts the surface energy budget and the carbon cycle. In this dissertation, I explore how the surface energy budget contributes to ET uncertainty, I apply new satellite soil moisture observations to improve global ET estimates, and I link the carbon and water cycles from space to characterize how vegetation responds to stressful conditions.

First, the differences of ground heat flux models are evaluated against 88 locations with *in situ* observations. I discuss the mechanisms which control ground heat flux and quantify how errors in this measurement have the potential to impact evapotranspiration. A new optimized model is presented to reduce this potential uncertainty.

Second, I apply integrated observations of soil moisture and evapotranspiration to improve a satellite-based evapotranspiration algorithm. I demonstrate how observations from soil moisture improve evapotranspiration estimates in water-limited regions and use this new model with soil moisture observations from the Soil Moisture Active Passive (SMAP) mission to compute evapotranspiration globally. I compare the new model with the original model

and quantify how evapotranspiration is partitioned. This is the first global satellite-derived evapotranspiration dataset to incorporate water availability limitations from SMAP.

Finally, I link independent measurements of the carbon and water cycle from space. I use satellite derived transpiration and new observations of solar induced fluorescence from the Orbiting Carbon Observatory -2 (OCO-2) to characterize how vegetation responds to hotter and drier climate perturbations.

Overall, this dissertation advances remote sensing evapotranspiration algorithms through quantifying the uncertainty contribution from ground heat flux models and provides a new relationship to link soil moisture observations to evapotranspiration. Additionally, I present the first study to apply transpiration and solar induced fluorescence from OCO-2 to explore how vegetation responds to hotter and drier conditions by regulating the carbon and water cycles. This dissertation delivers new ideas of how to leverage earth observing satellites to advance ET science and address knowledge gaps in the earth system.

Chapter 1

Introduction

1.1. Evapotranspiration and the earth system

By linking the water cycle, carbon cycle, and surface energy budget, evapotranspiration (ET) is arguably the most important process in the earth system (Fisher et al., 2017). When plants open stomata to ingest CO_2 for photosynthesis, water more readily transpires to the atmosphere, and large amounts of energy convert water from liquid to vapor. Over the global land surface, ET is the second largest flux in the terrestrial water cycle returning two thirds of the water from precipitation back to the atmosphere (Rodell et al., 2015; Trenberth et al., 2009). Using the water budget, we can compute ET over basins as:

$$ET = P - Q - \frac{dS}{dT} \tag{1}$$

where P is precipitation, Q is discharge, and $\frac{dS}{dT}$ is the change in terrestrial water storage. The carbon and water cycles are connected through plant regulation of stomata. A metric to quantify how this relationship varies across plants is the ratio of carbon uptake to water lost:

$$WUE = \frac{GPP}{ET} \tag{2}$$

where WUE is the water use efficiency, GPP is the gross primary production. Lastly, the energy used to convert water from liquid to vapor accounts for 1/2 of available energy at the earth surface (Trenberth et al., 2009).

$$ET\lambda = LE = R_{NET} - H - G \tag{3}$$

where λ is the latent heat of vaporization, *LE* is latent energy, R_{NET} is net radiation, *H* is sensible heat, and *G* is the ground heat flux. Therefore, any perturbations in ET carry large implications for water storage and potential runoff, determining whether a region is a carbon source or carbon sink, and regulating the surface energy budget including the mitigation or exacerbation of heat waves (Gedney et al., 2006; Long et al., 2013; Miralles et al., 2014; Reager et al., 2016; Wolf et al., 2016).

Warming of global surface air temperatures resulting from increased greenhouse gas concentrations hold the potential to increase intensity the hydrologic cycle (Syed et al., 2010). Rising temperatures increase the saturated vapor pressure of the atmosphere and therefore the vapor pressure deficit between wet surfaces and the above lying air. Changes in ET can impact the distribution of water availability and carbon uptake (Greve et al., 2014; Wada et al., 2017). Therefore, models of ET are needed to understand how changes in water availability, land cover, human management, and climate impact the energy, water, and carbon cycles in the earth system (Castle et al., 2016; Jung et al., 2010a; Lo and Famiglietti, 2013; Miralles et al., 2014; Sorooshian et al., 2011). Accurate ET observations can quantify the biospheres role in and the strength of land-atmosphere feedbacks that are currently poorly represented in many land surface and earth system models (Dirmeyer et al., 2010, 2006; Levine et al., 2016). Satellite-derived ET observations are a useful tool to evaluate such impacts on local and regional climate (Lo and Famiglietti, 2013; Sorooshian et al., 2011). Additionally, ET data are useful for evaluating how drought frequency, intensity, and duration impacts the terrestrial biosphere (Fisher et al., 2017; Miralles et al., 2014; Wolf et al., 2016). Due to the importance of this flux, numerous methods have been developed to measure and model ET.

1.2. Methods to measure and model ET

1.2.1. Observations

ET is a difficult process to directly measure and requires complex instrumentation and methods. The most widely used methods to measure ET at remote locations include: lysimeters, Bowen Ratio (BR) systems, and eddy covariance (EC) towers. Lysimeters use mass balance to calculate ET by burying circular or square (1-5 m^2) container scales below ground to depths of 1-4 m (Holmes, 1984; Scanlon et al., 1997). Additional measurements of precipitation and/or irrigation are required to measure time-variations in total water storage in order to calculate the amount of ET. Lysimeters are an instrumental tool used in the development and evaluation of ET models for agricultural applications. These instruments provide long-term ET observation records, but require intense operator attention and only observe ET across limited spatial extents (<10 m^2). Additionally, lysimeter observations are best suited for homogenous land covers and are therefore limited for global studies.

The BR and EC observation systems overcome the limitations of spatial coverage by measuring ET at scales relevant for land surface model development and satellite observations (10-1000 m^2). Both of these techniques measure the vertical gradients in water vapor and temperature and the orthogonal turbulent air movement to calculate ET. The sensor heights impact the area with which these towers observe, e.g. taller towers measure a larger footprint (Alfieri et al., 2012). The BR method relies on the ratio between sensible heat (H) and latent heat (LE) (Bowen, 1926).

$$\beta = \frac{H}{LE} \qquad (4)$$

where B is the Bowen Ratio. The BR method assumes the aerodynamic resistances for water vapor and heat to be equal and is most often applied over grasslands or crops.

EC towers quantifies ET by measuring the high frequency covariance of moisture and heat fluxes in the vertical component of turbulent flux (Baldocchi et al., 1996). The EC technique is best suited for measuring ET over a variety of land cover types and the EC instrumentation has been configured to execute continuous long-term measurement records (Goulden et al., 1996). At present a global network of EC observations covering a variety of climates and land covers exists through FLUXNET (Baldocchi et al., 2001). Limitations of this method include the lack of energy balance closure (Foken, 2008; Wilson et al., 2002) and data gaps from instrumentation malfunctions or unfavorable environmental conditions (e.g. rainfall) that violate the measurement method (Falge et al., 2001b). Despite these limitations, extensive studies have demonstrated appropriate methodology to fill in missing data and close the energy balance according to the BR (Falge et al., 2001a; Twine et al., 2000). Additionally, effort has been made to produce water and carbon observations with uniform processing and quality control standards (e.g. FLUXNET Marconi, FLUXNET La Thuile, and FLUXNET 2015). The success and advancement of these observation techniques provides the foundation to develop and evaluate point source models of ET, land surface models, and satellite-based remote sensing (RS) ET algorithms.

1.2.2. Modeling evapotranspiration

A variety of models have been developed to apply meteorological observations to calculate ET with varying levels of complexity (Hargreaves and Samani, 1985; Monteith, 1965; H L Penman, 1948; Priestley and Taylor, 1972). Preliminary evaporation models were developed for open water surfaces (H L Penman, 1948) and have since been modified to include biological resistances (Monteith, 1965). The atmospheric demand for water or the potential ET rate is the

basis for many models. The Penman-Monteith equation combines the Monin-Obukov similarity theory with the surface energy balance to calculate ET.

$$PET = \frac{\Delta(R_{NET}-G)+\rho C_p \frac{[e_s(T_a)-e_a]}{r_h}}{\Delta+\left(1+\frac{r_c}{r_h}\right)\gamma} \tag{5}$$

where Δ is the slope of the saturation vapor pressure temperature curve [kPa C^{-1}], ρ is the density of air [kg m^{-3}], C_p is the specific heat of air [J kg^{-1} C^{-1}], e_s is the saturation vapor pressure [kPa], e_a is the vapor pressure [kPa], r_c is the canopy resistance [s m^{-1}], r_h is the aerodynamic resistance [s m^{-1}], and γ is the psychometric constant [kPa C^{-1}]. The PM equation is the most physically defensible equation, but requires numerous meteorological variables to execute including: air temperature (T_a), relative humidity (RH), wind speed, net radiation (R$_{NET}$), and ground heat flux (G). Additionally, these models require extensive field studies to constrain parameterizations of both surface and physiological resistances for a given land surface.

Because of the complexity of the Penman-Monteith equation, empirical and semi-empirical models have been developed to estimate potential ET rate with less observational demands for more practical global applications (George H. Hargreaves and Zohrab A. Samani, 1985; Priestley, C.H.B., 1972; Taylor, 1972). The Priestly-Taylor (PT) equation is a simplified version of the Penman-Monteith equation where available energy ($R_{NET}-G$) and air temperature are the only required meteorological variables.

$$PET = \alpha\frac{\Delta}{\Delta+\gamma}(R_{NET}-G) \tag{6}$$

where α is the PT coefficient, a parameter representing the atmospheric surface and biological resistance terms which is commonly set to 1.26, and Δ is the slope of saturation vapor pressure to temperature curve, and γ is the psychometric constant.

Each of these models have been demonstrated to be successful given the appropriate environment, time-scale, quality forcing datasets, and non-water limiting conditions. Despite the intent to model the same variable, a global inter-comparison of potential ET models uncovered large disparities for certain climates and temporal scales (Fisher et al., 2011). Often, actual ET rates are calculated using these potential ET equations.

To calculate the actual ET, potential ET rates are scaled back by modeling increased stomatal resistance due to extreme temperatures or vapor pressure deficits, by applying ecophysiological stresses which occur under suboptimal environmental conditions, or by deriving empirical coefficients related to the stage of crop growth (Allen et al., 1998; Cleugh et al., 2007; Fisher et al., 2008; Jarvis and Mcnaughton, 1986; Mu et al., 2011). Much uncertainty still exists surrounding when and to what degree environmental conditions reduce potential ET rates. For example, a wide range in the sensitivity of transpiration to soil moisture exits across numerous ET models (Fig. 1.1; Table 1.1). In order to estimate global rates of ET, variations of these equations are applied within prognostic land surface modeling frameworks or remote sensing (RS) ET algorithms driven by satellite datasets.
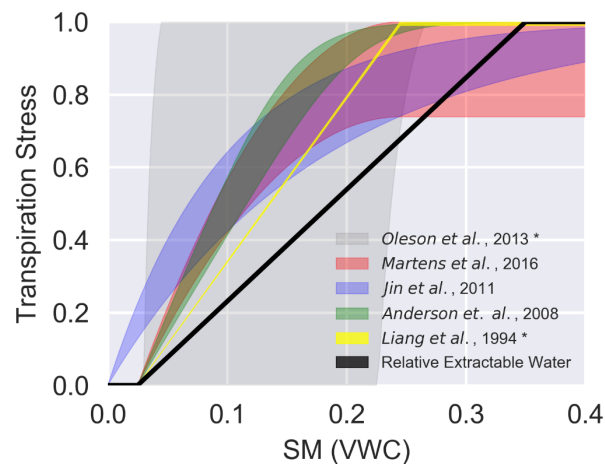
Figure 1.1 Transpiration sensitivity to soil moisture (SM) across numerous models. Each model is described in Table 1.1.

1.2.3 Prognostic land surface models

Land surface models (LSM) were developed to represent the hydrologic system at the basin scale to evaluate the impact from climate perturbations and land management. Over time, LSMs have been coupled to atmospheric models and applied to study the coupled climate system. Each LSM applies equations to represent ET by linking atmospheric conditions and land surface characteristics to calculate the drying rate of the soil. These models were often developed with limited observations from small study areas and then applied broadly to compute basin and global scale fluxes at coarser spatial resolutions. The different observational datasets and subsequent model formulations and parameterizations contributes to large disparities across models.

The current state of ET partitioning between soil evaporation, canopy transpiration, and canopy interception across LSMs shows large disagreement (Wang and Dickinson, 2012). Plant access to varying depths of soil water and the different sensitivities to the amount of water in the soil contributes to this large disparity. For certain LSMs plant transpiration is too sensitive to surface soil water availability and drought conditions. These types of LSM limitations have contributed to over-estimating the land-atmosphere feedback loop (Levine et al., 2016). Additionally, many LSMs do not simulate human water management limiting their ability in heavily populated and managed basins (Castle et al., 2016; Rodell et al., 2011). Because of LSM complexity, the computational requirements for fine spatial and temporal resolutions in addition to the uncertainty for human management applications, RS ET algorithms provide a holistic estimate of ET to overcome limitations from LSMs. Data-driven RS ET algorithms have been successfully used to benchmark models and used to circumvent LSM limitations such as tracking human water management (Castle et al., 2016; Mueller et al., 2013; Rodell et al., 2011).

Table 1.1 Transpiration reduction equations across multiple ET models. ' fT$_{SM}$ applied to the canopy resistance " fT$_{SM}$ applied to the minimum stomatal conductance.

Transpiration Reduction Equation	Source
$$f_{TSM} = \begin{cases} 1 & \theta \geq \theta_{FC} \\ \left[\dfrac{\theta - \theta_{WP}}{\theta_{FC} - \theta_{WP}}\right] & \theta_{WP} < \theta < \theta_{FC} \\ 0 & \theta \leq \theta_{WP} \end{cases}$$	*Best et al.,* 2011 *Boussetta et al.,* 2013
$$f_{TSM} = \begin{cases} 1 & \theta \geq \theta_{CR} \\ \left[\dfrac{\theta - \theta_{WP}}{\theta_{CR} - \theta_{WP}}\right]^{q} & \theta_{WP} < \theta < \theta_{CR} \\ 0 & \theta \leq \theta_{WP} \end{cases}$$	*Egea et al.,* 2011 *Martens et al.,* 2016
$$f_{TSM}' = \begin{cases} 1 & \theta \geq \theta_{CR} \\ \left[\dfrac{\theta - \theta_{WP}}{\theta_{CR} - \theta_{WP}}\right] & \theta_{WP} < \theta < \theta_{CR} \\ 0 & \theta \leq \theta_{WP} \end{cases}$$	*Liang et al.,* 1994
$$f_{TSM}'' = 0 \leq \frac{\psi_c - \psi_s}{\psi_c - \psi_o} \leq 1$$ ψ_s **is the soil matric water potential** ψ_c **is the soil matric water potential when stomata are fully closed** ψ_o **is the soil matric water potential when stomata are fully open** **This function is applied to the minimal stomatal conductance, g$_o$**	*Oleson et al.,* 2013
$$f_{TSM} = f\lvert f_{REW}\rvert = \frac{\ln(W)}{\ln(W_f)}$$ $$W = \frac{W_0 W_f}{W_0 + (W_f - W_0)e^{-\mu f_{REW}}}$$ **where Wf,, W0 ,and μ are stress parameters. μ controls the intensity of stress when soil moisture is below field capacity.**	*France and Thornley*, 1984 *Anderson et al.,* 2007
$$f_{TSM} = 1 - e^{(c1 - d1 \cdot \theta)}$$ **where c and d are parameters related to the sensitivity of soil moisture.**	*Jin et al.,* 2011

$$f_{TSM} = 1 - \frac{(1 - f_{REW}) \cdot T_{Event}}{k \cdot T_{Growing\ Season}}$$

T_{Event} **is time in soil water deficit,** $T_{Growing\ Season}$ **is the growing season length defined by temperature greater than 0ºC, and k is the sensitivity to the growing season length.**

Laio et al., 2001

Porporato et al., 2001

1.2.4 Satellite-based ET algorithms

Earth observing satellites contributed to the advancement in ET science by providing global measurements of vegetation characteristics, land surface temperature, soil moisture, and deviations in total water storage at spatial resolutions and frequencies necessary to accurately map ET (Entekhabi et al., 2011; Huete and Justice, 1999; Justice et al., 1985; Kerr et al., 2001; Njoku and Entekhabi, 1996; Tucker, 1979; Wahr et al., 2004). RS ET algorithms ingest satellites observations of relevant land surface variables to calculate spatially explicit ET (Allen et al., 2007a; M. C. Anderson et al., 2011; Bastiaanssen et al., 1998; Cleugh et al., 2007; Fisher et al., 2008; Miralles et al., 2011b; Mu et al., 2011; Senay et al., 2011; Su, 2002). Since RS ET models apply vegetation and land surface observations they inherently account for human management and land use changes. These algorithms have been developed for a range of applications with varying in levels of complexity. The spatial resolutions at which satellites observe the land surface and the revisit frequencies largely control ET model applications.

Fine spatial resolution (<100m) satellites with longer revisit frequencies (>10 days) facilitate quantification of farm-scale water consumption and basin-scale water demands (Allen et al., 2007a; M. C. Anderson et al., 2011; Castle et al., 2016; Melton et al., 2012; Senay et al., 2011). RS ET algorithms at these scales typically solve directly for ET using crop coefficients, empirical relationships based on greenness, or compute sensible heat and solve for LE as the residual of the surface energy balance. Crop coefficients provide a simple direct way to scale PET to actual ET

rates, using greenness to estimate crop stage (Allen et al., 1998; Melton et al., 2012). Empirical approaches calibrate ET to changes in vegetation indices provide reasonable estimates over riparian areas in semi-arid regions (Nagler et al., 2013, 2005). Models that utilize the surface energy balance (Eq. 3) apply differences in land surface temperature and vegetation 'greenness' to infer where LE is at the atmospheric demand and where LE is 0 and interpolate between these two extremes. Surface energy balance models were developed for semi-arid agricultural applications and are best suited for regions where there is a large contrast in dry, barren areas and highly evaporative areas (Allen et al., 2007a; Bastiaanssen et al., 1998).

Two widely used energy models are Mapping EvapoTranspiration using Inverse Calibration (METRIC) and Atmosphere-Land EXchange Inverse (ALEXI). The METRIC model relies on model operators to identify locations of maximum and minimum ET rates for a given area and uses on-ground weather data to calibrate each time-step. The ALEXI model solves for regional sensible heat constrained by changes in the boundary layer. The model infers higher spatial resolutions using the assumption of partitioning LSTs between the canopy and soil surface (Anderson and Kustas, 2008). Many models use vegetation indices and LST to identify the areas where ET is happening close to the atmospheric demand and areas where sensible heat occurs near its maximum and ET is negligible. These models often require local calibration and *in situ* meteorological observations over irrigated locations at or near the potential ET rate (Allen et al., 2007b), diurnal geostationary observations (M. C. Anderson et al., 2011), and highly accurate land surface temperature to compute ET with minimal error. Additionally, less frequent revisits introduce uncertainty because models become more reliant on temporal extrapolation to calculate daily ET values relevant for on-farm management and basin water use quantification (Ryu et al., 2012; Senay et al., 2011). Because of these reasons, these algorithms are best suited for local and

regional studies. For global applications, satellites that have coarser spatial resolutions and higher frequency revisits provide a suitable alternative.

Satellites such as the Moderate Resolution Orbiting Spectrometer (MODIS) and Advanced Very High-Resolution Radiometer (AVHRR) sacrifice fine spatial resolutions for more frequent revisits providing daily observations in the visible, near-infrared, and thermal infrared wavelengths of the electromagnetic spectrum. These observations facilitate spatially explicit global estimates of ET. Empirical upscaling algorithms have been developed that utilize multi-tree-ensemble and neural networks to scale *in situ* observations using relationships to remotely sensed data (Jung et al., 2011). Despite their ability to capture comparable estimates of global ET, these models do not represent the mechanistic processes necessary to evaluate and diagnose the source of perturbations in modeled ET.

Data-driven algorithms need to be physically defensible and robust over various land covers and climate zones to accurately quantify ET globally (Fisher et al., 2008; Jin et al., 2011; Miralles et al., 2011b; Mu et al., 2011). The official MODIS ET product MOD16 utilizes the PM equation to compute ET globally (Mu et al., 2011). Because resistance terms in the PM equation are not directly observable, MOD16 relies on land surface classifications, meteorological conditions, and a biome-specific lookup table to calculate actual ET. RS ET algorithm inter-comparison studies have documented how the MOD16 data underestimate global ET due to over-estimating stomatal and surface resistance (Miralles et al., 2015). For these reasons, less complex approaches have been developed.

The Priestley Taylor – Jet Propulsion Laboratory (PT-JPL) ET algorithm was developed at coarse (1º) monthly global applications from continuously observable limited inputs, but has since been applied to compute ET daily at much finer spatial resolutions (1-5 km with MODIS). The

PT-JPL ET model is rooted in the PT equation (Eq. 7) and applies eco-physiologically inspired stress functions to reduce potential ET to actual ET rates. This ET model has outperformed more complex approaches in global inter-comparison studies (Ershadi et al., 2014; Mccabe et al., 2016; Michel et al., 2016; Vinukollu et al., 2011). Despite the strong performance in these studies, the PT-JPL ET model has a high bias compared to other global datasets for certain water-limited regions. RS ET algorithms provide value in spatially explicit representation of many processes but still possess limitations.

1. 3 Opportunities to advance RS ET science and applications

RS ET algorithms successfully provide global estimates of ET, but still have many opportunities to improve upon current limitations and applications. ET algorithms rely on temporal interpolation, apply different methods to partition radiation and compute ground heat flux across models, have a limited representation of soil moisture, and have yet to be directly linked to carbon uptake.

RS ET algorithms deliver observation-driven estimates of ET, but are limited by the quality of input datasets, cloud cover obstructing data collection for certain regions, and temporally extrapolating instantaneous observations (1-16 days) to daily and multi-day estimates. Data driven models often rely on the mid-morning instantaneous evaporative fraction (EF) calculated as actual ET divided by potential ET to estimate daily ET. Studies have demonstrated how these assumptions provide reasonable weekly estimates (Ryu et al., 2012). However, to properly diagnose how plants and ecosystems respond to water-limiting conditions and stressful conditions, spatially explicit diurnal observations are needed. One main limitation of RS ET methods with long gaps between EF observations is that the algorithms are entirely reliant on radiation and temperature to interpolate between quality satellite observations.

12

Net radiation and available energy are first order controls on ET (Badgley et al., 2015; Fisher et al., 2017). These datasets are used extrapolate ET temporally using the EF, therefore any uncertainty in radiation, temperature or vapor pressure is propagated into ET uncertainty (Fig. 1.2) (Polhamus et al., 2013). However, ET algorithms compute available energy differently. Some models completely ignore G, which is an integral component of available energy (Purdy et al., 2016). Additionally, G is extremely important to appropriately model ET at sub-monthly time-scales and to partition ET into soil evaporation and canopy components. By completing process-level analyses on these components would enable ET model harmonization across areas of the largest uncertainty and facilitate more direct ET model comparisons. These steps will be needed to address current knowledge gaps in ET-based science such as how to appropriately partition ET between soil evaporation, canopy transpiration, and canopy interception in addition to how to appropriately represent soil water limitation on each component.
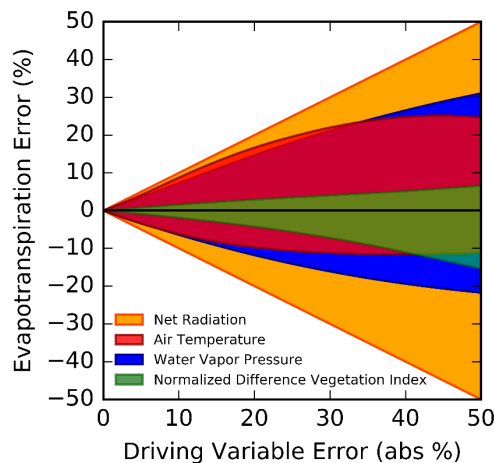
Figure 1.2 Forcing variable error impact on global ET error. Net radiation or available energy (R_{NET} -G) uncertainty are first order controls on ET error followed by air temperature, water vapor pressure, and NDVI for global importance in the PT-JPL ET model.

The water for ET is extracted from the top layers of the earth's surface. Therefore, incorporating soil water availability into ET algorithms should improve these estimates, especially in regions

where water availability controls ET rates. However, varying rooting depth, vegetation sensitivity to soil water availability, and the absence of accurate global soil moisture observations at relevant depths have prevented such an integration (Dirmeyer et al., 2004; Gao and Dirmeyer, 2006; Schenk and Jackson, 2002). Previous research has identified soil moisture as a leading control on ET for a variety of land covers (Burba and Verma, 2005; Granier et al., 2007). But, robust parameterizations of these equations across numerous landscapes has not been feasible due to the lack of available high-quality soil moisture datasets at relevant scales and depths. Previous limitations of available high-fidelity soil moisture observations have been lifted with the launch of the Soil Moisture Ocean Salinity (SMOS) and the Soil Moisture Active Passive (SMAP) satellites in recent years (Entekhabi et al., 2011; Kerr et al., 2016). However, to date no ET algorithms directly incorporate explicit soil moisture with other environmental constraints. Instead ET algorithms use relationships between soil moisture and EF to estimate soil moisture and temporally extrapolate ET observations (Anderson and Kustas, 2008; Hain et al., 2009). Or ET algorithms have relied on modeled soil moisture or applied soil moisture observations in data-assimilation frameworks to estimate ET while overlooking constraints from other environmental variables (Jin et al., 2011; Miralles et al., 2011b). These approaches may over-estimate the sensitivity of ET to soil water availability. Therefore, an opportunity exists to capitalize on new global soil moisture observations from SMAP to overcome previous limitations and incorporate explicit soil water control on ET in concert with other environmental variables. Integration of soil water control is key to representing ecosystem responses to stressful environmental conditions, and to better understand how strongly coupled changes in ET relate to changes in vegetation control on the carbon cycle (Biederman et al., 2017; Fisher et al., 2017).

Since the process of transpiration often dominates the total ET flux, an opportunity exits to link the water and carbon cycles from space with independent observations. This linkage at aggregate scales can help quantify whether the biosphere provides a positive or negative climate feedback to both short-term and long-term climate perturbations through changes in LE and GPP (Biederman et al., 2016; Phillips et al., 2009). Studies have examined the coupled energy, water, and carbon cycles responses using EC towers (Biederman et al., 2017; Wolf et al., 2016, 2013). Despite these studies that examine the carbon and water cycle at point scales, the extent to which vegetation to regulate the carbon and water cycles to drought and more stressful conditions remains largely uncertain (AghaKouchak et al., 2015). Global studies to link the carbon and water cycles using satellite datasets and quantify responses to potentially stressful conditions suffer from a lack of independence (Mu et al., 2013). With new independent observations of solar induced fluorescence (SIF), an indicator of GPP, an opportunity exists to link these cycles from space to understand the coupled water and carbon response at ecosystem and regional scales (Frankenberg et al., 2014). RS ET models that partition ET into the canopy and soil components enable this direct link to help close another gap in knowledge related to the earth system.

1.4 Organization of Research

With this dissertation, I address knowledge gaps related to ET in the earth system from the lenses of the surface energy budget, the water cycle, and the carbon cycle. In the following chapters I detail how ground heat flux should not be overlooked and how it is an integral component of the surface energy budget with large implications for modeling ET (Chapter 2; Purdy et al., 2016). In Chapter 3 I demonstrate how recent satellite observations of surface soil moisture from SMAP improve ET estimates in water limited regions (Purdy et al., *in review*). In Chapter 4 I compare new observations of SIF with transpiration from the PT-JPL ET model to link the carbon and water

cycles from space to characterize how vegetation responds to stress. Lastly, in Chapter 5 I discuss how the work presented in Chapters 2, 3, and 4 address knowledge gaps in ET science and the earth system and I conclude with what I hope to research moving forward.

Chapter 2

Ground heat flux: an analytical review of 6 models evaluated at 88 sites and globally

Adapted from:

Purdy, A. J., J. B. Fisher, M. L. Goulden, and J. S. Famiglietti (2016), Ground heat flux: An analytical review of 6 models evaluated at 88 sites and globally, J. Geophys. Res. Biogeosci., 121, 3045–3059, doi:10.1002/2016JG003591.

2.1 Introduction and Background

Ground heat flux (G) is an integral part of the surface energy budget ($R_{NET} - G = LE + H + V$). Net radiation, R_{NET}, and G are balanced by latent heat (LE), sensible heat (H), and chemical energy provided by metabolism or used by photosynthesis in plants (V), a negligible amount. Ground heat flux accounts for the energy gained or lost during belowground warming or cooling. Commonly used approaches to calculate LE and evapotranspiration (ET), such as the Penman-Monteith equation, the Priestley-Taylor equation, and the residual of the energy balance, not only need high-fidelity R_{NET} but also require G to calculate the available energy (Monteith, 1965; Penman, 1948; Priestley and Taylor, 1972). The magnitude of G varies greatly across different landscapes. In wet areas with dense canopy G is small, while in arid regions with sparse canopy midday G reaches comparable amounts of energy to H and often larger amounts than ET. With G varying orders of magnitude across different landscapes and being an

17

essential part of available energy to support global ET applications, the need for robust and accurate estimates of G is evident. However, many approaches to model G were formulated with limited spatiotemporal sampling and have since been broadly applied. A clear characterization of the discrepancies and potential sources of bias in current G models has the potential to improve estimates of available energy, increase the accuracy and consistency of ET estimates, and facilitate scrutiny of mechanistic model differences across ET algorithms, which is an actively ongoing focus of research (Chen et al., 2014; Ershadi et al., 2014; Jiménez et al., 2011; Mccabe et al., 2016; Michel et al., 2016; Mueller et al., 2013; Vinukollu et al., 2011).

Remote sensing algorithms developed to calculate daily ET at high spatial resolutions created a need for spatially explicit G estimates. Subsequently, many methods to quantify G using satellite data were developed. Initial approaches assumed G to be a constant fraction of R_{NET} or G to be negligible at daily or longer times (Seguin and Itier, 1983). Later work derived linear and nonlinear empirical relationships between G/R_{NET} and vegetation indices (Choudhury et al., 1987; Clothier et al., 1986; Daughtry et al., 1990; Kustas et al., 1993; Reginato et al., 1985) and G/R_{NET} and surface temperatures (Jacobsen and Hansen, 1999; Mu et al., 2011). Recently, G models have employed physically based analytical solutions to thermal diffusion equations (Bennett et al., 2008; Holmes et al., 2008). The assumption that G is always negligible is not appropriate, especially at midmorning times near satellite overpasses or in areas with sparse vegetation cover (Fig. 2.1 & Fig. 2.2) (Daughtry et al., 1990). Setting G as a constant fraction of R_{NET} discounts the impact of spatially varying soil properties, neglects the influence from vegetation insulation, and disregards conservation of energy, unless efforts are taken to equally weight periods when G is positive (daytime/summer) and negative (nighttime/winter). Variables that influence the magnitude of G/R_{NET} include soil properties, vegetation cover and height, and temperature

fluctuations (Santanello and Friedl, 2003). These different factors impart different magnitudes of influence at instantaneous or daily time scales. Consequently, models have been developed to quantify G instantaneously or aggregated across daily or longer times. The G model formulations and variable selection can be seen in Table 2.1, but models primarily use vegetation characteristics or temperature.
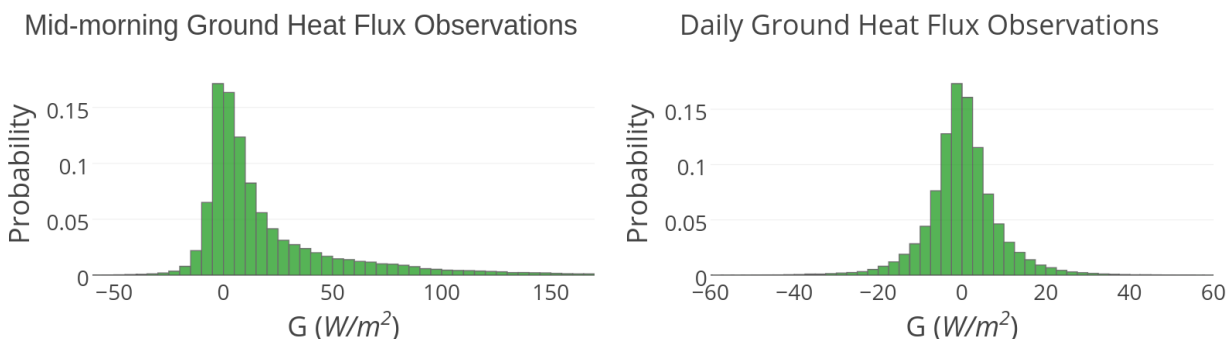
Figure 2.1 Probability density distributions of observed instantaneous mid-morning and daily G from the 88 FLUXNET towers used in this analysis. Left) Probability density distribution of mid-morning instantaneous G. Though G has the highest probability of being near 0, the long tail at the positive end of G indicates that G is an integral term in the instantaneous energy balance. Right) Probability density distribution of daily G. Daily G is more often than not 0. However, a normal distribution around G that spans from -40Wm^{-2} to 40Wm^{-2} demonstrates the seasonality of G at daily time steps.

Vegetation cover density impacts G by attenuating incoming radiation and temperature fluctuations at the soil surface. As vegetation cover increases, the ratio of G/R$_{NET}$ decreases. Despite the general agreement of this relationship, G/R$_{NET}$ varies for distinct amount vegetation cover across models, especially for areas with sparse to no vegetation (Fig. 2.2). Previous research reported G/R$_{NET}$ to range from 0 at complete canopy cover to 0.39 for bare soil (Mu et al., 2011). Other studies indicated smaller ranges: Kustas and Daughtry (1990) found G/R$_{NET}$ spanning from 0.15 at full canopy to 0.30 for bare soil, while Reginato et al. (1985) observed a much smaller range from 0.05 for full canopy and 0.1 for bare soil. The breadth of these ranges demonstrates

how localized measurements for one particular environment do not translate toward broader applications and that factors other than vegetation cover regulate G/R_{NET}.
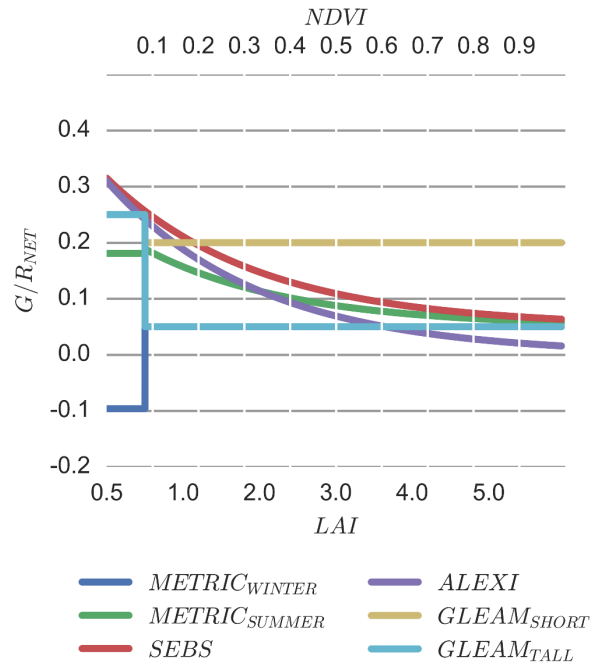
Figure 2.2 Vegetation influence on instantaneous modeled G/R_{NET} ratios. The separation between these models is greatest at low vegetation cover.

Soil properties and land surface temperature are also known to impact G. Idso et al. (1975) measured G/R_{NET} to be 0.5 for dry bare soil and 0.3 for the same bare soil when saturated. Land surface temperature (LST), also known as the radiometric skin temperature, has been shown to correlate to G. Empirical relationships and thermal diffusion solutions have been successful at modeling G over aggregated daily time steps (Bennett et al., 2008; Holmes et al., 2008). A linear empirical relationship developed for the Arctic tundra between simultaneously measured surface temperature and G exhibited high correlation and low error and has since been adopted for global applications (Jacobsen and Hansen, 1999; Mu et al., 2011). However, a linear relationship between skin temperature and G may not capture other factors that impact G, such as attenuation due to vegetation cover, the thermal conductivity of soil, or the temperature gradient of thawing tundra.

Thermal diffusion solutions use the integrated time difference between land surface temperatures

to calculate G. This approach mimics a physically accurate method to transfer heat from the

atmosphere into the Earth surface while relying on knowledge of soil surface thermal inertia

estimates. Bennett et al. (2008) bypass the need for spatially explicit global soil properties by

parameterizing a constant thermal inertia for each location globally. To date, this method has only

been applied globally at relatively coarse scales (1°–3°) using reanalysis data sets (Bennett et al.,

2008; Vinukollu et al., 2011).

Table 2.1. Widely used G modules in current LE algorithms including the equations to calculate both instantaneous G and daily G. fc is the fractional cover, LAI is the leaf area indices, and Tday/night is the surface air temperature.

Model	Equation	Source
	Developed for Instantaneous Applications	
METRIC	$G/R_{NET} = 0.05 + 0.18e^{-0.521 \times LAI}$　　　LAI > 0.5 $G/R_{NET} = 1.8 \times \frac{(T-273.15)}{R_{NET}} + 0.084$　　LAI < 0.5	*Allen et al., 2007*
SEBS	$G/R_{NET} = \Gamma_C + (1 - f_c) \times (\Gamma_S - \Gamma_C)$ $\Gamma_C = 0.315$ fraction of $G : R_{NET}$ for full canopy cover $\Gamma_S = 0.05$ fraction of $G : R_{NET}$ for bare soil	*Su 2002*
ALEXI	$G/R_{NET} = 0.31 \times (1 - f_c)$	*Anderson et al., 2007*
	Developed for Daily Applications	
GLEAM	$G/R_{NET} = 0.05$　　　　　　　Tall Canopy $G/R_{NET} = 0.20$　　　　　　　Short Canopy $G/R_{NET} = 0.25$　　　　　　　Bare Soil	*Miralles et al., 2011*
MOD16	for $T_{an} > -8°C$ & $T_{an} < 25°C$ & $T_{dif} > 5°C$: $G_{s(day/night)} = 4.73 \times (T_{day/night} - 273.15) - 20.8$ for $T_{dif} < 5°C \mid T_{an} < -8°C \mid T_{an} > 25°C$: $G_{s(day/night)} = 0$ Then G is capped at: $G_s[G_s > LE + H] = 0.39 \times (LE + H)$	*Mu et al., 2011*
Thermal Diffusion	$G(t) = \frac{I}{\sqrt{\pi}} \cdot \frac{dT(0,s)}{\sqrt{t - s}}$ $I = \sqrt{\rho ck} \mid I$ = thermal inertia $\mid \rho$ = soil bulk density $\mid$ c = specific heat $\mid k$ = thermal conductivity	*Bennett et al., 2008*

Many previous studies demonstrate success at tuning a G model for specific a location, but many of these G models and their optimized parameter sets have not been tested across a robust observation data set with a variety of land cover types and various climates. With a push for global high-resolution spatiotemporal ET data, some ET models and their respective G representations that were constructed to function over specific land uses have since been applied to continental applications without scrutiny (Allen et al., 2015). The limited studies which have investigated differences in G models have only focused on irrigated agricultural land uses (Cammelleri 2009, Irmak 2011). These studies found overall poor performance compared to mean in situ G observations and concluded that local calibration is necessary for successful model application. Additionally, the differences between methods to quantify G at both instantaneous and daily resolutions need to be better understood to aide appropriate G model selection in global ET algorithms.

Globally distributed observations of G at FLUXNET eddy covariance towers and global satellite observations of vegetation and LST facilitate the direct comparison of numerous G models across a robust global observation data set to address the limitations of previous work. Determining the best method to quantify G will lead to a high-fidelity G data set to apply to global ET algorithms and reduce the energy budget closure uncertainty at towers that have poor or missing G measurements. We compare several currently used methodologies ($N = 6$) to answer three main questions with this study: (1) What is the best G model structure for both instantaneous and daily ET algorithms? (2) What mechanisms govern G across instantaneous and daily time scales? (3) What is the impact of G uncertainty on ET globally?

2.2 Methods

Global energy flux and meteorological observations from the FLUXNET eddy covariance site network provide a robust data set to assess current remote sensing G models. In this section, we introduce the FLUXNET synthesized data set, describe the satellite vegetation and temperature data, the radiation data used to perform this analysis, and detail the statistical metrics used to evaluate model performance.

2.2.1 Datasets

2.2.1.1 FLUXNET La Thuile Dataset & validation sites

The FLUXNET eddy covariance tower network provides a decadal set of carbon, water, and energy cycle observations across a numerous biomes and climates (Baldocchi et al., 2001). The La Thuile data set is a subset of this network providing harmonious quality control treatment and gap filling to limit potential biases arising from data-processing techniques. Data are available from the FLUXNET database (http:///www.fluxdata.org). Despite being the best available collection of globally distributed observations, many locations lack a full year of observations, experience instrument quality degradation, and locate ground heat flux plates and soil thermocouples to calculate storage at different depths (2–15 cm) to measure G. We subset and filtered the La Thuile data set for sites with data that met our requirements for remote sensing G model evaluation. Selected towers for this study contain at least 90% high-quality G and R_{NET} observations for 330 days for a given year based on the La Thuile table of core variables present for each year (http://www.fluxdata.org). Only original observed data or high-quality, gap-filled data for both G and R_{NET} are used in this analysis. Overall, we used measurements from 88 towers across 11 climates and 10 biomes to evaluate modeled G (Appendix Table A.1.1). All tower data used in this analysis were open access.

The inherent uncertainty associated with small-scale variability of G due to soil moisture, soil conductivity, vegetation cover, sensor placement, and sensor accuracy contributes to the limited performance against coarser resolution remote sensing footprints in more heterogeneous landscapes. The large sample size (N = 88) mitigates potential bias from tower representativeness or sensor placement that may exist with a smaller sample size. Previous energy balance closure assessments have pointed out that limited sampling of G may contribute up to 15% of the closure uncertainty (Twine et al., 2000). Additionally, the variability for G measurements is highest in the early morning and midday, the time when many ET algorithms require high-fidelity energy balance flux observations (Kustas et al., 2000). To reduce bias from gridded forcing data and remote sensing observations to in situ tower comparison we use in situ observations of R_{NET} for forcing data for models that calculate G as a fraction of R_{NET}. Models are compared against instantaneous midmorning (9:30–10:30) G and daily G tower observations. The tower data are only used to assess models forced by high-resolution remote sensing data.

2.2.1.2 Moderate Resolution Infrared Spectroradiometer Data

The Moderate Resolution Infrared Spectroradiometer (MODIS) provided continuous high-resolution global coverage of vegetation phenology and land surface temperature. These observations span from 2000 to present at resolutions of 250 m–5600 m. Observations at 250 m and 1 km were used to evaluate G models against FLUXNET point observations of G and R_{NET}. We utilized the Oak Ridge National Laboratory MODIS land product subset tool and apply quality control filters to extract good to excellent quality MODIS normalized difference vegetation index (NDVI) and land surface temperature data to evaluate each remote sensing model (http://daac.ornl.gov/MODIS/).

2.2.1.2.1 MODIS Vegetation data

The MOD13Q1 16-daily 250 m normalized difference vegetation index (NDVI) data set was sampled at each of the FLUXNET. Linear interpolation from 16-daily to daily NDVI was used for daily analysis. This interpolation method is commonly used to fill missing data gaps in current LE algorithms (Ershadi et al., 2014). For global spatial comparisons, the 16-day MOD13C1 0.05o NDVI data set was applied. Fractional cover is calculated assuming a linear relationship with NDVI. This is based on the fraction of photosynthetic active radiation intercepted by total vegetation cover (Fisher et al., 2008). LAI is calculated from fractional cover as $LAI = \frac{-\ln(1-f_c)}{0.5}$ (Ross 1976).

2.2.1.2.2 MODIS Land Surface Temperature

Land surface temperature (LST) at 1 km from MOD11A1 was sampled at FLUXNET site locations daily, while daily MOD11C1 0.05° LST was used in spatial comparisons. MODIS quality control flags were used to filter each data set to avoid cloud contamination. The LST data encompass both the soil skin temperature and the canopy skin temperature for partially vegetated areas.

2.2.1.3 Reanalysis data

The National Center for Environmental Prediction (NCEP) provides global reanalysis data sets including short-wave radiation, long-wave radiation, skin temperature, and ground heat flux. The reanalysis data set uses data assimilation to combine observations and model simulations. We used daily (24 hourly) radiation, skin temperature, and ground heat flux at 2.5° by 2.5° gridded data to complete this analysis. Skin temperature was used to calibrate the thermal inertia parameters by land classification for the heat diffusion approach (Bennett et al., 2008).

2.2.2 Models

We compared models from six widely used ET algorithms that also calculate G. Three of these models were developed with the intent to model instantaneous G, while two other models were developed for use at daily time steps, and one model was developed to model G separately for day and night. The G models either apply vegetation properties to reduce R_{NET} to G or use skin temperature to model G (Table 2.1).

For instantaneous applications, we compare three models that use different vegetation properties (LAI and fractional cover) and R_{NET} to calculate G. The Mapping EvapoTRanspiration using Inverse Calibration (METRIC) algorithm relies on measures of LAI to partition controls of G, where for sparse cover a linear relationship of LST normalized by R_{NET} estimates G. At moderate and high vegetation cover, the fraction of G/R_{NET} decreases exponentially with increasing LAI. The Surface Energy Balance System (SEBS) model uses fractional cover to determine the portion of R_{NET} that contributes to G (Daughtry et al., 1990; Monteith, 1981; Su, 2002). Similar to SEBS, the Atmospheric Land EXchange Inverse (ALEXI) model assumes G to be a constant fraction of the R_{NET} that reaches the soil surface (Anderson et al., 2007). All the instantaneous approaches (METRIC, SEBS, and ALEXI) incorporate vegetation phenology through calculating and removing radiation intercepted by the canopy, after which a fraction of the energy which reaches the soil determines G.

Three distinct theoretical approaches are used to compare modeled G at daily resolution. The Global Land-surface Evaporation: the Amsterdam Methodology (GLEAM) quantifies the daily G from set fractions of R_{NET} based on canopy height and canopy cover. Tall canopies reduce the magnitude of G more than short canopies (Daughtry et al., 1990; Miralles et al., 2011b). The MOD16 ET algorithm (Mu et al., 2011) models G at both daytime and night using a linear

relationship with surface temperature. Additionally, this method includes temperature constraints to set G equal to 0 for extremely hot climates, extremely cold climates, and in areas with small diurnal temperature changes. Furthermore, a maximum fraction of G/R_{NET} is set for the incoming radiation that reaches the soil surface. Daily G for MOD16 is computed from the average of daytime and night values. Lastly, a thermal diffusion (T-DIFF) approach is applied to quantify G using the amount of heat that is transferred from the atmosphere to the soil. This approach requires parameterization of soil properties that represent the soil thermal inertia (Bennett et al., 2008). We force the T-DIFF model with nighttime LST from MODIS. Model equations and variables are described in detail in Table 2.1.

We evaluate all models against each other and use the original model parameterization while changing the temporal resolution of the forcing data to compare instantaneous and daily G separately. At midmorning instantaneous times, we evaluate five models (ALEXI, METRIC, SEBS, MOD16, and GLEAM), while at daily time steps we compare all six models. The T-DIFF model structure and forcing data requirement prevent modeling G at the instantaneous time steps.

Many of the G models evaluated here were originally calibrated for specific land uses; therefore, model performance should vary across these different plant functional types (PFTs). For example, the METRIC and ALEXI G models were developed for use over cropland cover and grasslands, the G model in MOD16 was originally developed for Arctic tundra, and the GLEAM and T-DIFF G models were developed for global applications. Because sampling across PFTs for FLUXNET towers is limited with respect to high-quality G/R_{NET} observations, we evaluate model performance across the four most sampled PFTs: grassland (GRA; N = 25), cropland (CRO; N = 15), evergreen forest (ENF; N = 23), and deciduous forest (DBF; N = 13). As in the above

27

global comparison, models are evaluated at both the instantaneously and daily temporal resolutions.

2.2.3 Statistical evaluation

The above models and data are used to evaluate modeled G. Statistical metrics, including the mean bias (BIAS), root-mean-square error (RMSE), and the Kendall's tau (KT) coefficient, are used to objectively rank instantaneous and daily G models against in situ observations. Model performance and skill are evaluated using in situ observations from FLUXNET. Measurement errors may degrade model comparison to in situ observations, but these errors do not impact the relative ranking of model performance because all models are subjected to error equally. Inter-model uncertainty is quantified from the standard deviation of modeled G normalized by R_{NET}. This allows for global seasonal model assessments to identify where high model disagreement exists. The spatial comparison calculates the difference in G models normalized by R_{NET} to highlight the times and regions with the largest model disagreement. These steps will help determine the optimal G model to capture instantaneous midmorning G and daily G, the mechanisms that control G at these different time scales, and the potential impact of modeled G uncertainty on ET algorithms.

2.3. Results

2.3.1 Model evaluation against in situ observations

2.3.1.1 Mid-morning instantaneous model evaluation

The G models in currently applied ET algorithms exhibit a wide range in performance across the FLUXNET sites. Site-wide analysis reveals that the ALEXI, METRIC, SEBS, GLEAM, and MOD16 models more often than not overestimate instantaneous G observations with the slope

between modeled G compared measured G greater than 1.0 coinciding with a positive BIAS (Fig.

2.3). Models' individual performances vary across all sites with average RMSE ranging from the

least error from MOD16 (RMSE = 26.93 Wm^{-2}) to the highest error from SEBS

(RMSE = 42.08 Wm^{-2}; Table 2.2). The site-wide average absolute BIAS ranges from a low of

14.96 Wm−2 from MOD16 to a maximum BIAS of 31.59 Wm^{-2} from SEBS. The average model

KT spans from the worst KT at 0.36 from ALEXI to the highest KT at 0.45 from GLEAM. Of all

the G models analyzed at the towers used in this study, MOD16 exhibits the strongest performance

with the lowest overall error (RMSE = 26.93 Wm−2and BIAS = 14.85 Wm^{-2}), while maintaining

similar ability to other models at capturing G variability (KT = 0.41; Table 2.2).
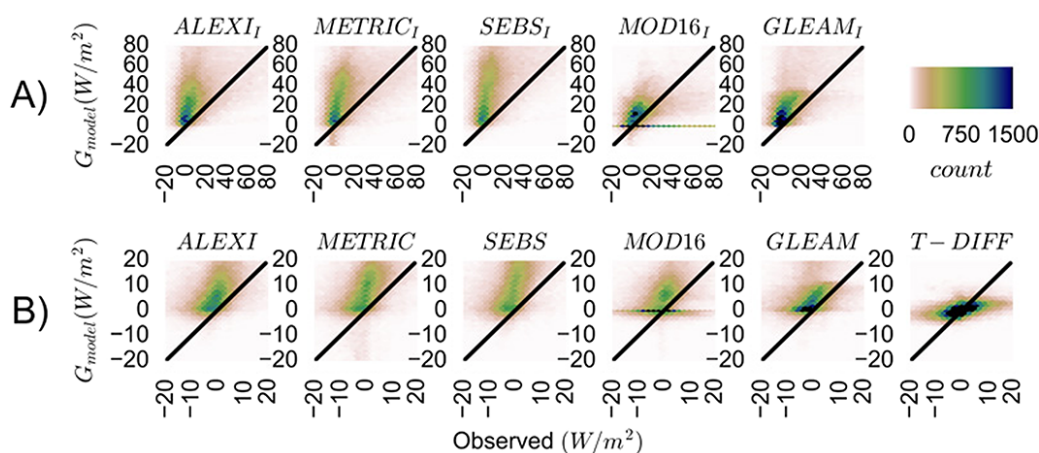
Figure 2.3 Top row (subscript I), frequency scatterplots of modeled and observed midday instantaneous G. The instantaneous models all overestimate instantaneous G as seen by deviation above 1:1 line. Bottom row, frequency scatterplots of daily G. Scatterplots are truncated from 80 Wm 2 to 20 Wm 2 for instantaneous comparison and 20 Wm 2 to 20 Wm 2 for daily comparison to maximize G observations.

Table 2.2 Instantaneous Model Performance Across All FLUXNET Sites.

Model	RMSE	BIAS	KT	Slope	Int	R^2
ALEXI	35.20	23.54	0.36	0.37	22.27	0.12
GLEAM	35.14	24.86	0.45	0.48	15.50	0.21
METRIC	32.40	21.31	0.43	0.40	22.49	0.11
MOD16	26.93	14.85	0.41	0.27	9.62	0.10
SEBS	42.08	31.59	0.40	0.42	26.12	0.10

2.3.1.2 Daily model evaluation

Of the six models, the thermal diffusion model (T-DIFF) best fits the observations with both the lowest average error given the towers and conditions for this analysis (RMSE = 7.34 Wm−2; BIAS = 1.45 Wm−2) and the second highest explanation of variance (KT = 0.38; Table 2.3). The T-DIFF model underestimates the magnitude of daily G with a negative bias and a slope between modeled G and measured G less than 1, while the other models all overestimate G with slopes greater than 1 and a positive BIAS (Fig. 2.3). The GLEAM approach only explains slightly more variance (KT = 0.40) than T-DIFF, but GLEAM has average errors across all sites that are twice as large (RMSE = 14.00 Wm−2; BIAS = 10.21 Wm−2) as T-DIFF. Like GLEAM, MOD16 has twice as much error compared to the T-DIFF model and explains the least G variability (KT = 0.27). The other models originally suited to quantify instantaneous G, ALEXI, GLEAM, METRIC, and SEBS all explain a similar amount of variance to T-DIFF but exhibit larger errors (Table 2.3). The RMSEs of each model are at least 1.75 times greater than T-DIFF, and the absolute BIASs are at least 5 times greater than T-DIFF.

Table 2.3 Daily Model Performance Across All FLUXNET Sites

Model	RMSE	BIAS	KT	Slope	Int	R^2
ALEXI	12.63	9.02	0.36	0.32	8.86	0.12
GLEAM	14.00	10.21	0.40	0.23	5.02	0.08
METRIC	12.91	8.07	0.37	0.39	7.07	0.12
MOD16	10.75	6.39	0.26	0.22	4.78	0.06
SEBS	14.98	11.51	0.37	0.07	9.90	0.01
T-DIFF	7.34	1.45	0.38	0.16	0.61	0.17

2.3.1.3 Model performance by Land Use

We evaluate G models across the four most sampled land covers, grassland, cropland, evergreen forest, and deciduous forest. Four FLUXNET sites were selected to provide an example of the wide range in modeled G across a year for these distinct land covers (Fig. 2.4). For the

30

instantaneous model statistics averaged over grasslands, METRIC results in the lowest errors

(RMSE = 32.20 Wm−2; BIAS = 15.75 Wm−2), and GLEAM explains slightly more variance
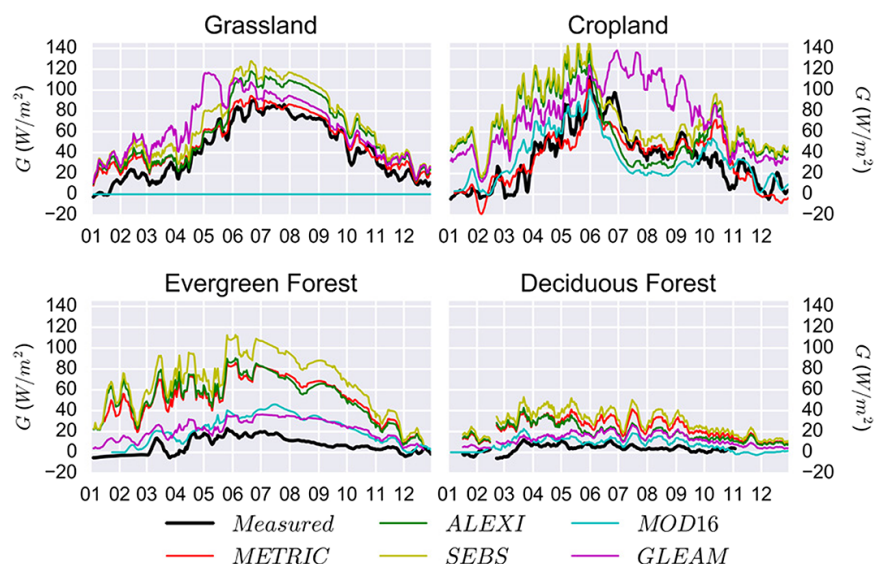
Figure 2.4 Instantaneous model performance compared across four different land covers at individual representative sites ((top left) grassland U.S.-Var, (top right) cropland U.S.-Ne1, (bottom left) evergreen forest U.S.-Blo, and (bottom right) deciduous forest UK-Ham). Data are plotted for one calendar year; the numbers along the bottom axis indicate each month in the year. The METRIC model most closely matches measured G for grassland and cropland cover, while GLEAM and MOD16 more closely match measured G over forested land cover. Model spread is high for each site demonstrating need for appropriate model choice for certain PFTs and potential for model improvement through global calibration.

(KT = 0.51) than other models. For cropland cover, METRIC again has the lowest errors

(RMSE = 30.03 Wm−2; BIAS = 10.82 Wm−2), while METRIC and GLEAM share the highest

explanation of variance (KT = 0.52). For evergreen needleleaf forests MOD16 results in the lowest

error (RMSE = 15.90 Wm−2; BIAS = 8.10 Wm−2) and is again followed by GLEAM (RMSE

16.13 Wm−2; BIAS 10.49 Wm−2). METRIC explains the most variance (KT = 0.45) for evergreen

needleleaf forests. In deciduous broadleaf forests, MOD16 has the lowest error

(RMSE = 14.75 Wm−2; BIAS = 8.79 Wm−2) followed by GLEAM (RMSE = 15.41 Wm−2;

BIAS = 11.30 Wm−2), while GLEAM explains the most variance (KT = 0.36). Figure 2.5 shows

the range in model performance for each of these statistics across all sites for each PFT. The MOD16 and GLEAM models exhibit more consistent performance over deciduous broadleaf forest and evergreen needleleaf forest with tighter error statistic box plots compared to other PFTs. Explanation of variance is generally higher for grassland and cropland cover compared to forests. Model errors, specifically, MOD16 and ALEXI BIAS and RMSE have the widest ranges over grassland, while ALEXI and SEBS BIAS and RMSE have the widest range for evergreen needleleaf forests.
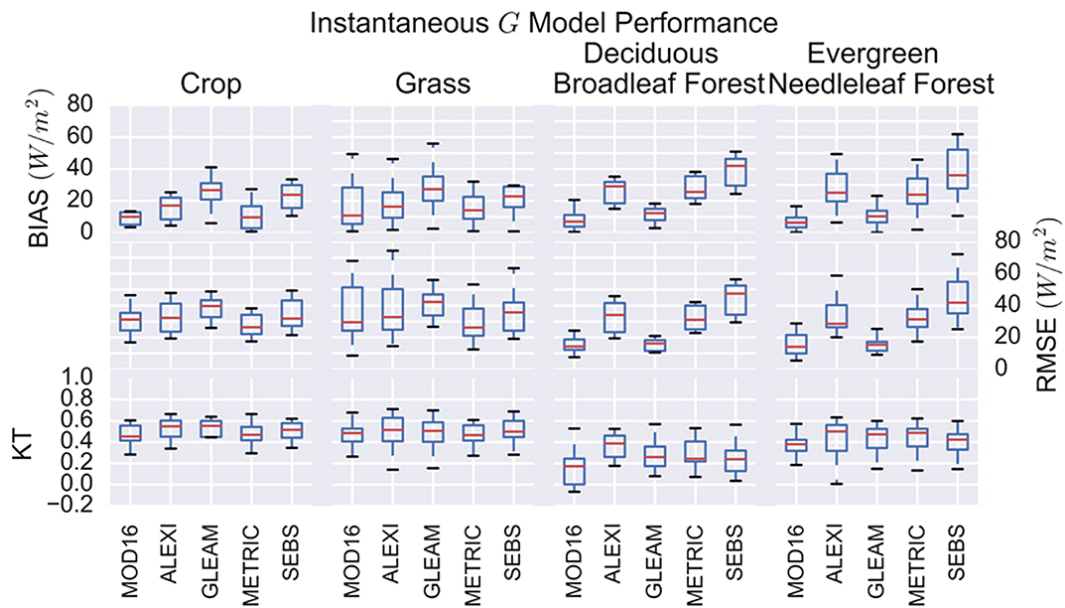
Figure 2.5 Instantaneous model performance across four most sampled PFTs in the observation data set. The METRIC G model is strongest for cropland and grassland cover. The MOD16 and GLEAM models show the strongest performance for both deciduous broadleaf forest and evergreen needleleaf forest.

The daily G models show more varied performance among the different PFTs (Fig. 2.6 and Fig. 2.7). The T-DIFF model consistently results in the lowest RMSE and BIAS and exhibits comparable explanation of variance to GLEAM, MOD16, ALEXI, METRIC, and SEBS for the four land covers (Fig. 2.7). The T-DIFF model has more varied performance for cropland and grassland compared to other land uses due to underestimation of thermal inertia (Fig. 2.6 and Fig.

2.7). We also compare a scaled version of the T-DIFF model at each of the four locations to show that the parameterized coarse resolution thermal inertia inhibits the T-DIFF model's ability to capture high and low G values. The scaled version demonstrates the strength of the model's structure by improvement in model performance with local calibration of thermal inertia.

The GLEAM and SEBS models show similar explanation of variance with the highest average Kendall's tau at three of the four PFTs (GRA, CRO, and ENF; Fig 2.7). Despite high explanation of variance across these particular PFTs, the GLEAM and SEBS G models have errors more than twice as large as the T-DIFF over GRA and CRO due to overestimation of daily G (Fig. 2.6 and Fig. 2.7). For GLEAM, model error improves in deciduous forest and evergreen forest (Fig. 2.6 and Fig. 2.7). The MOD16 model shows the widest range in model error across both grassland and cropland covers, with the highest error for one site out of all the models, most likely from setting G = 0 at a location where this is not appropriate as seen in the annual plot of grassland in Figure 6. For evergreen forest and deciduous forest, the MOD16 model shows reduced error and interquartile range in errors but exhibits a wide range in explanation of variance. The differences in model formulation yield a wide range of results for G estimation across these different biomes and climates.

2.3.2 Spatial and seasonal model inter-comparison

We model G from 2001 to 2006 at 5 km globally using MODIS NDVI, LST, and NCEP net radiation. The 2001–2006 model average midmorning G is not negligible in all areas globally (Fig. 2.8). Areas with dense vegetation such as the Amazon and boreal forested regions exhibit low G, but in areas with little vegetation G is greater than 150 Wm−2. Global G is lowest during the boreal winter and is at maximum during the boreal fall. High latitudes during winter months have the lowest G. Less vegetated regions, such as the southwestern United States, the Saharan
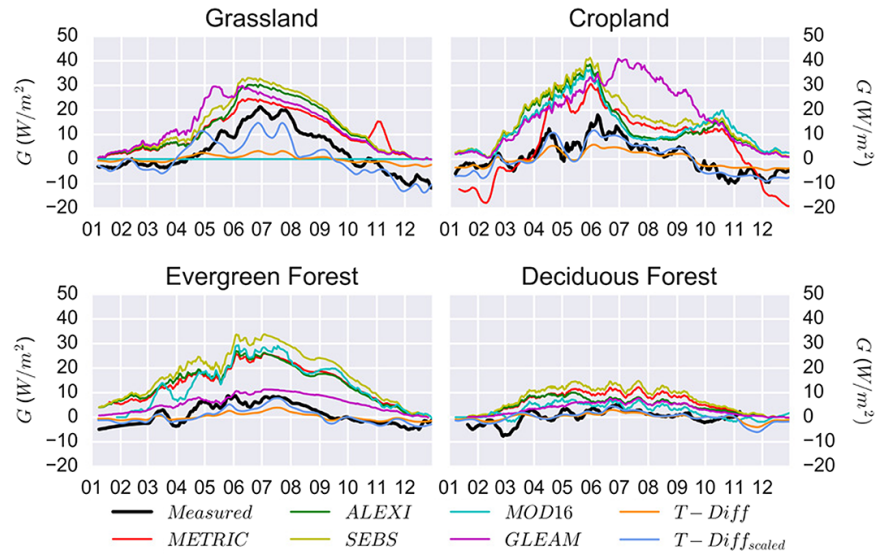
Figure 2.6 Daily model performance compared across four different land covers at same representative sites as seen in Figure 4. The T-DIFF model most closely models G throughout the year across all sites when the thermal inertia parameter is scaled.
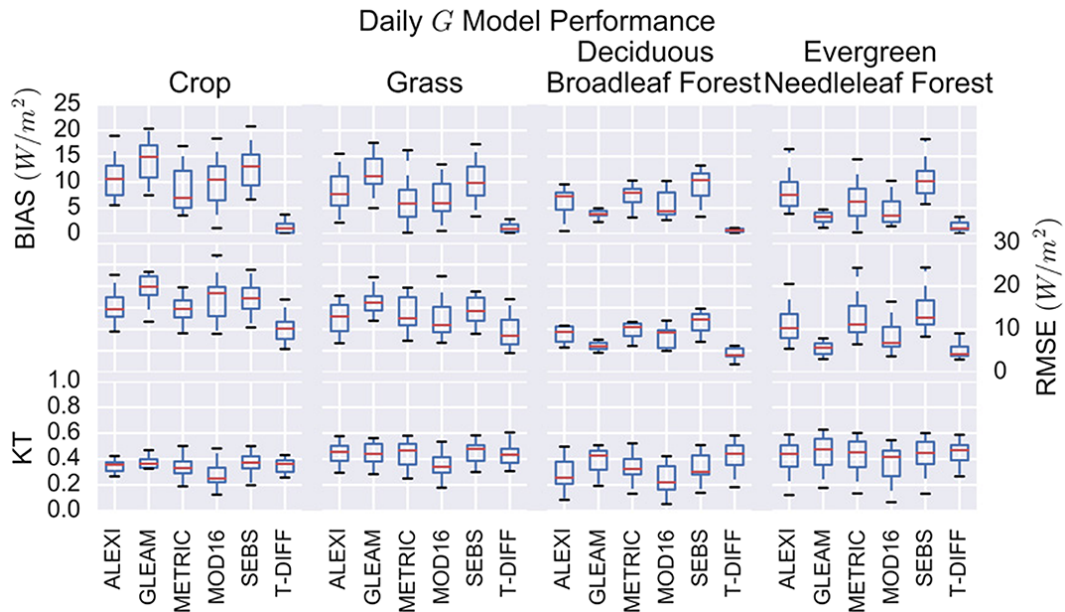
Figure 2.7 Daily G model performance across the four most sampled PFTs in the observation data set. The T-DIFF model has the lowest BIAS and RMSE across all sites along with the lowest spread in model performance, along with an explanation of variance at similar levels and reduced range compared to all other models.
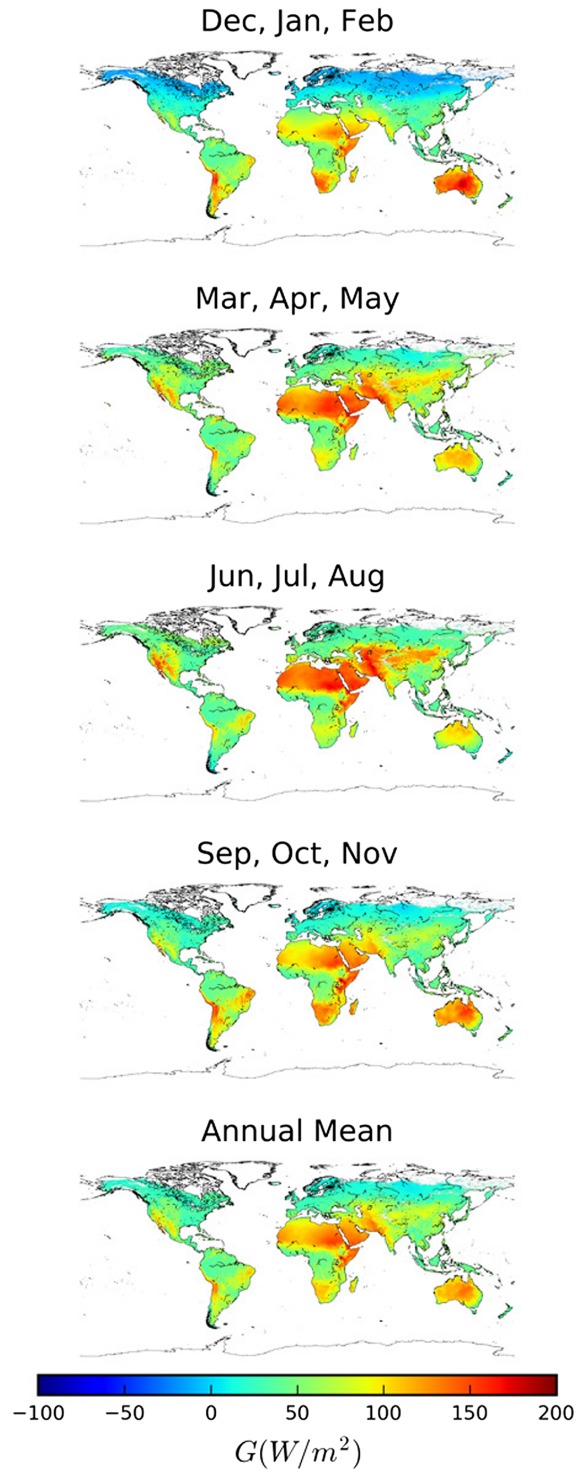
Figure 2.8 Seasonal and annual multi-model mean mid-morning G averaged from 2001 to 2006.

desert, the Arabian Peninsula, central Australia, and southern Africa, show the highest average

modeled G during warmer months. Modeled G differs more at low vegetation cover compared to

35

high vegetation cover (Fig 2.2). A spatiotemporal comparison highlights these seasonally driven model differences globally. We evaluate the G model uncertainty from 2001 to 2006 by normalizing the multi-model standard deviation of G by the mean R_{NET} for each season (Fig 2.9). During December, January, and February the largest regions of model disagreement are boreal Canada, Siberia, the southwest United States, and high-mountain Asia. Over the boreal spring and summer (March, April, and May and June, July, and August) models generally agree globally. For the months of September, October, and November, similar to the winter months high-latitude areas in the northern hemisphere experience more disagreement. The regions of disagreement are predominantly areas where bare soil, dormant vegetation, low radiation, and low temperature drive model divergence. The model formulations (Table 2.1) which quantify G/R_{NET} from empirical relationships to vegetation cover or temperature disagree most under periods of low vegetation cover and low R_{NET} (Fig 2.2). For areas with peak seasonal greenness the models converge to estimate similar magnitudes of G/R_{NET}.

2.4. Discussion

2.4.1 Strengths and weaknesses of models for instantaneous and daily G calculations

Despite potential scaling issues in relating remote sensing footprints to in situ data, we find that most models provide reasonable estimates of G across a variety of land uses and climates. For instantaneous estimation of G, we identify the linear relationship to LST used in MOD16 to provide the lowest error across all the sites (minimum average BIAS and RMSE). However, the current model formulation results in unrealistic G for regions with very hot (Tan >25°C) or cold (Tan <−5°C) temperatures or low diurnal temperature swings (Tdif <5°C) and can result in misclassification for some locations (Fig 2.6). This approach assumes that vegetation cover does not impact G for these regions, which is contradictory to much preliminary work developing G

models (Choudhury et al., 1987; Daughtry et al., 1990; Kustas et al., 1993). Therefore, the METRIC formulation presents an attractive alternative where G is modeled using vegetation cover for areas of moderate to high vegetation (LAI > 0.5), a common characteristic of models that capture more day-to-day instantaneous G variance, while still using a linear relationship to temperature for barren and sparsely covered areas (LAI < 0.5). The METRIC G model exhibits lower errors over grasslands and croplands compared to other land covers, which was the environment under which the original empirical relationship was calibrated (Allen et al., 2007b). Initial exploration into recalibration for the different PFTs indicated parameters for this formulation convergence for tall (mixed forest, DBF, evergreen broadleaf forest, and ENF) and short canopy (GRA and CRO) covers, respectively. This suggests that canopy structure not just leaf cover density influences G at these time scales (Clothier et al., 1986; Miralles et al., 2011b; Reginato et al., 1985). For midmorning instantaneous G calculations, the METRIC formulation shows the most potential from parameter recalibration for a more robust representation by incorporating canopy height.

For G needed at daily or longer time scales the T-DIFF model bests all other models. The T-DIFF model exhibits low errors while explaining a similar level of variance to models forced by R_{NET}. We find the optimal thermal inertia parameters to minimize error are greater than reported values for daily time steps (Fig 2.6) (Bennett et al., 2008). Despite the difference, the integrated time difference in nighttime LST is the best method to model G at these time scales. Further work on parameterization of the soil thermal properties and the incorporation of changing properties such as surface soil moisture creates the opportunity to enhance model performance globally (Idso, 1978; Santanello and Friedl, 2003).

2.4.2 Mechanisms that control G across instantaneous and aggregated timescales

The instantaneous and daily G models each share a common set of variables: R_{NET}, vegetation properties (NDVI, LAI, and fc), and LST (Table 2.1). These variables are used to model the environmental processes that control G. Vegetation impacts the magnitude of G in multiple ways. Dense vegetation reduces G through shading the ground from incoming radiation and by buffering temperature gradients in areas with high rates of ET. We analyze the results from the instantaneous and daily model evaluations to determine if these processes are appropriately represented.

For instantaneous models the highest explanation of day-to-day variability is achieved by GLEAM, a model forced with R_{NET} (Table 2.2). The models forced by only LST miss higher-frequency variability in G that is captured by models forced with R_{NET}; this is in contrast to previously published correlation coefficients for a model forced only by LST data (R2 = 0.90) (Jacobsen and Hansen, 1999). Models that use vegetation properties to scale R_{NET} to G (ALEXI and SEBS) result in more error compared to models that use both vegetation properties and LST to estimate G (METRIC and MOD16). Comparing the explanation of variance between the GLEAM scalar approach and the models that only use vegetation phenology (ALEXI and SEBS) would imply that vegetation changes might not even play a major role in the calculation of instantaneous G (Table 2.2 and Figure 2.5). This suggests that the phenological changes in vegetation are less indicative of seasonal changes in G compared to seasonal fluctuations in R_{NET} and LST or that LST implicitly incorporates phenological changes from the impact of vegetation on LST. This finding is contrary to early work built on the foundation that G/R_{NET} is proportional to vegetation density (Choudhury et al., 1987; Kustas et al., 1993). However, for specific locations, such as the cropland cover where large changes of vegetation occur with cultivation practices, this

is not the case (Fig 2.4). Here the GLEAM model deviates from the observation and the other G

models between May and June due to a change in vegetative cover unaccounted for by annually

invariant canopy height forcing data sets. Not every model applies vegetation properties to scale

R_{NET}; instead, models rely on LST data to reflect changes in canopy conditions appropriate for

modeling G.

For daily or longer times, temperature is the most important variable for accurately

modeling G. As evidenced above the T-DIFF model outperforms all other models, suggesting that

the integrated time differential in nighttime LST is a sound method to model G at daily time steps.

Additionally, the T-DIFF structure implicitly accounts for energy storage and conserves energy by

summing both increases and decreases in the time derivative of LST to calculate G. For these time

scales, models that reduce R_{NET} to G using vegetation attributes (NDVI, LAI, or canopy height)

have errors close to twice as large as T-DIFF and do not explain considerably more variability in

daily G (Table 2.3 and Fig. 2.7). The poor performance by these models might be traced to model

formulations that neglected energy storage. Energy storage is important for aggregated times but

not necessary for snapshots of energy partitioning. At daily or longer frequencies temperature

fluctuations explain just as much variability in G as R_{NET} does. The GLEAM G model, which

directly scales R_{NET} to G, only explains slightly more daily G variability than T-DIFF (Table 2.3).

The T-DIFF model error suggests that other factors, such as soil properties, may help explain the

magnitude of G, but parameterizing these uncertainties using PFT specific calibrations is an

appropriate way to handle the uncertainty surrounding spatially explicit specific soil properties.

However, since a relatively low amount of daily G variability is explained by this model

(KT = 0.36), the assumption that the thermal inertia calibrated for this model evaluation remains

constant across a year warrants further exploration. Future work to calibrate soil thermal inertia with soil moisture might enhance model performance.

We find that G models forced by R_{NET} better portray diel variability while models forced by temperature changes better capture seasonal variation. Since R_{NET} and temperature are largely independent, we hypothesize that a model incorporating both variables will best represent the environmental processes that drive G, such as absorption of incoming R_{NET} and energy gain or loss through the temperature gradient. Additionally, we posit that models that incorporate physical principles such as conservation of energy will outperform models that do not. Taking these environmental processes into account might offer a path toward G model reformulation and improvement.

2.4.3 Optimized G model to reduce ET uncertainty

For instantaneous G quantification, the METRIC G model provides a sound structure relating canopy density to reduce incoming radiation. We build upon this model by leveraging other G model strengths. For example, we incorporate canopy height to categorically model G as presented in GLEAM. We optimize the METRIC model to short and moderate to tall canopies. For moderate to tall canopies (CH > 1.0 m) we compute G/R_{NET} as:

$$
\begin{aligned}
\frac{G}{R_{NET}} &= a + b \cdot e^{-c \cdot LAI} \quad for\ LAI > 0.5\ CH > 1.0m \\
\frac{G}{R_{NET}} &= 0.05 \quad\quad\quad for\ LAI < 0.5\ CH > 1.0m
\end{aligned}
\tag{1}
$$

where a = 0.087, b = 0.15, c = 0.88. For short canopies we compute G/R_{NET} as:

$$
\begin{aligned}
\frac{G}{R_{NET}} &= a + b \cdot e^{-c \cdot LAI} \quad for\ LAI > 0.5\ CH < 1.0m \\
\frac{G}{R_{NET}} &= 0.20 \quad\quad\quad for\ LAI < 0.5\ CH < 1.0m
\end{aligned}
\tag{2}
$$

where a = 0.019, b = 0.079, c = 0.44. The optimized parameterizations reduce model BIAS by over 40% (Original Model: 18.9 Wm^{-2}| Optimized Model: 11.2 Wm^{-2}) and reduce RMSE by 30% (Original Model: 31.9 Wm^{-2}| Optimized Model: 22.1 Wm^{-2}). The largest improvements are for land covers with taller canopy heights (Appendix Fig. A.1.1). For daily applications, we find support for the thermal diffusion model with calibration (Figure 2.6). The thermal inertia for this model are dependent on soil moisture and vegetation cover, however at this time the limited number of quality soil moisture observations at the EC towers used in this study limits such parameterization. The new instantaneous model parameters have potential to reduce uncertainty in global ET model inter-comparisons by reducing the present uncertainty from different G models.

2.4.4 Current impact of G uncertainty on global ET

The G model disagreement is highest for areas and seasons when the magnitude of global ET is lowest. We quantify G uncertainty as a proportion of R_{NET}. ET is directly impacted by errors in available energy ($R_{NET} - G$ for evaporation or R_{NET} for transpiration) in both the Penman-Monteith and Priestley-Taylor equations. Depending on the radiation partitioning method for evaporation and transpiration for each algorithm the magnitude of the impact will differ across models. The spread in model disagreement is greatest in seasons with low R_{NET} and cold weather and in areas with low vegetation (Fig. 2.2). Snow cover negatively impacts remote sensing observations of vegetation and should decrease G due to lower net radiation as a result of a high albedo and smaller thermal inertia of snow relative to soil (Bennett et al., 2008). The spatiotemporal occurrences of minimum ET occur across the seasons and areas where model differences in G/R_{NET} are largest. Therefore, the timing of the differences in G/R_{NET} would have

41
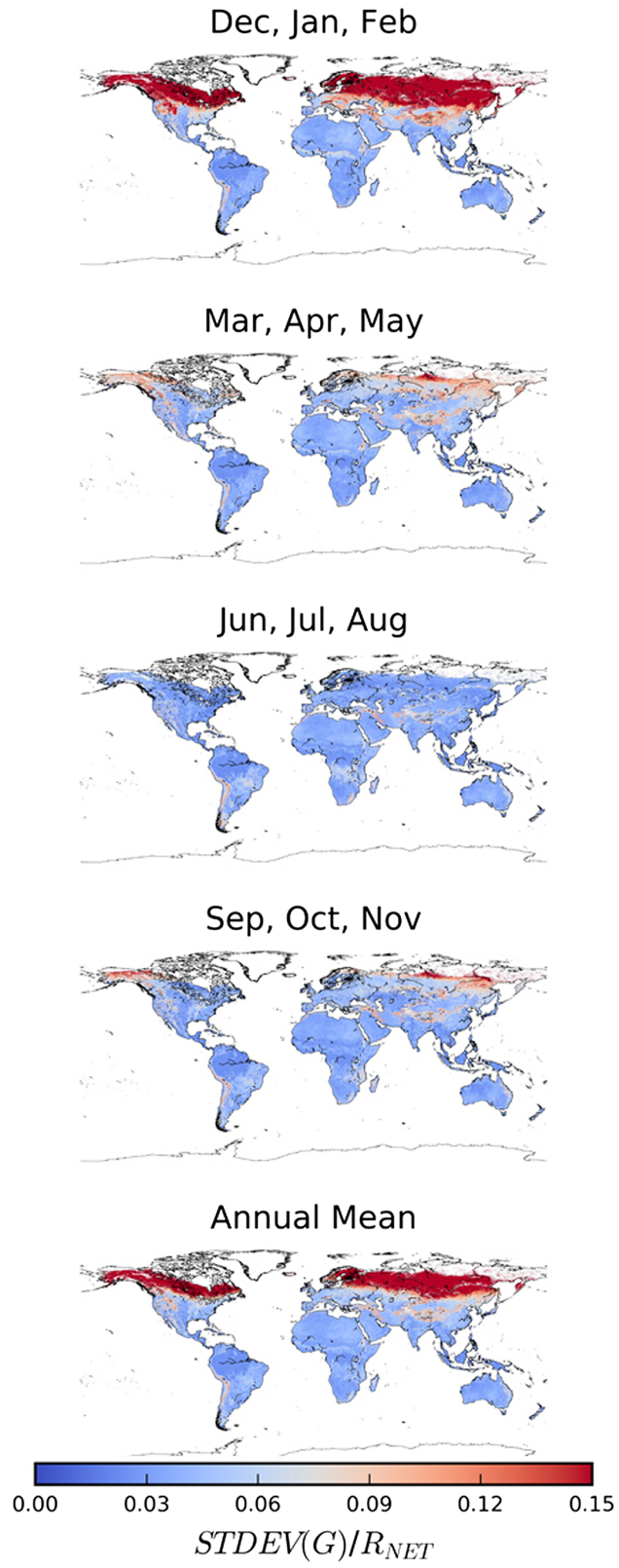
Figure 2.9 Average seasonal G model uncertainty from 2001 to 2006. The red areas indicate the greater model disagreement.

minimal impact on annual magnitude of ET models, especially because of smaller differences in available energy during seasons of peak ET (i.e., June, July, and August) (Miralles et al., 2011a; Vinukollu et al., 2011). However, during periods of low energy the importance of G is amplified since it is a larger component of available energy ($R_{NET} - G$) and subsequently the impact on ET. The occurrences of the largest modeled G disparities highlight seasons and areas where mechanistic differences in modeled ET and H would be most difficult to disentangle. Despite potential limitation to the impact on ET estimates globally, this analysis reveals regions ripe for G model refinement and demonstrates the importance to choose and calibrate the correct G model for regional studies, especially those focusing on the arctic regions (December-January-February and September-October-November; Fig. 2.9). Moreover, the limited performance by each instantaneous G model compared to in situ observations reveals a great opportunity to reduce uncertainty in ET model performance from uncertain G by recalibrating models to broader more robust data sets.

2.5. Conclusion

This study evaluates a suite of different G remote sensing methods in current ET models. Six different G models from highly regarded ET algorithms were compared. Previous studies have not evaluated G models against a global set of in situ observations or investigated seasonal model divergence globally. We use in situ G observations from the FLUXNET La Thuile synthesis data set in combination with MODIS vegetation and LST data to evaluate model performance across 88 sites globally. Global G flux estimates produced using MODIS NDVI and LST data along with NCEP R_{NET} were evaluated globally from 2001 to 2006. We identify which G models perform best globally, which models perform best across different plant functional types, and the areas with the largest seasonal disagreement among G models.

The results from this study uncover potential for improvement in energy balance closure at the site level through leveraging remote sensing data, provide guidance on how best to model G at different time scales for different land covers, and identify regional and seasonal model biases with implications for global ET and H estimates. Poor model performance at some locations ($KT < 0$) reveals potential issues of comparing models to in situ G observations. These potential issues include the scaling of situ observations to remote sensing footprints or the observation technique used to measure G, the depth of heat flux plate, and how soil heat storage above the sensor is modeled using soil thermocouples. For regional studies, utilizing finer spatial resolution remote sensing products would help minimize scaling issues in heterogeneous areas such as croplands and harvested forests. Much work is still needed to enhance understanding on how limited point measurements impact scaling this flux to much larger areas. Additional high-fidelity observations at high latitudes, where model disagreement is greatest (Fig. 2.9), would provide opportunity to scrutinize and improve G models under low-energy conditions.

The G models that only rely on vegetation may introduce seasonal biases in areas with large phenology swings, and areas with small vegetation changes may mask a seasonal cycle directly observed by LST. The G models that only use LST may overestimate G in areas with tall canopies and/or dense vegetation cover. Future work should incorporate physical principals and the environmental processes that control G and optimize the best structural formulations to many land uses and canopy heights. Preliminary results for these efforts suggest that calibration by PFT delivers optimal performance for both instantaneous and daily estimates. Despite often being the smallest term in the surface energy budget, this study reveals that G is not negligible and warrants appropriate representation in ET algorithms. Making such improvements can facilitate better

process level understandings of ET including appropriate partitioning and the sensitivity to other

environmental variables such as soil moisture.

Chapter 3

SMAP soil moisture improves global evapotranspiration

Adapted from:

Purdy, A.J., Fisher, J.B., Goulden, M.L., Colliander, A., Halverson, G., Tu, K., Famiglietti, J.S., SMAP soil moisture improve global evapotranspiration, submitted to *Remote Sensing of Environment*

3.1. Introduction

Water movement from land to the atmosphere, or evapotranspiration (ET), is an integral part of earth's ecological and climate systems, linking the water, carbon, and energy cycles in the earth system. Accurate observations of ET facilitate detection of the human fingerprint on the water cycle and surface energy budget (Lo and Famiglietti, 2013; Sorooshian et al., 2011), studies on land-atmosphere feedbacks related to heat wave intensity (Diego G. Miralles et al., 2014), quantification of agricultural and ecosystem water use (Allen et al., 2007b; R. G. Anderson et al., 2011; Goulden et al., 2012; Goulden and Bales, 2014), identification of droughts where plants may become vulnerable to other biotic stressors and potential mortality (Anderson et al., 2013; McDowell, 2011; Mu et al., 2013), and provide benchmarks to evaluate and improve parameterizations in land surface models (Mueller et al., 2013; Rodell et al., 2011). With increasing global temperatures and the subsequent greater atmospheric capacity for water vapor, the potential acceleration of the water cycle may alter global water distribution making certain regions drier (Huntington, 2006; Syed et al., 2010). As land begins to dry, (Greve and Seneviratne,

2015; Jung et al., 2010) quantifying where and to what degree reductions in water availability limits ET becomes increasingly important.

Remote sensing algorithms are an effective way to derive observationally-constrained ET estimates at the necessary spatiotemporal resolutions to support earth observations (Fisher et al., 2017, 2008; Miralles et al., 2011a; Mu et al., 2011; Su, 2002). Multiple manuscripts have reviewed the state and needs for ET remote sensing (Fisher et al., 2017; Wang and Dickinson, 2012) and one common theme across these remote sensing approaches is a limited or absent representation of soil moisture. Of the ET remote sensing algorithms, few approaches remain both physically defensible and globally applicable without reliance on data assimilation and prognostic land surface models.

The Priestley-Taylor Jet Propulsion Laboratory (PT-JPL) ET model, a widely used remote sensing retrieval algorithm, has outperformed many models for the majority of globally distributed eddy covariance towers within model inter-comparison studies achieving both high explanation of variance and low error (Ershadi et al., 2014; Michel et al., 2016; Vinukollu et al., 2011). Despite a strong performance in these studies, the PT-JPL algorithm lacks soil moisture control and is restricted by its dependence on a combination of atmospheric conditions and vegetation characteristics to represent surface conditions. These limitations become especially evident in regions where the coarse near surface air temperature and water vapor pressure deviate from the underlying surface soil water availability at fine temporal frequencies, in areas with highly heterogeneous land covers, in areas of active land management, or in regions prone to atmospheric advection conditions (Fig. 3.1). Incorporating soil moisture observations has great potential to address these limitations and improve global ET estimates but large challenges exist.

47
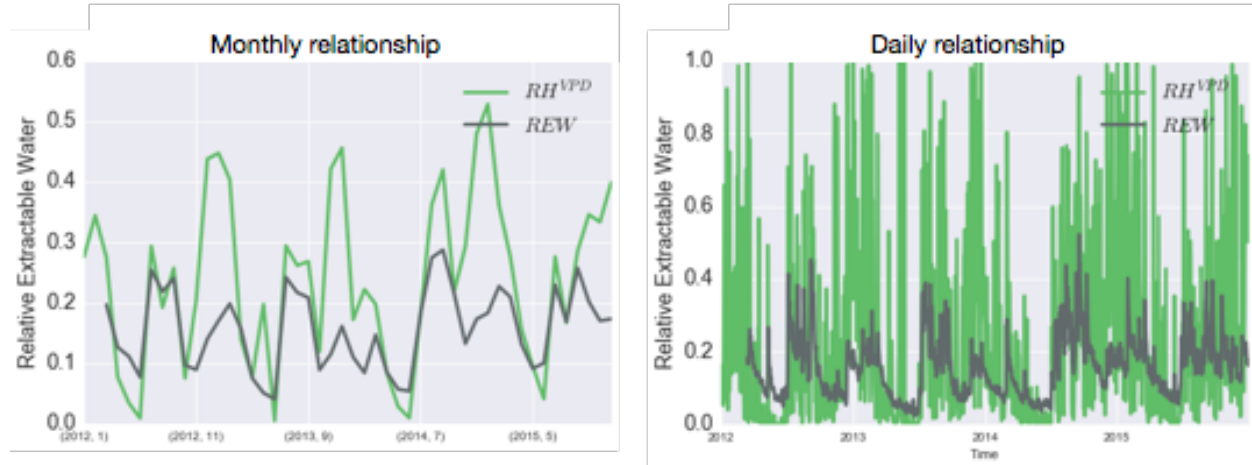
Figure 3.1 Atmospheric variable ability to explain REW. Monthly REW (left) and daily REW (right) demonstrates how moving to higher temporal frequencies hinders this method. Also, for this location (US-Wkg), we see overestimation of this approach at monthly and daily times.

There are two main challenges to improve global estimates of ET using soil moisture: 1) observing accurate integrated values of soil moisture; and, 2) appropriately modeling how limitations from soil moisture interact with other environmental constraints to quantify ET.

The launch of the Soil Moisture Active Passive (SMAP) satellite (2015) addresses the first challenge through providing global soil moisture observations (Entekhabi et al., 2010). The SMAP mission has leveraged lessons from other global soil moisture observing satellites, such as the Advanced Microwave Scanning Radiometer- EOS (Njoku et al., 2003) and the Soil Moisture Ocean Salinity (Kerr et al., 2016) satellites to detect and mitigate potential radio frequency interference and provide observations at relatively high spatio-temporal [9-36 km, 3-daily] resolutions at a depth [5-cm] applicable to improve modelled ET (Johnson et al., 2016; Mohammed et al., 2016; Oliva et al., 2012; Piepmeier et al., 2014). These observations have been extensively evaluated as part of a rigorous calibration and validation campaign and shown to be within mission accuracy requirements and thus capable of supporting improvements to global ET quantification (Colliander et al., 2017a).

To address the second challenge, model testing and updates needs to be done with coterminous observations of meteorological conditions, soil moisture, and ET. Observations of soil moisture and ET are made globally in distributed networks of eddy covariance (EC) towers as part of FLUXNET (Baldocchi et al., 2001). However, sites often include measurements of soil moisture at only 1-4 points and these points may misrepresent actual land surface conditions within the EC footprint making model parameterization and calibration difficult. Despite this, EC observations of water and energy exchange at the earth's surface provide a valuable dataset which approaches the resolution at which satellites observe environmental variables necessary to test and evaluate ET models (Baldocchi et al., 2001).

Generally, land surface and remote sensing models relate the amount of ET to water availability and the atmospheric demand for ET, but vary to what degree and at what point water availability limits and eventually prevents ET. Various adaptations of soil moisture normalized by soil properties to compute the relative extractable water (REW) have been applied to limit transpiration (Fig. 1.1, Table 1.1). Yet, soil moisture is just one of many environmental variables that limits the maximum stomatal conductance, as temperature and vapor pressure extremes have been found to regulate transpiration (Fisher et al., 2008; Jarvis and Mcnaughton, 1986; Monteith, 1965; Mu et al., 2011; Novick et al., 2016). This idea has been adopted for approaches that use the Priestley Taylor equation where REW-based stressors are applied in series with other scalar stressors, such as temperature and vapor pressure, to reduce PET based on sub-optimal environmental limitations (Fisher et al., 2008; Jin et al., 2011; Miralles et al., 2011a). Additionally, plant access to soil moisture varies with rooting depth and much uncertainty exists with the role deep roots play in mitigating limitations from soil water availability during drought (Schenk and Jackson, 2002). Plant type, canopy height and aboveground biomass provide indicators of rooting

depth and the potential to access to deeper soil water (Canadell et al., 1996; Fan et al., 2017; Jackson et al., 1999). Miralles et al. (2011) postulate taller vegetation is less sensitive to soil water deficits compared to shorter canopy plants due to deep rooting potential to alleviate plants from seasonal drought conditions (i.e., when precipitation occurs outside of the of summer maximum atmospheric demand). Recent global observations of canopy height hold create an opportunity to further inform plant sensitivity to environmental conditions (Simard et al., 2011).

We present an update to the PT-JPL algorithm by incorporating explicit surface soil moisture constraint from SMAP to model ET globally. To address previous model parameterization limitations, we use integrated in situ observations of soil moisture and ET to implement soil moisture control within the PT-JPL model. Then, we apply the new PT-JPL$_{SM}$ model globally using soil moisture data from the Soil Moisture Active Passive mission (SMAP). The following sections will provide: (1) a description of the PT-JPL algorithm with updates detailing soil moisture constraints on evaporation and transpiration, (2) details on the datasets used in this study, (3) results evaluating the updated PT-JPL$_{SM}$ model compared to the original PT-JPL model using eddy covariance towers from Ameriflux and globally using satellite datasets, and (4) discussion on the implications of soil moisture on global ET quantification improvement.

3.2. PT-JPL algorithm

3.2.1 PT-JPL ET Algorithm

The Priestley Taylor-Jet Propulsion Laboratory (PT-JPL) ET algorithm applies ecophysiological constraints to model reductions of ET from the atmospheric potential ET due to sub-optimal environmental conditions (Fisher et al., 2008). The model incorporates a variety of data sources from satellite observations and reanalysis datasets (Fig. 3.2; Table 3.1). Potential ET, or latent energy *LE,* is computed using the Priestley-Taylor model:

$$PET = \alpha \frac{\Delta}{\lambda(\Delta+\gamma)}(R_N - G) \tag{1}$$

where PET is the potential ET based on temperature and radiation, α is the Priestley-Taylor coefficient that is set to 1.26, Δ is the slope of the saturated vapor -pressure relationship [kPa $^{\circ}C^{-1}$], and γ is the psychrometric constant [kPa $^{\circ}C^{-1}$], and R_N is the net radiation [W m^{-2}], G is the ground heat flux [W m^{-2}], and λ is the latent heat of vaporization [MJ kg^{-1}] (Priestley and Physics, 1972). The water cycle and energy cycle are linked through ET and latent heat LE such that the latent heat of vaporization such that ET λ = LE. The model is constructed to compute LE, but we refer to output in terms of the water component ET throughout the remainder of the manuscript. The PT-JPL algorithm is a three source ET model where each component of ET is calculated as:

$$LE = LE_I + LE_T + LE_S \tag{2}$$

where LE_I is evaporation from plant intercepted water, LE_T is transpiration from vegetation, and LE_S is soil evaporation. Ecophysiological *f-functions*, scalars between 0 and 1.0, limit each component from the potential rate.

Canopy interception is computed as:

$$LE_I = f_{WET}\alpha \frac{\Delta}{(\Delta+\gamma)} R_N{}^C \tag{3}$$

where f_{WET} is the fraction of saturated soil computed as $f_{WET} = RH^4$, where RH is the relative humidity, $R_N{}^C$ is the canopy net radiation calculated as $R_N{}^C = R_N - R_N{}^S$. $R_N{}^S$ is the net radiation at the soil surface computed as $R_N{}^S = R_N e^{(-k_{Rn}LAI)}$ where $k_{Rn} = 0.60$ and LAI is the leaf area index.

Canopy transpiration is computed as:

$$LE_T = (1 - f_{WET})f_G f_T f_M \alpha \frac{\Delta}{(\Delta+\gamma)} R_N{}^C \tag{4}$$

where f_G is the fractional canopy greenness computed as $f_G = \frac{f_{APAR}}{f_{IPAR}}$ where f_{APAR} is the fraction of absorbed photosynthetically active radiation (*PAR*) and f_{IPAR} is the fraction of intercepted *PAR*; f_T

is the sub-optimal temperature constraint computed as $f_T = e^{\left(-\left(\frac{T-Topt}{Topt}\right)^2\right)}$ where T is the maximum daily air temperature and T_{OPT} is the optimum temperature computed as $T_{opt} = T_{max}$ at $\max\left\{\frac{PARf_{APAR}T_{max}}{VPD}\right\}$; and f_M is the vegetation moisture constraint computed as $f_M = \frac{f_{APAR}}{f_{APARmax}}$ where $f_{APARmax}$ is the annual maximum f_{APAR}.

Soil evaporation is computed as:

$$LE_S = [f_{WET} + f_{SM}(1 - f_{WET})]\alpha \frac{\Delta}{(\Delta+\gamma)}(R_N{}^s - G) \tag{5}$$

where f_{SM} is the soil moisture constraint computed as $f_{SM} = RH^{VPD}$, VPD is the vapor pressure deficit. For further detail reference *Fisher et al.*, 2008.

Soil water control on evaporation is implicitly represented through $f_{SM} = RH^{VPD}$, where f_{SM} is the soil moisture constraint on E_S, RH is the relative humidity, and VPD is the vapor pressure deficit. This equation is formed from Bouchet's theory of land atmosphere equilibrium. However, the assumption that land and atmosphere are in equilibrium at the fine spatial resolutions and acute temporal scales fails for certain regions (Fig 3.1). Similarly, plant water availability is implicitly represented by observations based on plant greenness and therefore phenological changes from peak greenness introduces potential latency in vegetation response to water limitations.

3.2.2 Updates to the PT-JPL model

We update the new model, here-after called PT-JPL$_{SM}$, to incorporate explicit soil water availability control on evaporation and transpiration. We also incorporate a new cold-temperature limitation constraint for frozen ground and a new G parameterization.
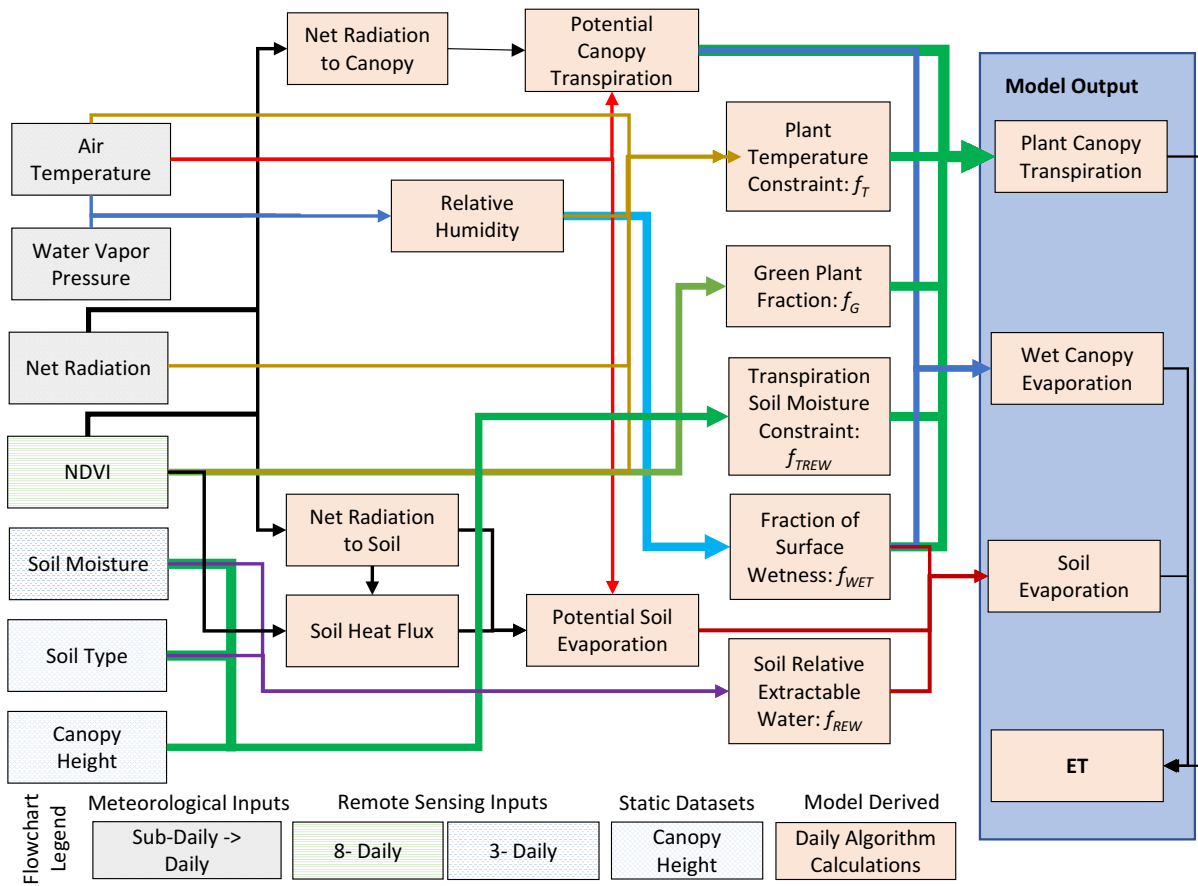
Figure 3.2 Flow chart showing data processing stream for the original PT-JPL model.

Table 3.1 Global gridded forcing dataset characteristics.

Variable	Product Name	Time Available	Frequency	Spatial Resolution	Reference
Net Radiation	MERRA2 M2T1NXLND	1979-present	Daily	0.5^o x 0.5^o	GMAO 2015a
Temperature	MERRA2 M2I1NXASM	1979-present	Daily	0.5^o x 0.5^o	GMAO 2015b
Vapor Pressure	MERRA2 M2I1NXASM	1979-present	Daily	0.5^o x 0.5^o	GMAO 2015b
NDVI	MOD13A2 MYD13A2	2000-present	8-Daily	5km x 5km	NASA LP DAAC 2017
Soil Moisture	SPL3SMP_E v1 SPL3SMP v4	4-2015-present	3-Daily	9km x 9km 36km x 36km	Oneil et al., 2016a Oneil et al., 2016a
Soil Properties	SPL4SMLM	NA	NA	9km x 9km	Das et al., 2013
Canopy Height	NA	NA	NA	1km x 1km	Simmard et al., 2011

3.2.2.1 Soil moisture control on evaporation

Surface soil moisture and soil properties control the rate of evaporation. As such we employ the available water content to scale the rate of evaporation. The relative extractable water is a commonly used stressor that normalizes the impact from soil properties. The original model employs the f_{SM} scalar to limit the rate of evaporation from the soil surface. This scalar was formulated to represent relative extractable water through the Bouchet's theory of where the land surface and near surface atmosphere are in equilibrium across certain space and time scales. Here we update each model to represent true relative extractable water using:

$$f_{REW} = \frac{\theta_{obs} - \theta_{wp}}{\theta_{POR} - \theta_{wp}}$$ (6)

where θ_{obs} is the soil moisture observation, θ_{WP} is the soil-plant wilting point, and θ_{FC} is the soil field capacity. We replace f_{SM} with f_{REW} in the new evaporation algorithms.

$$LE_S = [f_{WET} + f_{REW}(1 - f_{WET})]\alpha \frac{\Delta}{(\Delta + \gamma)}(R_N{}^s - G)$$ (7)

This method has been implemented in other remote sensing ET algorithms that use ET to model surface and root zone soil moisture (Anderson et al., 2007; Martens et al., 2017).

3.2.2.2 Soil moisture control on transpiration

In the original PT-JPL formulation plant moisture stress is inferred from the deviation from maximum greenness (f_M). As the model was developed for application at monthly or longer timescales, latent responses from vegetation to moisture deficits did not impact quantification of ET, as this does at higher temporal frequencies, i.e. daily calculations. Therefore, we formulate and include an explicit soil water availability constraint on transpiration. We posit that canopy height is related to the rooting depth and plant capacity to access water from deeper sources. Therefore, these data enable continuous quantification of plant sensitivity to surface soil water

conditions (Canadell et al., 1996; Jackson et al., 1999; Martens et al., 2017; Nepstad et al., 1994). We calculate the new transpiration constraint as:

$$f_{TREW} = 1 - \left(\frac{\theta_{CR} - \theta_{obs}}{\theta_{CR} - \theta_{wp_{CH}}}\right)^{CH_{scalar}} \tag{8}$$

where θ_{CR} is the critical soil moisture at which soil water availability limits ET, $CH_{scalar} = \sqrt{CH}$ is a canopy height scalar that impacts the sensitivity to soil water availability, set the range from 1 to 5.

$$\theta_{CR} = (1 - p)\left(\theta_{POR} - \theta_{wp_{CH}}\right) + \theta_{wp_{CH}} \tag{9}$$

$$p = \frac{1}{1 + PET} - a\frac{1}{1 + CH} \tag{10}$$

$$\theta_{WP_{CH}} = \frac{\theta_{WP}}{CH_{scalar}} \tag{11}$$

where p is a parameter dependent on both *PET* [mm/day] and *CH* [m] that quantifies at which point soil water availability begins to limit transpiration below the potential rate, a is a parameter set to 0.1 represents the weight of influence *CH* imposes on θ_{CR}. Equation 8 was formed from the influence of Martens et al. (2016), but adjusted to incorporate the atmospheric demand and canopy height as continuous scalars to avoid dependence on land classification datasets. Equation 9 and 10 were amended from van Diepen et al. (1989), to account for the influences of plant access to deeper water reserves and atmospheric demand intensifying or mitigating vegetation sensitivity to water availability (van Diepen et al., 1989). The resulting relationship resembles those of previous models, but instead of being entirely reliant on soil properties to explain soil moisture impacts transpiration, our model uses the potential ET and canopy characteristics to quantify at what point and to what degree soil water availability limits LE$_T$ (Fig. 3.3). The new ecophysiological scalar f_{TREW} in Equation 8 is combined in series with the combined stresses from f_G and f_T, to equally weight the constraint from surface soil moisture on canopy transpiration f_{TREW}.

$$LE_T = (1 - f_{WET})f_{TREW}f_Gf_T\alpha\frac{\Delta}{(\Delta+\gamma)}R_N{}^C \tag{12}$$

3.2.2.3 Cold temperature limitation

We maintain optimal temperature stress f_T, but include a new frozen ground temperature limit on E_S and below freezing temperature constraints on E_C and E_I such that f_{FS} =0.0, f_{FT}= 0.05, and f_{FI} = 0.0, when daily maximum air temperature is below 0°C. Each cold temperature limitation is applied in series with all other f-functions for the respective ET component.
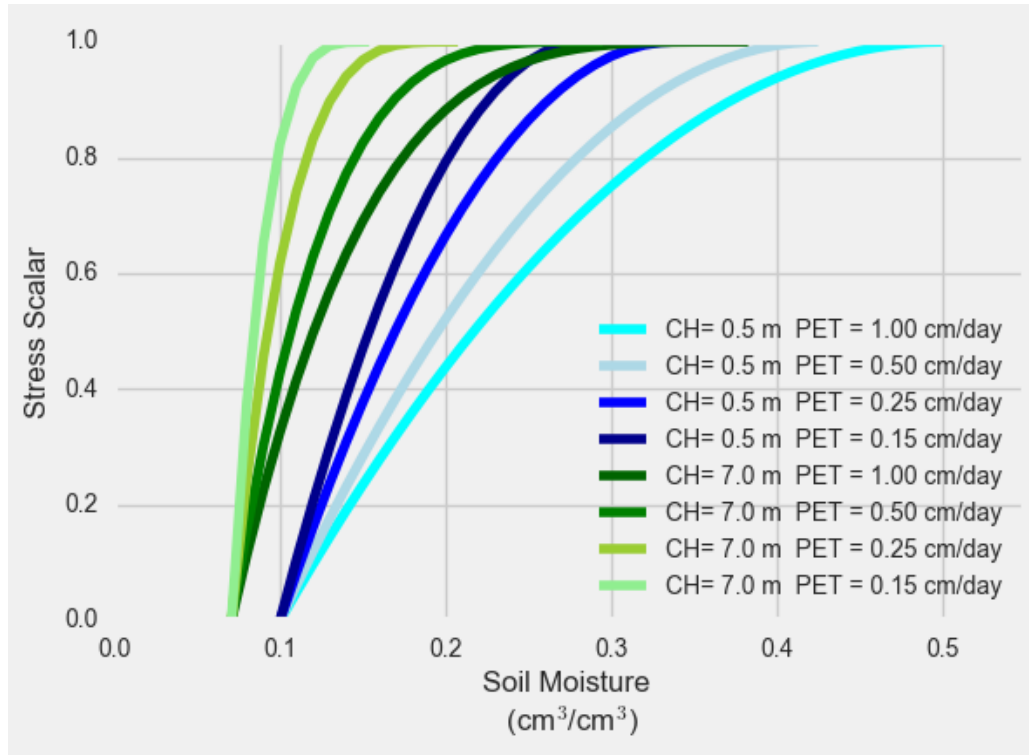
Figure 3.3 Model transpiration sensitivity to surface soil moisture. Differences in canopy height (green or blue) and potential ET (PET). The conceptual model response is shown for a wilting point of 0.01 cm³cm⁻³ and a porosity of 0.50 cm³cm⁻³.

3.2.2.4 Ground heat flux

Previously, since PT-JPL was implemented at monthly time resolution G was estimated to be 0. For daily calculation, we derive G as described in Allen et al., (2007), but update the parameterizations based on tall and short canopies. The updated model parameters were calibrated

to a *G* evaluation dataset (Chapter 2; Purdy et al., 2016). The equations used to model *G* and the updated parameterizations are presented in Chapter 2.

3.3. Datasets and data processing

3.3.1 Global and *in situ* model forcing datasets

We combine satellite observations of vegetation and surface soil moisture with meteorological data from a reanalysis dataset to model ET globally. We evaluate the model using both *in situ* and gridded forcing datasets. *In situ* meteorological (R_{NET}, T_{AIR}, e_A), soil moisture (θ), and latent heat observations at integrated spatial scales from these two networks facilitate updates to the PT-JPL algorithm. Gridded forcing data from MERRA, the MODerate resolution Imaging Spectrometer (MODIS), ICESat/GLAS, and SMAP provide spatially continuous data sources to model ET globally. All datasets are open access and available from: the NASA Land Process Distributed Archive Center (https://e4ftl01.cr.usgs.gov/; http://daac.ornl.gov/MODIS/), the Goddard Earth Sciences Data and Information Services Center (https://goldsmr4.gesdisc.eosdis.nasa.gov:443), the National Snow and Ice Data Center (https://n5eil01u.ecs.nsidc.org), the COsmic-ray Soil Moisture Observing System (COSMOS) (http://cosmos.hwr.arizona.edu), the Lawrence Berkley Livermore National Laboratory's Ameriflux repository (http://ameriflux.lbl.gov) and the FLUXNET data center (http://fluxnet.fluxdata.org). Table 3.1 describes the spatial extent and frequency characteristics of each dataset used in this study. Table 3.2 details the eddy covariance towers from Ameriflux used in this analysis including site locations, plant functional types, and climate and terrain sampled for the areas used to support this analysis.

3.3.2 MODIS NDVI (MOD13A2 & MYD13A2)

The normalized difference vegetation index (NDVI) facilitates monitoring vegetation green up and senescence. The MOD13A2 and MYD13A2 data products from MODIS, when combined, provide NDVI observations at 8-day and 0.05° from the Terra and Aqua satellites from 2000 to present for global estimates (NASA 2017). For *in situ* model runs, we use the Oak Ridge National Laboratory MODIS land product subset tool to extract higher spatial resolution (250m) NDVI observations from MOD13A1 and MYD13A1 for each eddy covariance tower location, or tower principal investigator suggested representative pixel (http://daac.ornl.gov/MODIS/). All NDVI data are filtered for only high-quality observations and linearly interpolated for daily application.

3.3.3 Canopy Height (ICESat/GLAS)

Global observations of canopy height (1-km^2) are used to model plant sensitivity to surface soil moisture. This canopy height dataset was generated with observations spanning 2003 to 2009 from the Geoscience Laser Altimeter System (GLAS) on the Ice, Cloud, and land Elevation Satellite (Simard et al., 2011). We spatially average this dataset to each of the EASE grids used in this study to model vegetation sensitivity to surface soil moisture.

3.3.4 SMAP surface soil moisture (SPL3SMP and SPL3SMP_E)

We use two SMAP soil moisture data products: SMAP_L3_SM_P and SMAP_L3_SM_P_E. The SMAP Level 3 Radiometer Global Daily 36km EASE-Grid Soil Moisture Version 4 and the SMAP Enhanced Level 3 Radiometer Global Daily 9 km EASE-Grid Soil Moisture Version 1 datasets were used to compare with *in situ* observations and model ET globally for this study (O'Neill et al.*,* 2016a; O'Neill et al.*,* 2016b). Each dataset provides global

coverage every 3 days. The SMAP mission leveraged lessons from previous soil moisture observing satellites such as the Soil Moisture Observing System (SMOS) to incorporate radio frequency interference detection and mitigation to provide more continuous high quality global coverage of soil moisture (Mohammed et al., 2016; Oliva et al., 2012).

Soil moisture data are filtered for high-quality data which prevents using SMAP observations in urban areas, areas with high fractions of surface water, areas impacted by radio frequencies in the same microwave wavelengths as SMAP, and densely forested or highly productive agricultural regions where vegetation water content is high. The densely forested and agriculture regions that have high vegetation water content suffer from degraded surface soil moisture retrieval accuracy from space. However, many of these areas exist in perceived non-water limiting regions, which mitigates potential issues of data value for ET modeling globally.

3.3.5 Soil properties

The soil properties used in this study are from the SMAP L4RZ dataset and sourced from the Harmonized World Soil Database version 1.2.1 (HWSD1.21) and the State Soil Geographic project (STATSGO2). These data have been re-gridded to the EASE-2 grid to maintain consistency with the SMAP Level 2 retrieval algorithms (Das et al., 2013). For the 36-km runs, we use the nested mean of the 9-km soil properties. For in situ analysis we extract data from the United States Department of Agriculture soil survey database (see Appendix 2).

3.3.6 MERRA2: Net Radiation, Temperature, Vapor Pressure

Net radiation, air temperature, and vapor pressure data from MERRA2 reanalysis datasets M2T1NXLND and M2T1NXASM were used in this study. The MERRA2 reanalysis data provides 3-hourly hourly data at a 0.5^o latitude x 0.625^o longitude global grid. We take a daily average air

temperature, water vapor pressure, and net radiation, daytime maximum temperature and net radiation, and daytime minimum water vapor pressure and resample these data to the EASE grid resolutions (9-km and 36-km) to complete this study. Resampling meteorological data to finer spatial resolutions introduces uncertainty but is required due to the lack of continuous global datasets.

3.3.7 Ameriflux and COSMOS: *in situ* evaluation datasets

Eddy covariance observations of LE with coincident integrated measures of soil moisture are used for model development and evaluation (Table 3.2). Many EC towers that are part of these networks measure soil moisture with 1 to 4 dielectric sensors. With limited observations, the inherent variability in soil moisture adds observational uncertainty with potential to confound model formulation and parameterizations (Ryu and Famiglietti, 2005). Soil moisture variability

Table 3.2 Eddy covariance tower characteristics. COSMOS soil moisture observations are taken at or near each of the towers used for in situ forcing evaluation or both. The towers used for gridded forcing evaluation contain data after 4/2015 and are ordered based on the aridity index calculated as annual potential evapotranspiration divided by precipitation.

Site	Latitude (°N)	Longitude (°W)	PFT	Precip (mm)	Temp (°C)	Elevation (m)	Aridity Index	Tower Use	PI / Citation
US-SCs	33.734	-117.696	OSH	375.44	18.545	475	3.29	*in situ*	Goulden 2017
US-Whs	31.743	-110.052	OSH	338.54	17.135	1370	3.08	grid	Scott 2017
US-SCg	33.737	-117.695	GRA	378.83	18.565	470	2.81	*in situ*	Goulden 2017
US-SRM	31.821	-110.866	WSA	409.04	18.445	1120	2.71	grid	Scott 2017
US-Wkg	31.736	-109.941	GRA	380.01	16.51	1531	2.43	both	Scott 2017
US-SCc	33.610	-116.450	OSH	371.39	15.045	1280	2.18	*in situ*	Goulden 2017
US-Ton	38.431	-120.966	WSA	610.68	16.39	177	1.95	both	Baldocchi 2017
US-SRG	31.789	-110.828	GRA	513.79	17.935	1291	1.87	grid	Scott 2017
US-Var	38.407	-120.951	GRA	608.35	16.4	129	1.86	grid	Baldocchi 2017
US-Me2	44.452	-121.557	ENF	555	7.215	1253	1.54	*in situ*	Law 2017
US-CZ2	37.031	-119.256	MF	883.31	13.785	1160	1.29	*in situ*	Goulden 2017
US-UMB	45.559	-84.713	DBF	770.29	6.01	234	0.95	*in situ*	Gough et al., 2017
US-MOz	38.744	-92.200	DBF	1089.87	12.8	219.4	0.88	*in situ*	Wood et al,2017
US-MMS	39.323	-86.413	DBF	1148.53	12.02	275	0.83	*in situ*	Novick et al., 2017
US-CZ3	37.067	-119.195	ENF	1033.73	9.225	2014	0.82	*in situ*	Goulden 2017
US-Ro1	44.714	-93.089	CRO	823.02	7.535	260	0.81	*in situ*	Baker et al., 2017
US-PFa	45.945	-90.2723	MF	823	4.33	470	0.77	grid	Desai 2017
US-Ho1	45.204	-68.740	ENF	1143.42	5.84	60	0.63	*in situ*	Hollinger 2017
US-GLE	41.364	-106.239	ENF	953.06	0.245	3197	0.59	*in situ*	Massman 2017

increases with spatial extent and during the transition from saturated to dry conditions, conditions critical for the success of modeling soil water control on ET (Famiglietti et al., 2008). The COsmic-ray Soil Moisture Observing System (COSMOS) overcomes issues of spatial representativeness by using observations of cosmic-ray neutrons to measure soil moisture at integrated scales similar to the footprints of ET measurements from eddy covariance tower (Köhli et al., 2015; Zreda et al., 2012, 2008). Coincident integrated observations of soil moisture, ET, and meteorological data from EC towers facilitates model updates and evaluation.

We use observations from 14 EC sites that cover 7 plant functional types and varying climatic conditions. Half of the 14 sites are classified as water limited based on the Budyko Classification where the aridity index, calculated as the mean annual potential evapotranspiration divided by the mean annual precipitation, is greater than 1. We supplement the meteorological observations of FLUXNET and soil moisture observations from COSMOS with satellite observations of vegetation characteristics. Vegetation observations of CH and NDVI are extracted from satellite sources at 1-km resolution (http://daac.ornl.gov/MODIS/).

Table 3.2 provides the site locations, plant functional types, terrain, and climate sampled of the locations. We indicate whether the site was used to evaluate model updates using *in situ* evaluation, gridded forcing variables, or both in situ and gridded forcing variables. Gridded forcing assessments were performed for sites with LE observations since March 31, 2015, the start date of SMAP observations. Data availability from Ameriflux *in situ* observations during this time period and the SMAP recommended quality flag limit the number of sites used in this analysis. Numerous studies have examined the impact on eddy covariance tower footprint to gridded forcing data mismatches, but this type of analysis is outside of the scope of the current study (Amiro, 1998; Chen et al., 2009). Since eddy covariance observations of LE suffer from energy closure

61

imbalance, we force closure according to the Bowen Ratio (Foken et al., 2011; Twine et al., 2000). *In situ* LE evaluations were only performed for sites with high quality meteorology, soil moisture, and LE observations with at least 1 year of data.

3.4. Results

3.4.1 Model evaluation with in situ forcing

The *in situ* modeled LE from both PT-JPL and PT-JPL$_{SM}$ shows strong agreement with observations (Fig. 3.4, Table 3.3). Figure 3.4 compares one year of mid-day modeled LE with in situ observations from 14 EC towers. Sites are ordered from dry (top) to humid (bottom) based on the aridity index, a ratio of annual precipitation to PET. The PT-JPL$_{SM}$ model demonstrates greater skill than PT-JPL model at water limited sites but not at non-water limiting sites (Table 3.3). On average the PT-JPL$_{SM}$ shows a decrease in BIAS (PT-JPL: 70.7 Wm^{-2}, PT-JPL$_{SM}$: 22.7 Wm^{-2}), an increase in explanation of variance (PT-JPL: 0.59, PT-JPL$_{SM}$: 0.73), and a large decrease in RMSE (PT-JPL: 87.8 Wm^{-2}, PT-JPL$_{SM}$: 39.9 Wm^{-2}) when compared to the PT-JPL. Mean annual BIAS improves across all water limited sites and explanation of variance improves at all sites except for US-Wkg, a dry grassland in Arizona, where no change is observed. RMSE improves at all water limited sites with exception to US-Wkg, where a small increase is observed. The greatest overall statistical improvement was observed at US-SCs and US-SCg. Both of these sites have very dry conditions and a large fraction of LE comes from soil evaporation. Additionally, the years examined for these sites were part of the multi-year California drought, which exacerbated the importance of soil moisture to model LE. In addition to US-SCs and US-SCg, the largest improvements in explanation of variance occurred US-Ton, US-Me2, and US- CZ2. At the US-Ton, US-Me2, and US-CZ2 the PT-JPL$_{SM}$ model demonstrates improvements to model estimation of LE during the seasonal dry down. Lastly, at US-SCc and US-Wkg LE response to increases and

subsequent dry down of soil moisture from short interval precipitation events is best modeled by PT-JPL$_{SM}$.
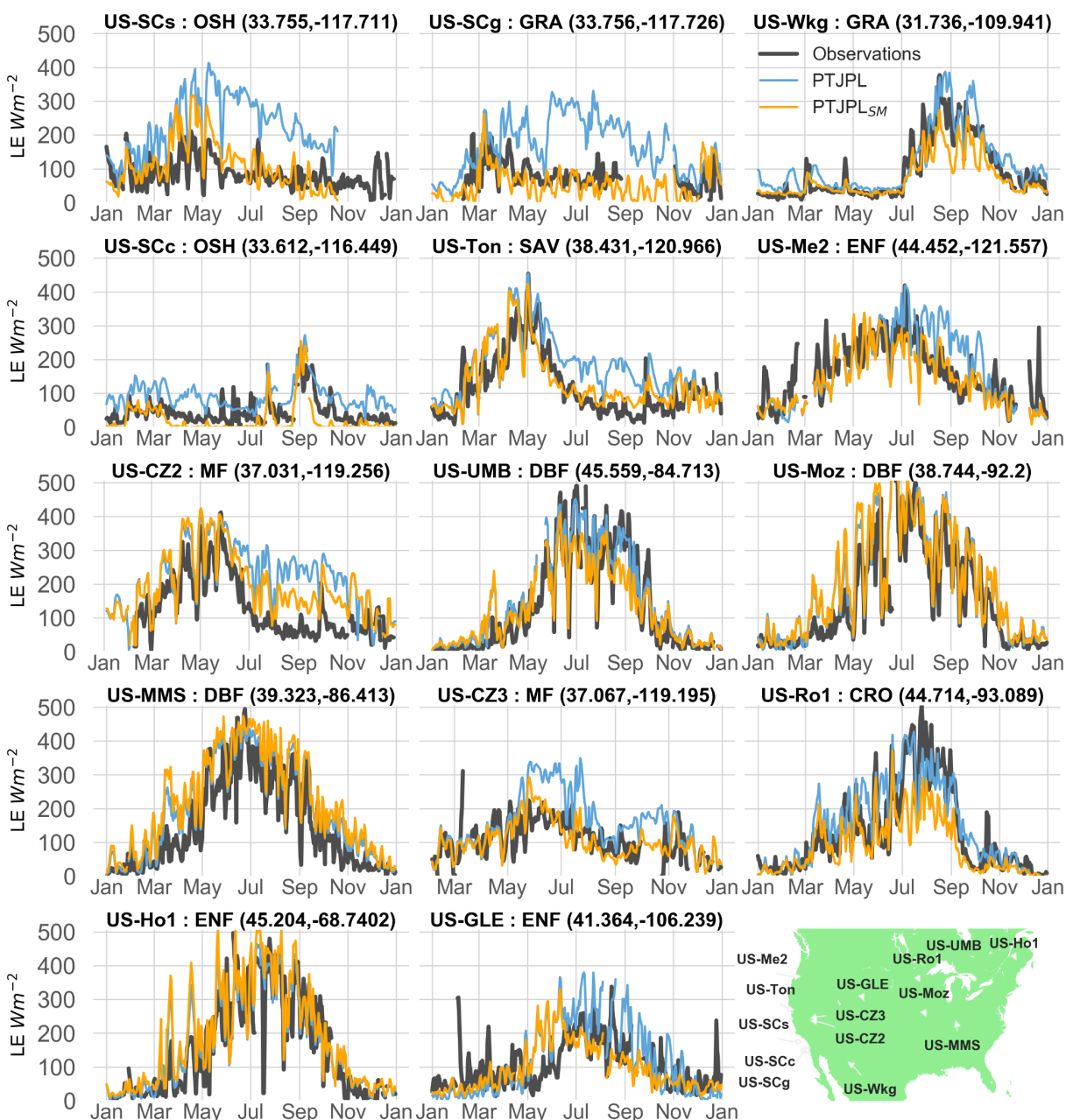

Figure 3.4 *In situ* model performance across 14 Ameriflux eddy covariance sites distributed across the US. The PT-JPLSM model is shown with orange and the original model is shown in blue. Sites are ordered based on their aridity index from top (more dry) to bottom (more wet) (Table 3.2). PT-JPLSM better estimates ET at more arid locations compared to PT-JPL.

Table 3.3 PT-JPL and PT-JPLSM model performance as indicated by BIAS, R^2, and RMSE.

Site	PT-JPL			PT-JPL$_{SM}$		
	BIAS	R^2	RMSE	BIAS	R^2	RMSE
US-SCs	137.8	0.37	145.1	32.9	0.55	46.9
US-SCg	105.5	0.01	137.9	8.2	0.41	33.7
US-Wkg	21.4	0.94	27.6	10.6	0.94	30.7
US-SCc	54.0	0.76	56.3	17.6	0.77	22.9
US-Ton	67.3	0.79	75.9	20.5	0.85	35.9
US-Me2	21.1	0.65	65.2	6.1	0.84	31.2
US-CZ2	87.9	0.63	106.6	63.1	0.77	77.7
US-UMB	29.4	0.90	50.3	15.5	0.80	62.0
US-Moz	43.3	0.97	49.4	49.2	0.96	56.3
US-MMS	52.5	0.97	57.6	71.5	0.95	77.1
US-CZ3	33.7	0.62	60.2	12.6	0.61	37.5
US-Ro1	19.1	0.90	40.0	38.4	0.89	64.3
US-Ho1	46.4	0.88	62.0	66.6	0.85	83.5
US-GLE	15.4	0.79	55.9	15.8	0.41	51.9
AI > 1	70.7	0.59	87.8	22.7	0.73	39.9
AI < 1	34.3	0.86	53.6	38.5	0.78	61.8
All Sites	52.5	0.73	70.7	30.6	0.76	50.8

For the non-water limited sites (US-UMB, US-Moz, US-MMS, US-CZ3, US-Ro1, US-Ho1, US-GLE) the original model outperforms PT-JPL$_{SM}$. On average, PT-JPL$_{SM}$ shows a marginal increase in BIAS (PT-JPL: 34.3 Wm^{-2}, PT-JPL$_{SM}$: 38.6 Wm^{-2}), decrease in explanation of variance (PT-JPL: 0.86, PT-JPL$_{SM}$ 0.78), and increase in RMSE (PT-JPL: 53.6 Wm^{-2}, PT-JPL$_{SM}$: 61.8 Wm^{-2}) when compared to PT-JPL. We posit transpiration from vegetation at these EC tower locations is more sensitive to atmospheric conditions and phenological changes. Therefore, the model re-formulation reduces sensitivity to atmospheric control on the exchange of water at the cost of introducing error at non-water limiting sites. The PT-JPL$_{SM}$ model only showed reduced errors at US-CZ3. This site was in the midst of a multi-year drought with the forest moving towards water-limiting conditions. The greatest decrease in model performance was recorded at the US-Ro1. At this site, PT-JPL$_{SM}$ underestimates peak LE during the growing season compared to observations. This large disparity is driven by observations and parameterization of the critical point at which soil properties soil moisture controls the rate of LE. Despite a small decrease in performance for non-water limiting sites, site-wide averages show PT-JPL$_{SM}$ better models LE.

We find site-wide average improvement in BIAS, R^2, and RMSE as a result of model improvements. Additionally, incorporating explicit soil moisture improved estimates of mean monthly LE (Fig. 3.5). The PT-JPL$_{SM}$ model shows greater explanation of variance (PT-JPL: 0.70, PT-JPL$_{SM}$: 0.75) and a slope (PT-JPL: 1.26, PT-JPL$_{SM}$: 1.05) closer to 1.0 compared to the PT-JPL model. Observations between 0 and 150 Wm^{-2} are better represented by the new model with a scatter closer to the 1:1 line from reduced overestimation in LE. The results of modeling LE using *in situ* forcing data demonstrates value in surface soil moisture observations for modeling ET. Next, we evaluate PT-JPL$_{SM}$ with gridded meteorology and surface soil moisture observations from SMAP with observations and compared to the original model.
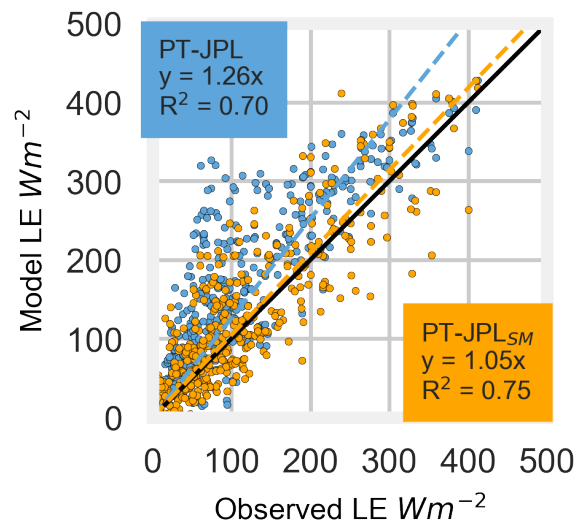
Figure 3.5 Monthly scatter plot of ET model without (blue) and with (orange) soil moisture integration.

3.4.2 Model evaluation of global SMAP soil moisture based PT-JPL$_{SM}$

The PT-JPL and PT-JPL$_{SM}$ algorithms were successfully applied globally using the SMAP SM_L3_P and SM_L3_P_E data. We evaluate the LE generated using the two SMAP soil moisture data products and at six EC validation sites that meet SMAP QA/QC for 2015. Figure 3.6 compares
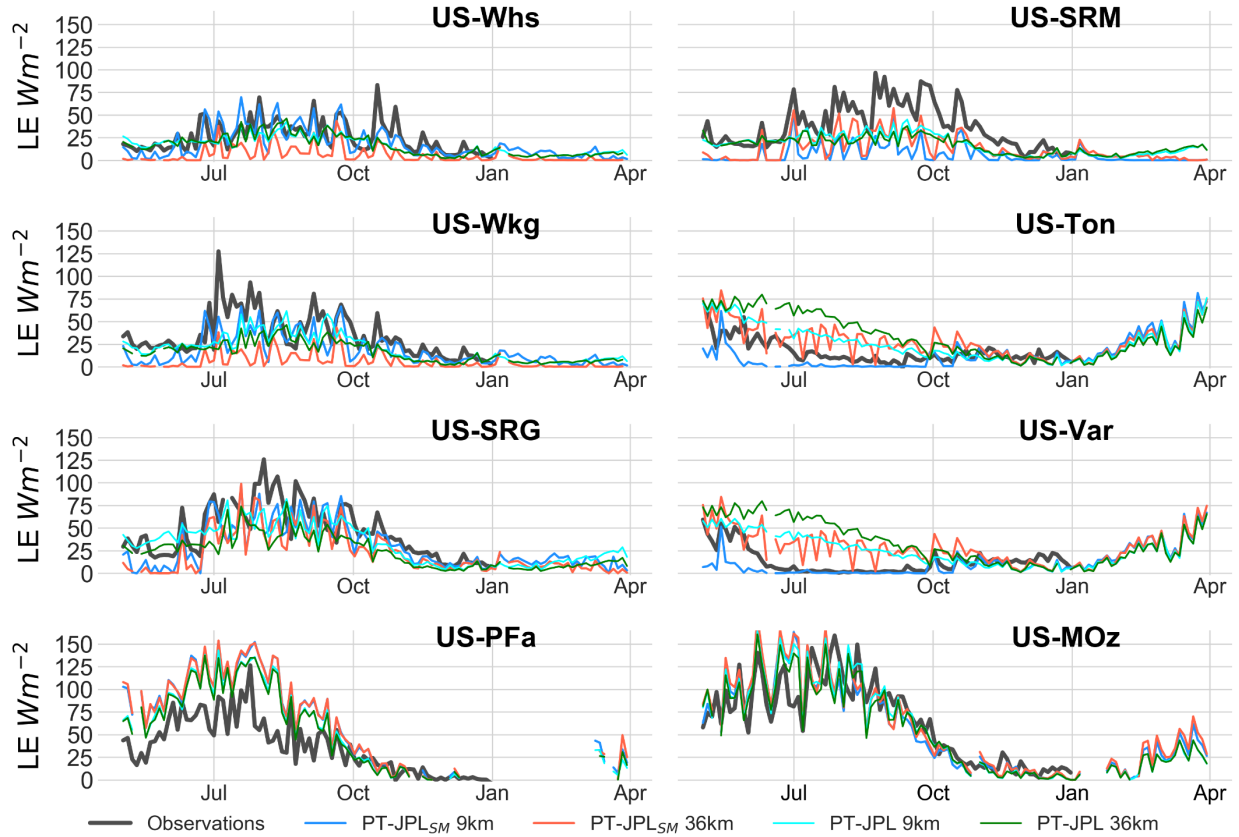
Figure 3.6 Model evaluation at 6 Ameriflux EC towers with gridded forcing data. A 3-day moving average is applied to all datasets. Observations are shown in black, ET modeled with PT-JPLSM using SMAP_L3_P_E shown in blue, and PT-JPLSM using SMAP_L3_P shown in red. The PT-JPL model is shown in cyan (9-km) and green (36-km).

the PT-JPL$_{SM}$ model using soil moisture from SM_L3_P (red) and SM_L3_P_E (blue) with the

PT-JPL model and the site observations from 4/1/2015 to 12/31/2016. Both the PT-JPL$_{SM}$ and PT-

JPL models capture the seasonal cycle of LE for each EC tower (Fig. 3.6). Similar to the *in situ*

analysis, PT-JPL$_{SM}$ demonstrates improved seasonal dry down and response to precipitation events

with both 9-km and 36-km products. For two sites that experience a Mediterranean climate (US-

Ton & US-Var), where winter precipitation precedes spring warm up, PT-JPL$_{SM}$ shows

improvements in modeled LE during seasonal dry downs when using SMAP data from May 2015

to October 2015, while the PT-JPL model overestimates LE. At US-Whs, US-Wkg, US-SRG, and

US-Var we find PT-JPL$_{SM}$ model evaluated at 9-km shows better agreement with observations

66

compared to the 36-km data. Despite soil moisture from SM_L3_P_E being influenced by L-band microwave radiation from a larger area, the observed soil moisture data are more centered on tower locations compared to the SM_L3_P. Poor model performance is observed for PT-JPL$_{SM}$ and PT-JPL at US-SRM. We posit that underestimation of modeled LE using SMAP data at the US-SRM might be due *in situ* LE observations not being representative over the heterogeneous area or as a result of soil properties controlling the point at which soil moisture limits ET. For the more humid sites, US-PFa and US-MOz, where soil water availability is non-limiting, we see similar performance for both PT-JPL$_{SM}$ and PT-JPL. Therefore, we find support for global inter-comparisons between old and new LE datasets created with and without soil moisture to demonstrate when and where soil water-limiting conditions create the greatest disparity for global LE quantification, how soil moisture impacts LE partitioning, and how LE modeled with soil moisture impacts inter-annual variability.

3.4.3 Changes in global ET patterns from SMAP data

We compare the PT-JPL and PT-JPL$_{SM}$ for 2016 modeled on the 9-km grid surface. Figure 3.7 shows ET from each model for 2016 and the difference between the models. Both PT-JPL and PT-JPL$_{SM}$ show expected global patterns of ET. ET is greatest in the tropics lowest at mid-latitudes. Model differences are evaluated spatially to determine where PT-JPL$_{SM}$ is greater than or less than the PT-JPL. PT-JPL$_{SM}$ modeled LE increases in Argentina, Northern and Eastern India, and Central America compared to PT-JPL. These regions are dominated by transpiration and we posit that shifting moisture stress from a 'greenness' index to soil moisture lessened phenological control on LE$_C$ (Fig. 3.8). EC observations were not available in these regions for this study to determine if the differences result in model improvement or degradation. The largest decreases
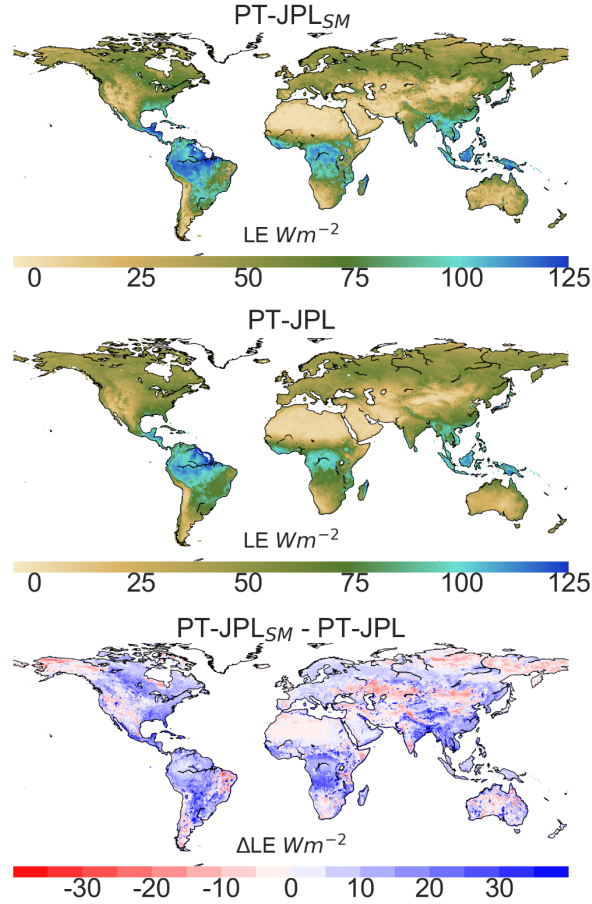
Figure 3.7 Mean annual PT-JPL$_{SM}$ ET for 2016 using SMAP_L3_P_E(top), mean annual PT-JPL ET for 2016 (middle) and PT-JPL$_{SM}$-PT-JPL difference (bottom). ET data are evaluated on the 9-km EASE 2.0 Grid.

from PT-JPL$_{SM}$ occur in regions, where soil evaporation makes up the largest fraction of ET. These areas include the Southwest United States and Northern Mexico, the East Coast of Brazil, Northern Africa, Southern Africa, The Horn of Africa, and Central Australia (Fig. 3.7). The largest decreases from PT-JPL$_{SM}$ occur in summer months for each respective region. These differences highlight the limited ability of f_{SM} to represent relative extractable water for daily ET modeling and highlight the value in calculating REW from using SMAP observations. Based on the results of the *in situ* evaluation (Section 3.4.1), we find support that the reduced soil evaporation better reflects true ET magnitudes for these regions. These lower ET estimates have implications for feedbacks between
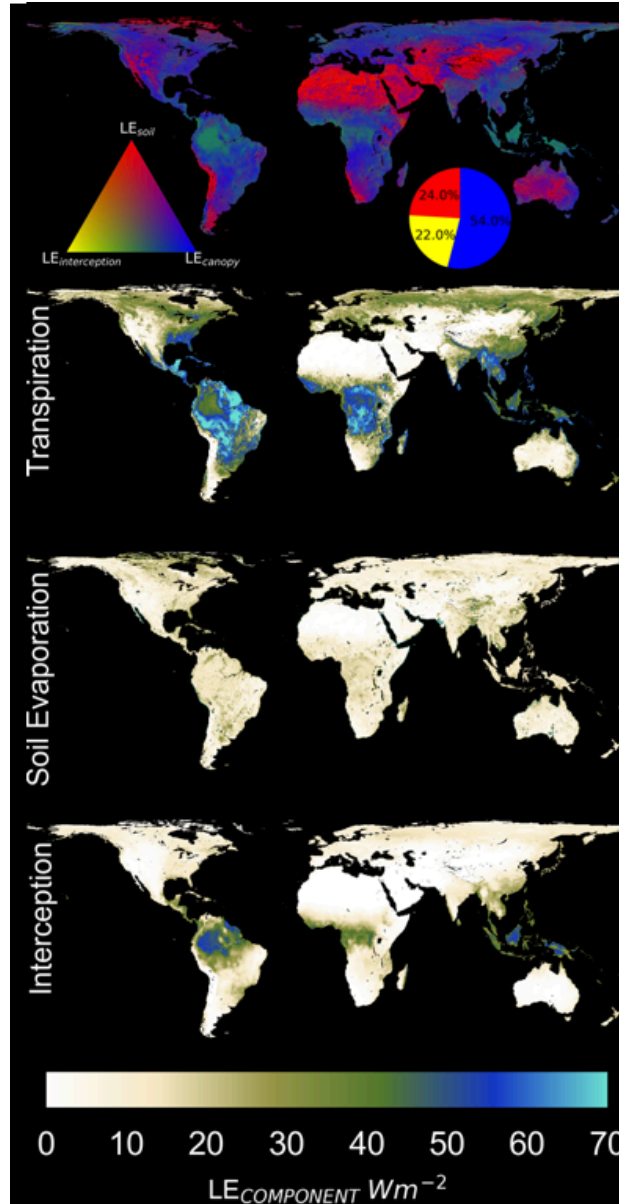
Figure 3.8 Evapotranspiration components as expressed as a percentage of total ET. Red indicates more soil evaporation, blue indicates more transpiration, yellow indicates more canopy interception evaporation. Below, total contribution to annual ET from transpiration, soil evaporation, and interception.

the water cycle and the carbon cycle. Arid and semi-arid regions have been identified as a major contributor to the inter-annual variability in CO_2 uptake and are key areas to better understand how strong coupling between land-atmosphere moisture exchange impacts carbon uptake (Levine et al., 2016; Diego G. Miralles et al., 2014; Miralles et al., 2012; Poulter et al., 2014). The lower

estimates provide a more accurate dataset to quantify water use efficiency and track impacts from drought and climate perturbations such as El Nino events.

3.5. Discussion

3.5.1 Inter-annual variability of ET for 2015-2017

Global LE datasets provide a valuable tool to quantify ecological responses to climate perturbations. We analyze inter-annual variability of LE for during the peak months of the 2015-2016 El Niño intensity and compare the data to the following year (Fig. 3.9). Previous studies have used LE to measure global hydrological response to El Niño. During El Nino years, global average negative LE anomalies occur relative to average LE (Diego G. Miralles et al., 2014). We find that PT-JPL$_{SM}$ mean global LE for the 2015-2016 El Nino was 2.2% less than the following year. Figure 7 shows the change in mean annual LE. For areas identified as having warmer or drier than average conditions during El Nino Years, such as Australia, Indonesia, Southeastern Africa, we find negative anomalies, e.g. lower LE when compared with the subsequent La Nina year (Vecchi and Wittenberg, 2010). In water-limited regions expected to experience more precipitation during El Nino, such as Argentina and the South West USA, we find positive LE anomalies. These subtle changes show the potential ability to distinguish explicit changes in LE as a result of soil water limitation and serve as a tool to identify vegetation stress and drought intensity. Overall, PT-JPL$_{SM}$ demonstrates the value of using soil moisture within LE models for capturing seasonal changes, especially in drier regions as soil moisture contributes to greater inter-annual variation.

70
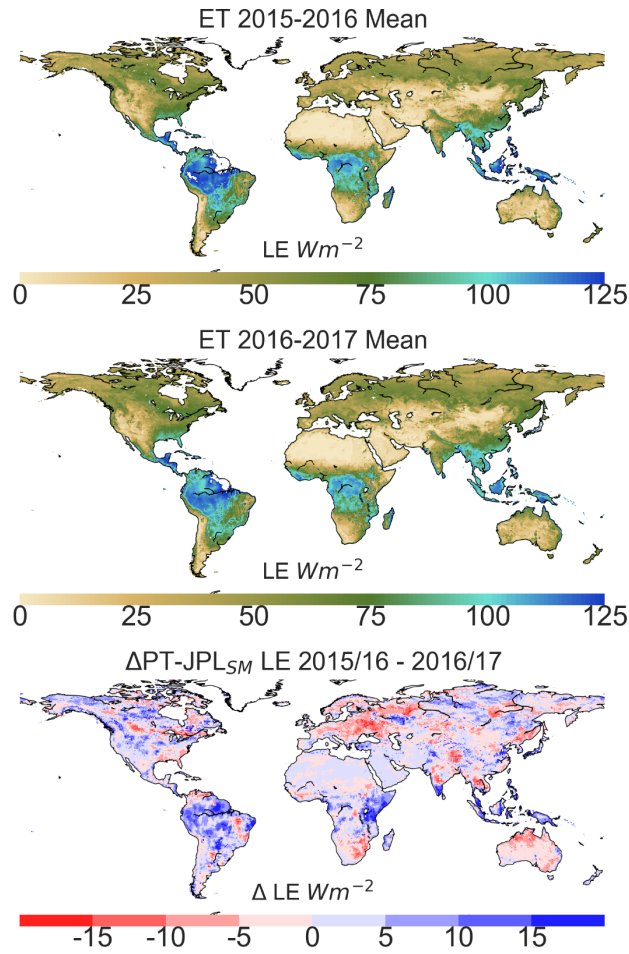
Figure 3.9 Inter-annual variation in PT-JPL$_{SM}$ LE. Top) 2015-2016 mean LE during El Nino. Middle) 2016-2017 mean LE. Bottom) Difference in LE.
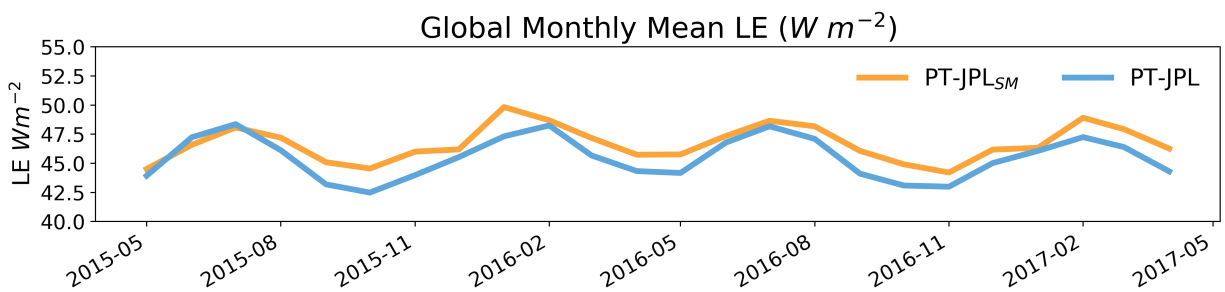
Figure 3.10 Monthly LE from May 2015 through April 2017. New modeled ET

3.5.2 ET Partitioning

Appropriate partitioning of ET into transpiration, canopy interception, and soil evaporation

is an overlooked area of ET science, yet greatly important to appropriately model these mechanistic responses to environmental conditions. Figure 3.8 shows the fraction of transpiration, interception, and soil evaporation globally and each components contribution to mean annual LE. The top map illustrates the percent contribution from each component and reveals expected global patterns of dominant ET components (e.g. soil evaporation is greatest in deserts, transpiration is dominant in forested regions, and interception is a large fraction in rainforests). Previous ET model partitioning estimates estimate transpiration to be between 25% and 65% (Wang and Dickinson, 2012) and recent remote sensing algorithms estimate transpiration to be as high as 80% of ET globally (Miralles et al., 2011a). We estimate soil evaporation, canopy transpiration, and evaporation from interception to be 24±1.6%, 54±1.6%, and 22±0.9% of total ET annually respectably. The PT-JPL$_{SM}$ fraction of soil evaporation and canopy interception are greater than similarly reported fractions from GLEAM model 7% and 11% respectively (Miralles et al., 2011a). Additionally, we calculate a lower fraction of canopy transpiration 54% compared to GLEAM (80%). The large disparity in soil evaporation and canopy transpiration can be traced to the radiation partitioning and the forcing datasets that influence R_N^C and R_N^S and the environmental stress imparted on the transpiration rate. We posit that the difference in canopy intercepted evaporation occurs as a result of the model's dependence on RH to calculate f_{WET}. Coarse resolution meteorological forcing resampled to finer spatial resolutions introduces larger fractions of wet surface area, especially in coastal and tropical regions where regions are more influenced by water vapor pressure. However, the difference in LE partitioning, we find the global patterns to be similar. These large differences warrant further investigation into appropriate partitioning methodology across biomes and climates. More ground-based observations of each component at scales relevant for modeling and remote-sensing comparison are needed to reign in this large uncertainty.

3.6. Conclusion

We present an update to the widely used PT-JPL ET model to address one of the model's main gaps: the implicit representation of soil water control. We incorporate soil moisture constraints on evaporation and transpiration. *In situ* analyses demonstrate improved ET estimates for dry regions and small changes in ET estimates for non-water limiting regions. We apply SMAP soil moisture observations to model ET globally using PT-JPL$_{SM}$. The PT-JPL$_{SM}$ model shows favorable comparisons to ground observations. The soil moisture constraint on evaporation resulted in lower global estimates of evaporation for water-limited regions. The updated PT-JPL$_{SM}$ ET model shows expected patterns of changes in ET for El-Nino and La Nina years. Based on the results in this study we conclude that modifications to the PT-JPL algorithm produce more realistic ET estimates globally. This dataset provides the opportunity to identify vegetation vulnerable to water limiting conditions and study the coupled carbon and water cycle response to such climate perturbations.

Chapter 4

Linking the carbon and water cycles from space: An evaluation of OCO-2 solar-induced-fluorescence, SMAP soil moisture, and the PT-JPL ET model to characterize vegetation stress

Adapted from:

4.1. Introduction

Plants link the carbon and water cycles through evapotranspiration (ET) and photosynthesis. When plant stomata open to ingest CO_2 for photosynthesis, water can more readily transpire into the atmosphere. This exchange of carbon and water is sensitive to a number of environmental variables including: soil water availability, temperature, atmospheric water vapor and carbon dioxide, canopy shading, and radiation (Field et al., 1995; Jarvis and Mcnaughton, 1986; Middleton et al., 2009; Monteith, 1965; H. L. Penman, 1948). Climate change is poised to intensify the energy cycle, speeding up the water cycle along with it as the atmospheric demand for water increases (Syed et al., 2010; Wild et al., 2008). When the atmospheric demand for water is high, plants avoid hydraulic failure by regulating the amount of water exiting leaves at the

74

expense of inhibiting carbon uptake. Over time, stress caused by this response limits plant growth and can even result in death by carbon starvation (McDowell, 2011). These distinct responses highlight the need to better understand how plants and ecosystems control water loss and carbon uptake (Fig 4.1). Despite its importance, to what extent plants respond to stressful conditions is an open science question (AghaKouchak et al., 2015; Dolman et al., 2014).

At the leaf scale, exchanges in carbon and water are regulated by stomatal control. Individual studies have explored how decreases in water availability and increases in the vapor pressure deficit between leaf and the overlying atmosphere impact carbon uptake and water loss (Biederman et al., 2016; Fisher et al., 2007; Schwalm et al., 2012; Wolf et al., 2016). These studies demonstrate regional responses to warmer and drier conditions result in large decreases in GPP and ET. Despite the foundational influence of the eddy covariance tower networks to develop process-level knowledge of the terrestrial biosphere, these networks are limited by the limited spatial coverage of the observations, non-continuous observational records, equipment and data quality standards, and underrepresenting the true global land cover distribution (Baldocchi et al., 2001).
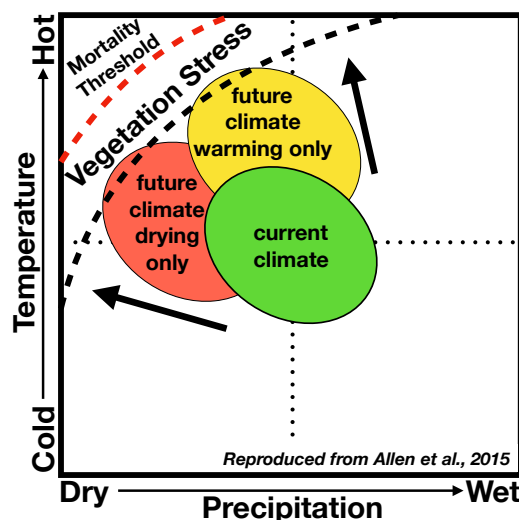
Figure 4.1 Conceptual diagram showing climate perturbation impacts on vegetation stress.

.

Satellite observations of water, carbon, and vegetation help bridge the gap by providing global coverage to monitor ecosystem-scale responses to sub-optimal environmental conditions. Drought indices based on 'greenness', moisture, and precipitation anomalies, have been used extensively to quantify anomalously dry conditions, but are removed from direct impacts of carbon and water fluxes in the earth system (AghaKouchak et al., 2015). Positive correlations between carbon flux anomalies and drought indices have been documented in arid regions while negative correlations were seen in boreal regions (Chen et al., 2013; Zhao et al., 2010), consistent with known global patterns of environmental constraints on plant productivity (Nemani et al., 2003). Recent studies have found evidence for expanding arid regions and a decrease in ET from soil moisture limitations (Greve and Seneviratne, 2015; Jung et al., 2010). Similar decreases in net primary production and regional GPP have also resulted from a limited moisture supply (Baldocchi et al., 2001; Zhao et al., 2010). However, plants regulate carbon uptake and water loss differently under stressful conditions resulting in different controls of ecosystem-scale water use efficiency (WUE) during drought (Yang et al., 2016). To date, the lack of application of independent simultaneously-flying high-fidelity carbon and water cycle observations has limited our ability to link and identify key differences between vegetation regulation on the carbon and water cycles.

Current simultaneous global observations of solar induced fluorescence (SIF), an indicator of GPP, from the Orbiting Carbon Observatory 2 (OCO-2), microwave radiation, an indicator of surface soil moisture, from the Soil Moisture Active Passive (SMAP) mission, and satellite driven ET models provide an opportunity to directly link observations of the carbon cycle and water cycle from space and characterize vegetation stress.

Global observations of OCO-2 SIF provide a state-of-the-art way to measure when and

where plants are taking in CO_2 from the atmosphere (Frankenberg et al., 2014). SIF provides a direct and distinct measure of photosynthetic activity independent of vegetation indices (Frankenberg et al., 2011; Guanter et al., 2014; Joiner et al., 2011; Lee et al., 2013). Compared to previous SIF-observing satellites such as GOME and GOSAT, OCO-2 has a finer spatial resolution along orbital tracks, records 25 times more soundings, resulting in lower observational error (Sun et al., 2017). SIF datasets provide an invaluable measurement to determine when and where plants photosynthesize at sub-optimal rates. To date, few studies have examined links between SIF and moisture availability or water stress (Lee et al., 2013; Sun et al., 2015).

The launch of SMAP in 2015 facilitates direct comparison of high-fidelity soil moisture observations with SIF. The SMAP mission provides the state-of the art observations validated to an accuracy of within 0.04 volumetric water content (VWC) at depths applicable for water and carbon cycle studies (Chan et al., 2016; Colliander et al., 2017; Entekhabi et al., 2010). The SMAP mission provides valuable information on the state of surface moisture availability.

Remote sensing (RS) ET models provide global observation-based estimates which support land surface model benchmarking, agricultural water use quantification, and drought identification (Fisher et al., 2017). Many RS models exit to compute ET with high accuracy, but few models are both globally applicable and capable of discerning mechanistic limitations on ET or GPP (Allen et al., 2007b; Fisher et al., 2008; Jung et al., 2011; Mu et al., 2011; Su, 2002). The Priestley-Taylor Jet Propulsion Laboratory (PT-JPL) ET model computes canopy transpiration independent of ET to facilitate a more direct comparison to SIF observations (Fisher et al., 2008).

Limited studies have linked carbon and water anomalies from space to explore how sub-optimal environmental conditions impact GPP and ET. Only Mu et al. (2013) applied ET data to create an evaporation-based stress index to compare with carbon uptake anomalies, but the study

77

derived GPP and ET from the same source variables subjecting the study to an inherent cross dependence of the vegetation indices observed from MODIS. Harnessing the current suite of carbon and water satellite observations has the potential to advance our understanding of how vegetation responds to hotter and drier conditions by evaluating changes from independent observational datasets. An important step forward is to use these independent observations to characterize the dominant controls of vegetation stress as seen by carbon and water cycle variables.

Despite the limited overlap between the OCO-2 and SMAP missions, the 2015-2016 El Niño serendipitously corresponds to the first full year of coincident SMAP and OCO-2 observations. During El Niño events, certain areas experience anomalously wet, dry, warm, or cold conditions relative to the respective climate norms for different parts of the globe under different seasons which causes distinct responses in the carbon cycle (Chen et al., 2017; Liu et al., 2017; Vecchi and Wittenberg, 2010). Therefore, we capitalize on this opportunity to characterize regional vegetation stress using changes in SIF from OCO-2 SIF, moisture availability from SMAP, and transpiration from PT-JPL. We evaluate reductions in SIF and transpiration during the 2015-2016 and characterize how environmental stress, as identified by hotter and drier conditions, impacts vegetation control on the carbon and water cycles in two semi-arid regions (Australia & Southern Africa) and two tropical regions (the Amazon & Maritime Continent). To our knowledge this is the first study to synchronize OCO-2 SIF observations with a satellite data driven ET model to characterize vegetation stress.

4.2. Data and Methods

4.2.1 OCO-2 SIF data

Observations from OCO-2 provide a new SIF dataset with a higher spatial resolution and

are less prone to cloud contamination than previous datasets resulting in stronger relationships to GPP and higher fidelity observations in the tropics and extra-tropics compared to other SIF datasets (Sun et al., 2017). SIF is directly related to GPP following the equations of Farquhar et al., (1980) and Monteith (1972) such that:

$$GPP = \frac{\Phi_{CO_2}}{\beta \Phi_F} SIF \tag{1}$$

where: Φ_{CO_2} is the light use efficiency of CO_2 assimilation, Φ_F is the SIF light use efficiency, and β is the probability of SIF photons escaping the canopy (Sun et al., 2017). Therefore, reductions in SIF provide a spatially explicit, independent measurement that is linearly related to GPP (Fig. 4.2) (Frankenberg et al., 2014).
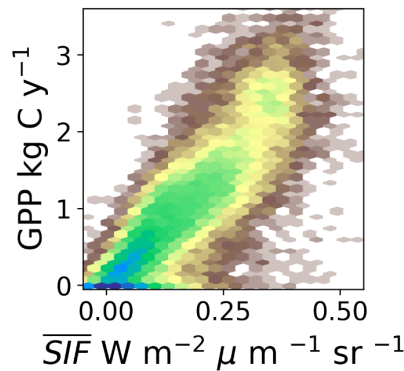
Figure 4.2 2015 mean annual OCO-2 SIF compared to 2015 mean annual MOD17 GPP. A linear relationship emerges from the global pattern of SIF and GPP.

The level 2 OCO-2 SIF data [W m^{-2} sr^{-1} μm^{-1}] are available daily at a spatial resolution of 1.3 x 2.25 km^2, with a 16-day global revisit from https://oco2.gesdisc.eosdis.nasa.gov/data/ (OCO-2 2015). Since we compare SIF data to a MODIS and SMAP-based ET model and SMAP soil moisture observations, we grid SIF observations on a 72-km equal-area-scalable (EASE) grid to support continuous global coverage (Brodzik et al., 2012). We follow the methodology of Sun et al., (2017) and combine the SIF$_{757}$ and SIF$_{771}$ to further reduce uncertainty when aggregating SIF

observations to monthly means on a global grid. We use data from 2014 and 2015 to evaluate SIF with GPP observations from the MOD17 product, and from April, 2015 to March, 2017, to compare SIF response to climate perturbations with the equivalent vegetation-controlled water cycle response, transpiration (Fig. 4.3).

4.2.2 PT-JPL: Priestley Taylor ET

We use the PT-JPL ET model with updates to include SMAP soil moisture to model transpiration (Fisher et al., 2008; Purdy et al., *in review* | Chapter 3). The PT-JPL model calculates each component of ET: soil evaporation, canopy transpiration, and interception evaporation. The model imposes eco-physiological stresses to reduce ET from the potential rate as calculated by the PT potential ET (PET) equation. Since this study focuses on vegetation control of the carbon cycle, water cycle, and surface energy budget, we only examine stresses imposed on canopy transpiration and interception calculated as:

$$T = f_G f_T f_{SM} \alpha \frac{\Delta}{\Delta + \gamma} R_{nc} \tag{2}$$

where T is the sum of canopy transpiration and interception, f_G is the green canopy fraction, f_T is a temperature scalar, f_{SM} is the soil moisture limitation imposed on transpiration, α is the Priestley-Taylor coefficient set to 1.26, Δ is the slope of change in water vapor pressure with temperature curve, γ is the psychrometric constant (0.666 kPa °C^{-1}), and R_{nc} is the radiation absorbed by the canopy.

The PT-JPL ET model has been identified as a high-performing in global RS ET model inter-comparison studies (Ershadi et al., 2014; McCabe et al., 2016; Vinukollu et al., 2011). Other physically-based models exist, but, complex parameterizations and numerous data requirements limit their performance with reduced bias compared to other ET models (Ershadi et al., 2014;

McCabe et al., 2016; Michel et al., 2016; Vinukollu et al., 2011). The transpiration dataset from PT-JPL exhibits strong seasonal changes with similar spatial patterns to OCO-2 SIF (Fig. 4.3).

4.2.3 SMAP datasets

SMAP products L3_SM_P Version 4 and L4_SM Version 3 facilitated this study. The L3_SM_P data provide global daily composites of surface soil moisture (VWC) at depth of ~5cm on a 36km EASE Grid 2.0 (O'Neill et al., 2016). Since the L3_SM_P dataset is limited in regions with dense canopies (e.g. tropical forests) we include the L4_SM data. The L4_SM data provide 3-hourly model assimilated root zone soil moisture (VWC) to depth of 1 m on a 9km EASE Grid 2.0 (Reichle et al., 2017). Each data product is aggregated to monthly mean values and gridded to the 72-km EASE grid. SMAP data products support modeling ET in addition to comparing changes in GPP or transpiration to soil moisture availability.

Compared to other global soil moisture datasets, SMAP observations provide moderate resolution (9-km to 36-km) and frequent revisit (3-day) microwave observations to support surface soil moisture observations at depths (5-cm) applicable for carbon and water cycle studies (Entekhabi et al., 2011). Other observations in this spectrum (~1.0-6.0 Ghz SMAP: 1.41 Ghz, SMOS: 1.4 Ghz, AMSR-E: ~6.0 Ghz) have provided continuous coverage to support soil moisture algorithms (Entekhabi et al., 2010; Kerr et al., 2016; Njoku et al., 2003). However, higher frequency observations are limited by soil penetrating depth, atmosphere attenuation, and demonstrate greater sensitivity to vegetation cover and surface roughness. Other, global satellites have been prone to interference from certain radio frequencies (Oliva et al., 2012). SMAP provides accurate global soil moisture observations validated to 0.04 m^3m^{-3} to help discern at what level soil moisture inhibits or exacerbates vegetation stress (Chan et al., 2016; Colliander et al., 2017a).
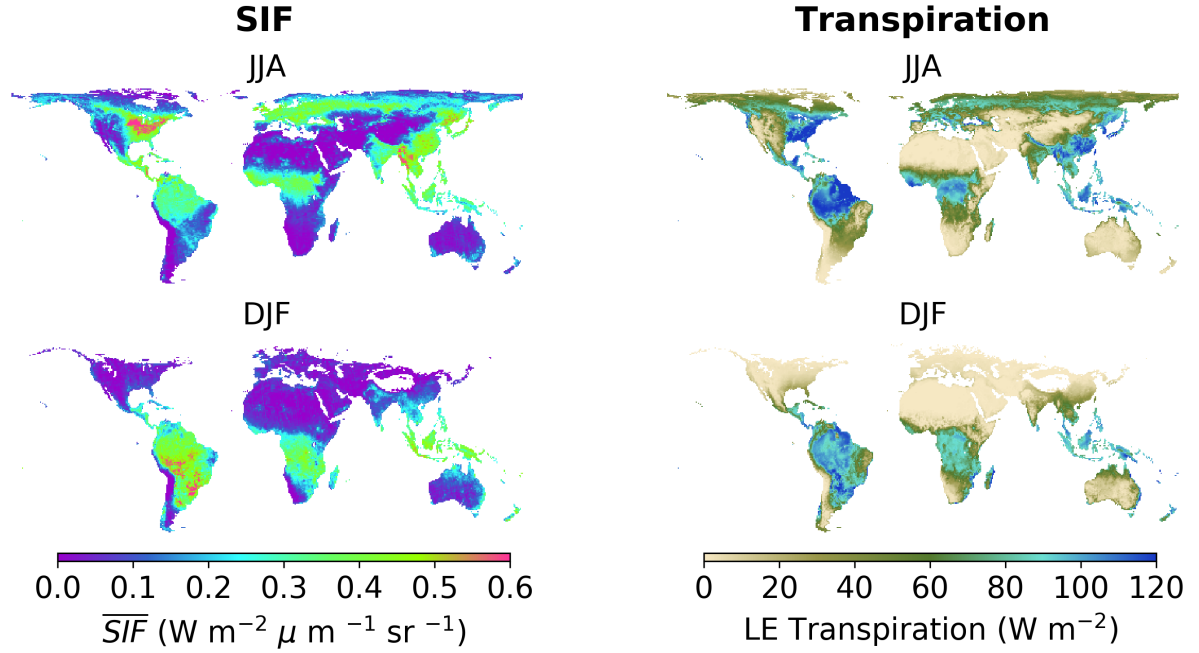
Figure 4.3 Left) Mean seasonal SIF for 2015-2017 for JJA (top) and DJF (bottom). Right) same as for SIF except for PT-JPL transpiration.

4.2.4 MERRA-2 Reanalysis Meteorological Data

Net radiation, air temperature, and vapor pressure data from MERRA-2 reanalysis datasets M2T1NXLND and M2T1NXASM were used in this study. The MERRA-2 reanalysis data provides 3-hourly hourly data at a 0.5° latitude x 0.625° longitude global grid. The datasets include M2T1NXLND for air temperature and water vapor pressure, and M2T1NXASM and net radiation. We use the maximum daily air temperature to characterize vegetation stress and use the vapor pressure and net radiation data to force the ET model.

4.2.5 GPCC Precipitation Data

The Global Precipitation Climatology Centre (GPCC) provides long-term monthly precipitation data (Schneider et al., 2016). We use the Version 7 monthly combined precipitation dataset constructed from station data (Schneider et al., 2015). Data are gridded at 1.0° degree grid

and resampled to the 72km EASE grid for this study.

4.2.6 CERES Radiation and Cloud Cover

The Clouds and Earth Radiant Energy System (CERES) dataset combines multiple satellite observations to provide global monthly observations of surface photosynthetically active radiation, surface shortwave radiation, and cloud cover datasets to support climate science. The CERES monthly SYN1deg dataset was available up to January, 2017 at the time of this study. We utilize both direct and diffuse short-wave radiation to supplement observations in SIF and transpiration. The CERES data are resampled to the 72km EASE grid similarly to the other supplementary datasets. All datasets are described in detail in Table 4.1.

Table 4.1 Characteristics of each dataset used in this analysis.

	Variable	Data Product	Spatial Resolution	Frequency	Time Span	Citation
OCO-2	SIF (757 & 771)	OCO-2 7 Lite	1.3 x 2.25 km	16-day	9/2014-present	(Frankenberg et al., 2014)
PT-JPL	Transpiration	NA	36 km	3-day	4/2015-present	(Purdy et al., *in review*)
SMAP	Soil Moisture Root Zone Soil Moisture	SM_L3_P SM_L4	36 km 9 km	3-day	4/2015-present	(Entekhabi et al., 2010)
MERRA2	Temperature	M2T1NXLND	0.5º x 0.625º	3-hourly	1/1980-Present	(Gelaro et al., 2017)
GPCC	Precipitation	Combined	1.0º x 1.0º	Monthly	1901-Present	(Schneider et al., 2011)
CERES	Radiation	SYN 1 deg	1.0º x 1.0º	Monthly	3/2000-Present	(Loeb et al., 2009)

4.2.6 Data analysis

Changes in SIF and transpiration from May 2015 - April 2016 and the next year, May 2016 - April 2017, are evaluated with changes in environmental conditions. The May 2015 – April 2016 time period has been identified as the months of peak intensity for the ENSO index. We capitalize on a period of expected patterns in precipitation and temperature deviations during the 2015-2016 El Niño to characterize 2-year changes in ET and GPP. Therefore, we supplement OCO-2, SMAP, and PT-JPL model with precipitation and temperature data with surface radiation satellite observations. We use long-term records of precipitation and temperature to normalize environmental perturbations in the context of climatological variability. The two-year deviations from each temperature or precipitation perturbation is measured as:

$$\sigma_{VAR} = \frac{\mu_{VAR_{15/16}} - \mu_{VAR_{16/17}}}{\sigma_{VAR_{clim}}} \tag{3}$$

where σ_{VAR} is the perturbation in precipitation or temperature, $\mu_{VAR_{15/16}}$ is the mean precipitation or temperature for the first year of record, $\mu_{VAR_{16/17}}$ is the mean of precipitation or temperature for the second year of record for this study, and $\sigma_{VAR_{clim}}$ is the 1980-2010 variability in mean annual precipitation or temperature. These normalized perturbations are used to evaluate the mean annual differences between SIF and transpiration.

We use a time series analysis to evaluate how quickly water-limiting conditions as seen from precipitation, soil moisture, and air temperature manifest into reductions of transpiration and GPP across four regions identified to experience warmer and drier conditions during 2015-2016 (Fig. 4.4). The comparison of these indicators of vegetation stress and identification of the dominant controls on them can be used to determine areas vulnerable to more variable rainfall, decreased cloud cover, persistent droughts, and extreme heat waves.
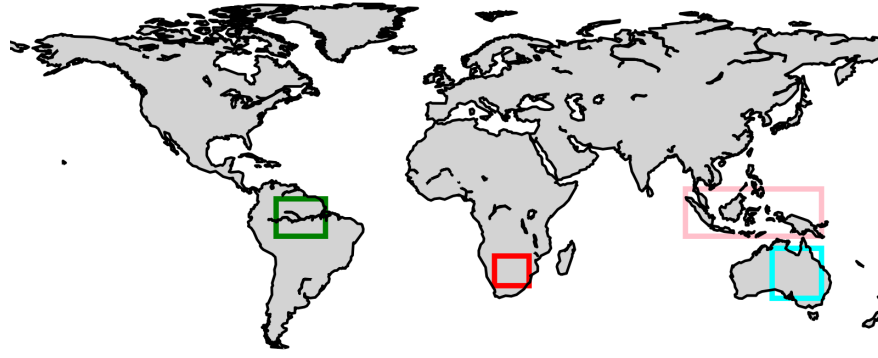
Figure 4.4 Focus areas used for this study. Amazon (Green), Southern Africa (red), Maritime Continent (pink), and Australia (cyan).

4.3. Results

4.3.1 Seasonal & Annual Differences in SIF and Transpiration

Figure 4.5 shows differences in mean annual SIF and transpiration. Red/blue areas indicate that the variable was lower/greater in 2015-2016 relative to 2016-2017. The largest concurrent decreases in SIF and transpiration occur in Southern Africa, Australia, northern South America, the Sahel, and Eastern Europe. Some of these regions, Southern Africa and Australia, coincide with expected decreases in precipitation and increased temperature during El Niño events. We explore these regions in depth as they experience simultaneous decreases in water availability and increases in temperature (e.g. moving towards vegetation stress as in Figure 4.1). Figure 4.5 also shows tropical forests have inverse carbon and water cycle responses to decreases in precipitation and increases in temperature. Specifically, we find decreases in SIF and increases in transpiration in the Amazon, the Congo, and the Maritime Continent. To characterize how perturbations in environmental conditions advance into changes in SIF and transpiration at sub-annual time-scales, we use four regions and supplement SIF and transpiration with precipitation, temperature, soil moisture and radiation datasets. The four focus regions were identified as places experiencing an

increase in temperature and a decrease in surface or root zone soil moisture, conditions expected to cause vegetation stress (Figure 4.4, Appendix Figure A.3.1).
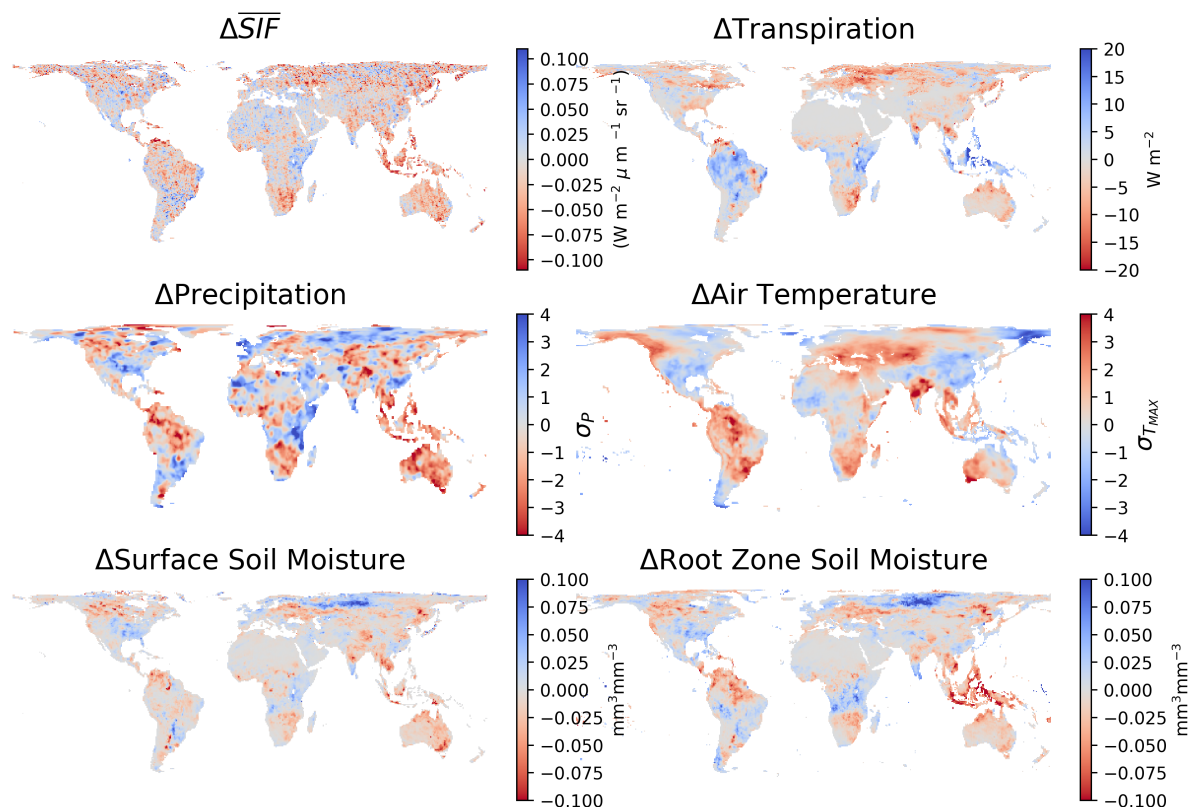
Figure 4.5 Mean annual changes in SIF (top left), transpiration (top right), precipitation (middle left), air temperature (middle right), surface soil moisture (bottom left), and root zone soil moisture (bottom right) for 2015-2016 minus 2016-2017. Precipitation and air temperature are represented as standardized deviations from 1980-2010 climatological variability. Red areas indicate reductions in SIF/transpiration, decreased water availability, or increased in temperature.

4.3.2 Characterization of Vegetation Stress

We analyze Southern Africa, Australia, the Amazon, and the Maritime Continent. Each region experiences decreases in water availability, as identified from SMAP and GPCC, and warmer temperatures over the 2015-2016 year compared to 2016-2017. These regions encompass two semi-arid water-limiting regions and two tropical radiation-limiting regions. Figure 4.6 shows how regional mean temporal changes in precipitation, temperature, and soil moisture evolve into

changes in SIF and transpiration. We find each area shows decreases in SIF, but only Australia and Southern Africa experience simultaneous decreases in transpiration. Interestingly, both the Amazon and the Maritime Continent experience greater transpiration rates during 2015-2016 relative to 2016-2017. The climate perturbation scatter plots show how short-term (mean-annual) changes in temperature and precipitation impact SIF and transpiration within each region (Figure 4.7).

In Australia, decreases in precipitation are evident for both December, January, and February and June, July, and August with smaller increases in temperature. SMAP observations during the same time period reveal the same seasonal differences in surface moisture availability. CERES observations indicate similar amounts of cloud cover by similar direct and diffuse radiation levels across this time span. We observe lower SIF and transpiration in 2016-2017 relative to 2015-2016 for both seasons coincident with less surface water availability. The climate scatter plots reveal this region to be impacted by both lower precipitation and changes in temperature across the focus region. SIF observations show larger decreases with decreases in precipitation and increases in temperature, evidenced by more intense red color moving from the center of the plot to the upper left corner. Changes in transpiration across the study region show similar scattered responses to the climate perturbation.

In Southern Africa, we find the largest changes in precipitation and temperature occur during December, January, and February. This period also experiences less surface and root zone soil moisture compared to the following year. These conditions result in large decreases in SIF and transpiration for 2015-2016 relative to the following year. The time series plot also shows how closely coupled the carbon and water cycles are in this region (Fig. 4.6). The climate scatter plots reveal decreases in SIF and transpiration co-occur with decreases in precipitation and increases in

temperature. The largest decreases in SIF occur under the hottest temperatures, while the largest

decreases in transpiration occur due to reduced water availability and increased temperature. For

the largest precipitation deficits, transpiration decreases more than SIF indicating ecosystem scale

increases in WUE. This response indicates plant resilience to sever shore term water limitations

(Fig. 4.7).

Juxtaposing the coupled carbon and water cycle responses in Australia and Southern

Africa, we find contrasting responses to warmer and drier conditions in the tropics. In the Amazon,

an increase in temperature and a decrease in precipitation is observed for June, July, and August.

These changes result in lower root-zone soil water availability, which persists through the austral

summer with higher temperatures (Fig. 4.6). During the decrease in precipitation, an increase in

direct short-wave radiation and decrease in diffuse short-wave radiation was observed as a result

of reduced cloud cover. With the increase in direct short-wave radiation an increase in transpiration

occurred. Similarly, as diffuse radiation decreased SIF also decreased. These responses continue

over the two-year timespan. The climate deviation scatter plots indicate transpiration is greater in

2015-2016 during warmer and drier conditions, while SIF decreases. The varied magnitude of

change across precipitation and temperature space signals that another factor, such as direct or

diffuse radiation, may be controlling the inter-annual changes such as direct or diffuse short-wave

radiation (Fig. 4.7).

In the Maritime Continent, we see similar responses from transpiration and SIF as observed

in the Amazon. Likewise the climate deviation scatter plots reveal a lack of control from

precipitation or climate perturbations (Fig. 4.7). However, the time-series plots indicate differences

in the seasonal response to SIF and transpiration. Compared to the Amazon, transpiration and SIF

both experience a biannual cycle. Transpiration increases during June, July and August, and
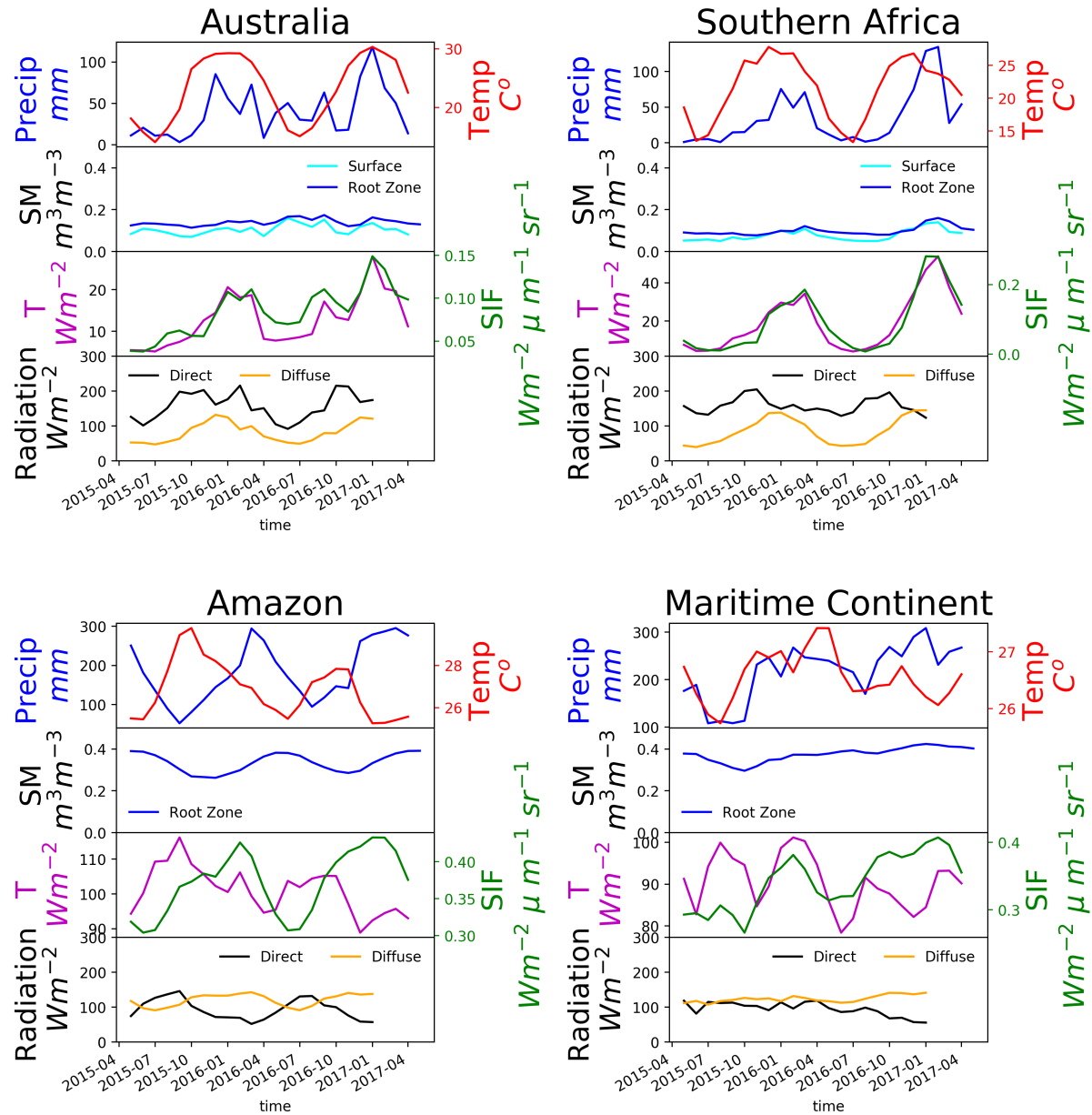
Figure 4.6 Monthly changes in precipitation and temperature, surface and root zone soil moisture, SIF and transpiration, and direct and diffuse short-wave radiation. These time series help characterization why changes in SIF and transpiration occur for each region. For example, the time series indicate Southern Africa SIF and transpiration are limited by lower precipitation and soil moisture during early in the first year. While in the Amazon, SIF is more closely linked to diffuse radiation and transpiration is linked to direct radiation.
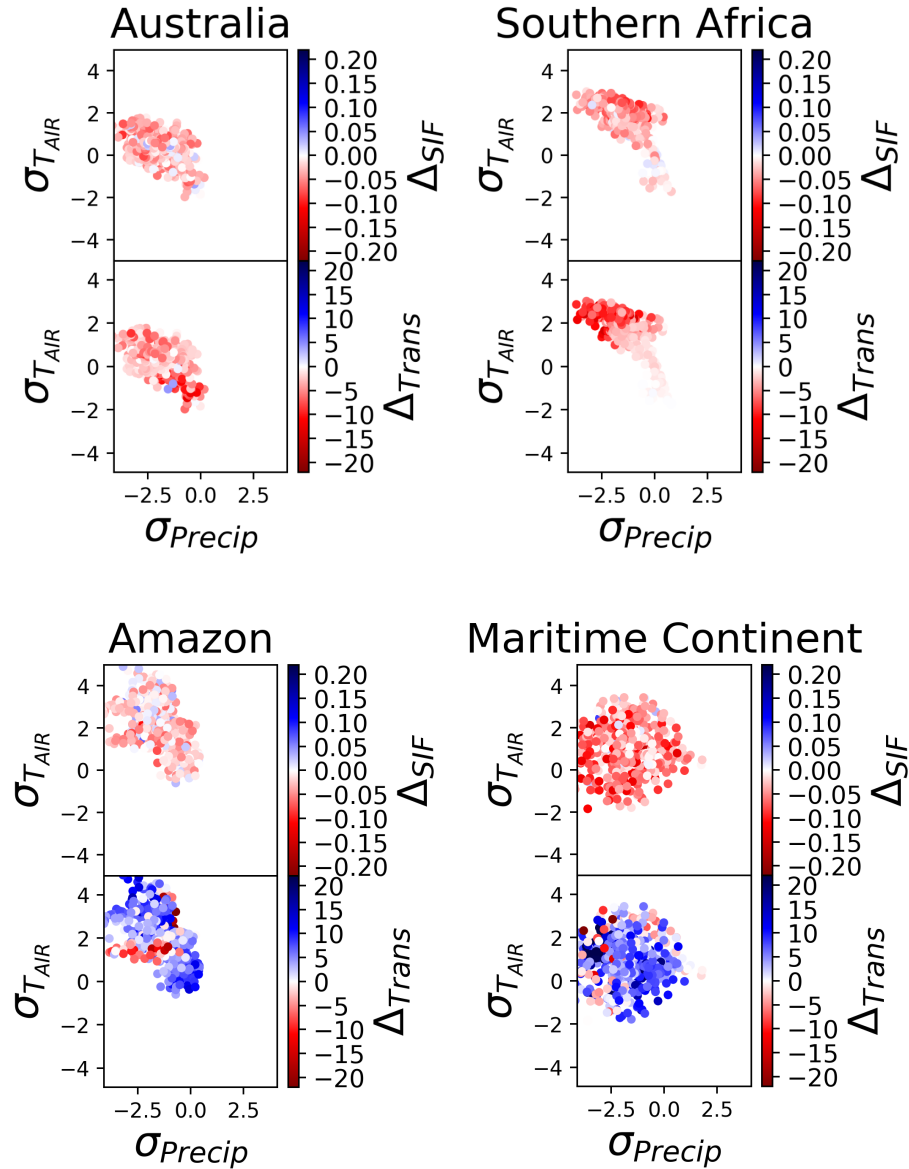
Figure 4.7 Climate scatter plots demonstrating how deviations in temperature (y-axis) and water availability (x-axis) impact SIF (top) and transpiration (bottom plot) for each study region. Study regions are ordered from clockwise top left) Australia, top right) Southern Africa, bottom left) Amazon, and bottom right) Maritime Continent.

December, January, and February (Fig 4.6). Though these cycles do not track changes in radiation

as closely as in the Amazon, the two-year change in SIF is mimicked by a 2-year increase in diffuse

radiation. Similarly, more transpiration during the El Niño year is reflected in the amount of direct

short-wave radiation. The differences observed in vegetation regulation of the carbon and water

cycles in semi-arid and tropical regions creates large uncertainty surrounding the ability of semi-arid and tropical ecosystems to mitigate increases in atmospheric CO_2.

4.4. Discussion

4.4.1 Vegetation response to regulate the carbon cycle and water cycle in tropics

Ecosystem carbon cycle and water cycle responses to warmer and drier conditions have been shown to vary across different climates to regulate water use efficiency (WUE) (Yang et al., 2016). In water limited regions, photosynthetic carbon uptake and ET have been shown to exhibit strong linear relationships (Biederman et al., 2016). Our results support a linear relationship between plant carbon uptake and water loss in water-limited regions and an increase in WUE for the hottest and driest perturbations (Fig. 4.8; Fig. S1). Precedent exits for less tightly coupled carbon and water cycles in tropical environments, as SIF and ET have been shown to exhibit a lagged relationship in the Amazon basin (Swann and Koven, 2017). However, managed drought experiments reveal declines in both GPP and ET (Fisher et al., 2007). Our analysis of tropical forest ecosystems, with deep roots (refs), reveals that a shift to warmer and drier conditions resulted in increased plant transpiration, reduced GPP, and a decrease in WUE. This response is observed in both the Amazon and the Maritime Continent and suggests other environmental factors restrict GPP and transpiration in the tropics.

We hypothesize that this difference in response to warmer and drier conditions may be due to changes of plant regulation on water transfer from soil or from changes in cloud cover and the subsequent shifts in the amount of direct to diffuse light. Previous studies have shown plants have a higher light use efficiency under diffuse light and that direct light increases ET rates but decreases carbon uptake (Doughty and Goulden, 2009; Gu et al., 2003; Mercado et al., 2009; Roderick et al.,

91

2001). Therefore, increased direct radiation has the potential to lower light use efficiency and/or induce leaf temperature limitations on the photosynthetic capacity of tropical forests. In the Amazon and the Maritime Continent changes in direct and diffuse short-wave radiation coincide with changes in transpiration and SIF respectively (Fig. 4.6). Greater amounts of direct radiation contribute to higher rates of transpiration during 2015-2016. Similarly, higher diffuse radiation coincides with more SIF.
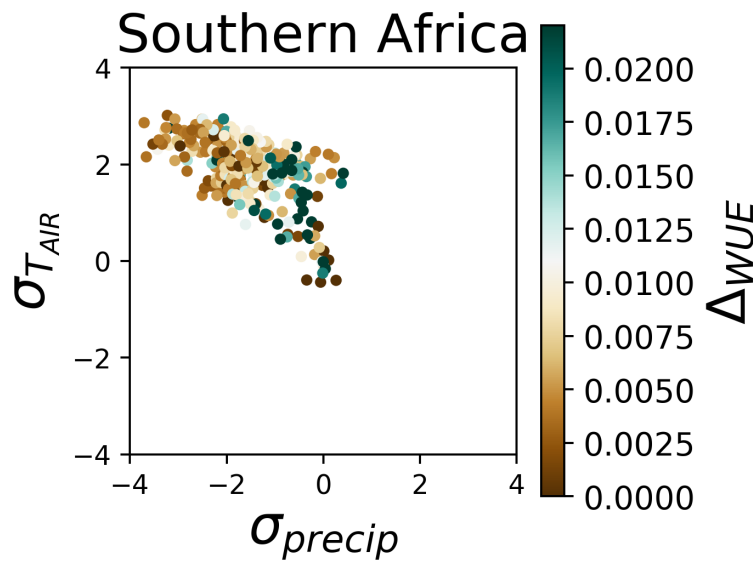
Figure 4.8 Change in WUE for the Southern Africa Study region. WUE increases for the hottest and driest perturbations in climate indicative of ecosystem resilience to drought. WUE is calculated as the change in SIF divided by the change in transpiration.

This distinct response in the tropics carries implications for long-term carbon and water cycle feedbacks on climate. Greater transpiration increases soil water drying rates with the potential to intensify tropical forest sensitivity to prolonged drought or abiotic stressors. Also, this feedback may ultimately lead to reduced carbon uptake during the dry season compared to wet season (Lee et al., 2013). Decreases in rainfall and intense droughts have directly impacted the carbon cycle in tropical forests through shrinkages in above-ground biomass and increases in forest fires in the Amazon (Aragão et al., 2007; O. L. Phillips et al., 2009). Future monitoring to inspect

how clouds and the amount of direct and diffuse radiation control vegetation regulation on carbon uptake and water loss could help constrain models. We find evidence showing that direct and diffuse short-wave radiation impact the carbon and water cycle responses differently. Ultimately, the capacity of the biosphere to buffer increases in atmospheric CO_2 depends on how ecosystems respond to changes in short term climate variability, long-term increases in temperature and decreases in water availability, and cloud cover impacts on quality of short-wave radiation.

4.4.2 Implications under future climate & rising CO_2

Under future climate, certain regions will experience warmer and drier conditions. These changes will ultimately contribute to more frequent occurrences of vegetation stress. Both semi-arid regions and tropical ecosystems play a large role in regulating atmospheric CO_2. Semi-arid control the inter-annual variability in GPP and are more susceptible to decreases in carbon uptake and transpiration during drought (Poulter et al., 2014; Zhang et al., 2016). However, the species compositions in these regions may be more resilient to changes in drought frequency compared to humid regions. We find evidence for such resilience in Southern Africa, where under the most stressful conditions WUE increased (Fig. 4.7). Tropical forests currently have the highest rates of carbon sequestration, but their future remains highly uncertain. Already, long term observations of above-ground biomass indicate the rate of carbon uptake by tropical forests in the Amazon has declined (Brienen et al., 2015). Increased vegetation stress events as a result of increases in drought frequency threatens to enhance forest dieback in certain tropical ecosystems. We find evidence for a large role in the quality of short-wave radiation regulating the water and carbon cycle responses. Further exploration into the extent of this control can help improve model projections. Additionally, how humans impact tropical forest ecosystems through deforestation and fire

management practices, especially during periods of vegetation stress, may ultimately determine how long tropical forests remain carbon sinks (Malhi et al., 2014; Oliveira et al., 2007).

While this study explores changes in SIF and transpiration as a result of short-term climate perturbations, long term changes from increases in atmospheric CO_2 may mitigate the impacts of drought through increases in WUE (Swann et al., 2016). Current remote sensing ET algorithms do not account for this impact and thus prevents predicting how increases in atmospheric CO_2 might impact vegetation's resilience. Despite the potential negative feedback form higher atmospheric CO_2, to what degree and how quickly tropical ecosystems respond to these changes is still largely uncertain. Future studies using other satellite datasets with longer records (e.g. GOSAT, GOME, SMOS, and AMSRE) may help elucidate how, where, and to what extent plants respond to these conditions.

4.5 Conclusion

Resolving the regions susceptible to climate-driven vegetation stress and the dominant climate controls helps piece together potential climate feedbacks from global water distribution to carbon uptake, and the intensification of the energy cycle. We used global observations from OCO-2, SMAP, CERES, and the PT-JPL ET model to identify and characterize vegetation stress as seen from carbon and water cycles. In water-limiting regions, we found the carbon cycle and water cycle to be closely linked and exhibit similar plant mediated responses to hotter and drier conditions. In tropical regions, we found contrasting responses with an increase in transpiration and a decrease in carbon uptake in the Amazon and the Maritime Continent. We find evidence that the amount of diffuse and direct short-wave radiation in these regions may play a critical role in the observed carbon and water cycle responses. Further exploration into the mechanistic reason behind this difference is warranted as potential feedbacks between the carbon and water cycle in

the tropical forests are of great importance to the climate system. Although we only evaluated 2-years of data to characterize vegetation stress in semi-arid and tropical regions, we found distinct and consistent responses to short-term climate perturbations across Australia and Southern Africa and the Amazon and the Maritime Continent. Extending the SIF and ET model records has the potential to help clarify our process-level understanding of the carbon uptake and water use and answer why tropical ecosystem respond differently to warmer and drier conditions.

Chapter 5

Conclusions

5.1 Summary of Results

As ET is a key climate variable linking the energy, water, and carbon cycles, my dissertation advanced ET science or applies ET data by exploring each sphere of its influence in the earth system. To accomplish this research, I have relied on globally distributed observations from the FLUXNET, Ameriflux, and COSMOS networks in addition to NASA satellite data and reanalysis datasets. My efforts contribute to the advancement of ET science through focusing on inter-algorithm uncertainty from the derivation of a small but important variable in the surface energy balance, the incorporation of new global observations of soil moisture into an ET model, and by linking the carbon and water cycles from space to quantify how vegetation responds to stressful conditions.

Chapter 2 focuses on the role of G in RS ET models and how to appropriately model G to reduce this uncertainty. Like many RS ET algorithms, G parameterizations were developed at one location and then applied broadly because of the need for global ET data. As a result, inter-ET-algorithm comparisons remain hindered by different methods to calculate G. In this chapter I discuss avenues to improve G models for both instantaneous and daily ET algorithm applications and present new optimized coefficients for the best G model. This study was accomplished using the largest ground-based comparison dataset ever assembled from FLUXNET. G models are often overlooked, and even completely ignored in some ET algorithms despite being a significant part to the surface energy budget. For example, G can account for as much as 50% of the incoming

radiation under sparse to bare canopy cover (Clothier et al., 1986). Additionally, G is especially important during peak hours of satellite overpasses and seasons where ET is often at its maximum (Kustas et al., 1993). Since all RS ET algorithms rely on varying versions of G models to calculate the available energy (R_{NET}-G) for soil evaporation, these different methods contribute to unnecessary uncertainty. Therefore, an opportunity existed to evaluate these G models across a wide range of observations and quantify G model variations contributions to ET uncertainty.

Multiple formulations exist to quantify G for both instantaneous and daily applications (Table 2.1). However, these models vary largely on which canopy characteristics influence G and to whether R_{NET} or LST are used to calculate G. Previous studies have limited G model inter-comparisons for irrigated agricultural applications (Cammelleri et al., 2009; Irmak et al., 2011). Chapter 2 expands G model evaluation beyond agricultural land cover and investigates how G models perform across a diverse set of land covers. I discuss what mechanisms govern G model performance, and how differences in G models propagate into ET uncertainty. Observations from 88 FLUXNET locations across 11 climates and 10 biomes from the La Thuile synthesis dataset were used to complete this study. Additionally, satellite and reanalysis datasets were used to quantify how differences in G models impact global ET uncertainty.

Results reveal that all instantaneous G models overestimate G when compared to observations. The lowest error statistics are achieved by the MOD16 G model, a model that applies LST. The highest explanation of variance is achieved by the GLEAM model, a model that uses canopy height and R_{NET} to calculate G. Despite the MOD16 G model showing strong performance for instantaneous modeling, we find models that calculate G from R_{NET} in conjunction with phenological changes of leaf cover density and canopy structure best fit observations. We reformulate the METRIC G model to account for tall and short canopies and found that this

structure best captures instantaneous mid-morning G. At daily time steps, we found different mechanisms control G.

For daily G models, a thermal diffusion model that utilizes LST best fit observations with an RMSE two times smaller than all other models. The GLEAM model, which includes canopy height, demonstrated the greatest explanation of variance but had poor error statistics. The thermal diffusion model quantifies G by accounting for the integrated changes in time derivative of LST and parameterizes the rate of energy exchange based on land cover. This method offers a strong structure to build upon because the model indirectly accounts for energy conservation. We find that when optimizing the thermal inertia parameter this model provides the best fit for daily G applications. More work needs to be done to optimize the thermal inertia globally by incorporating changes in canopy cover and soil wetness, two factors greatly influence the exchange of energy between the land surface and the atmosphere. The optimized thermal inertia parameters and the categorized METRIC parameters provide a robust means to minimize uncertainty of G across ET models.

The current uncertainty in ET from G models is significant for certain seasons and regions. Specifically, G uncertainty is greatest in the northern hemisphere during cooler months and is greater for regions with less vegetation cover. The present uncertainty from G limits diagnosing the impact from mechanistic model distinctions from inter-model comparison studies. For example, more uncertainty in RS ET models limits distinguishing the appropriate method to partition ET between soil evaporation and canopy transpiration. Chapter 2 demonstrates the importance of G in ET modeling and helps to address these types of limitations in ET model inter-comparisons. The presented optimized models and coefficients facilitate reducing ET uncertainty

in order to tackle other limitations in current RS ET algorithms such as representing limitations from soil moisture.

Many RS models exist that quantify ET across a range of spatial scales for different applications, however many models do not account for soil moisture and instead rely on atmospheric variables, LST, and vegetation indices when quantifying ET. Since water from the surface soil layers is the source for much of ET, including soil moisture observations should improve ET models. However, limitations such as accurately observing soil moisture at relevant scales for model development and global application prevented integration into RS ET algorithms (Dirmeyer et al., 2006). With the recent successful launch of the SMAP satellite, a new opportunity exists to incorporate accurate soil moisture observations into an RS ET algorithm. In Chapter 3, I use *in situ* observations of soil moisture and ET to formulate and incorporate soil moisture into an ET algorithm. Then I apply the new model with soil moisture observations from SMAP to produce a new global ET dataset.

Water availability regulates ET rates for certain regions globally. While prognostic models provide direct links to introduce soil moisture limitations on ET, LSMs are overly sensitive to soil moisture deficits and inter-model transpiration comparisons reveal a wide range transpiration fractions indicating different sensitivities to soil water availability (Figure 1.1) (Wang and Dickinson, 2012). This disparity presents an opportunity to incorporate soil moisture into a RS ET model by prescribing to what degree soil water availability limits soil evaporation and canopy transpiration. Chapter 3 addresses this limitation by capitalizing on integrated observations of soil moisture from COSMOS and ET from Ameriflux at similar spatial and temporal scales to test and advance current ET algorithms.

Results show that the new soil moisture constraints in the PT-JPL ET model reduce error. An *in situ* evaluation showed changes to soil evaporation and canopy transpiration improved modeled ET most in water limited regions identified by the aridity index. Soil evaporation was improved by limiting evaporation by the relative extractable water and canopy transpiration was improved by relating plant soil moisture sensitivity to canopy height, soil properties, and the atmospheric demand for water. Previously, the PT-JPL model overestimated ET in regions where seasonal dry downs occur due to its reliance on atmospheric variables and canopy changes to infer water limitations. Atmospheric observable variables such as temperature and humidity can only be used to infer surface conditions at certain spatial and temporal resolutions and break down when moving towards finer spatial and higher temporal frequencies. Likewise, vegetation response to water limitation, as observed from satellite, can lag the time when soil moisture limits canopy transpiration.

This research, for the first time, provided global ET dataset with soil moisture limitations from SMAP. Global ET estimates generated with PT-JPL$_{SM}$, the new model, indicate ET is lower than previously estimated for water limited regions. Analyzing gridded ET data at 8 eddy covariance towers revealed that the new PT-JPL$_{SM}$ shows strong agreement and improvement in representing seasonal dry downs for water-limited sites. Similar to other ET studies on El Niño, ET from PT-JPL$_{SM}$ global mean LE was lower during 2015-2016 compared to 2016-2017 and spatial patterns of ET reveal expected responses to changes in water availability and temperature (D G Miralles et al., 2014). As the need for ET data and other hydrologic data moves towards higher spatio-temporal resolutions, providing a global ET dataset with 3-day coverage helps to constrain land surface models and address other knowledge gaps in the earth system. By linking independent carbon cycle observations with water cycle observations from this new ET dataset,

we can begin to characterize how plants respond to regulate carbon uptake and water loss under changes in water availability and temperature (Fisher et al., 2017).

Vegetation regulation of the carbon and water cycle carries large consequences for the earth system. The coupled carbon and water cycle responses, or how plants respond to regulate carbon uptake and water loss, contributes in a large way to uncertainty in climate projections (Friedlingstein et al., 2006, 2003; Gregory et al., 2009). Under a warming climate and potentially accelerating water cycle, understanding how plants respond to stressful conditions and avoid mortality can help reduce this uncertainty and also support forestry management. Previous studies have linked changes in GPP to drought indices, but have relied on ET datasets derived from the same satellite observations (Mu et al., 2013). By combining independent observations of the water cycle with soil moisture from SMAP, ET from PT-JPL$_{SM}$, and the carbon cycle via SIF from OCO-2 I diagnose and characterize vegetation response to sub-optimal environmental conditions. In Chapter 4, vegetation response to hotter and drier conditions is evaluated across four regions in two climate zones using deviations of temperature and precipitation to characterize changes in transpiration and SIF.

The short-term (2-year) climate perturbations and the subsequent impacts on ET and SIF show differing responses between tropical and water-limited regions. A time series analysis reveals regional mean patterns have contrasting responses. For water limited regions, regional averages over Southern Africa and Australia show a closely coupled carbon and water cycle response. In both of these regions changes in transpiration and SIF are of similar relative magnitude and both SIF and transpiration decrease under hotter and drier conditions. A contrasting response is observed over tropical regions. In the Amazon and the Maritime Continent the carbon and water cycles are not tightly coupled and a decrease in SIF is observed while transpiration increases.

101

Climate scatter plots show similar patterns for both regions. For Southern Africa we find evidence of ecosystem scale responses of water conservation under the hottest and driest conditions (Fig. 4.8). In Australia, decreases in transpiration and SIF show less consistency across climate space, but overall decreases in both SIF and transpiration for warmer and drier climate deviations. In the tropics, a varied response over the Amazon and the Maritime Continent indicates that other variables may be needed to diagnose changes in SIF and transpiration across climate space. Despite the scatter, both regions show a consistent response in overall decreases in SIF and an increase in transpiration under warmer and drier climate deviations. The differences in vegetation response to warmer and drier conditions reveals secondary impacts from cloud cover may explain inter-annual changes in transpiration and SIF. Our analysis shows support for previous theories about reduced light-use-efficiency under more direct short-wave radiation (Roderick et al., 2001) and lower carbon uptake in response to increased amounts of short-wave radiation (Doughty and Goulden, 2009; Taylor et al., 2017). Figure 4.6 shows that SIF more closely corresponds to changes in diffuse light and is reduced during periods of high amounts of direct radiation in the tropics. The distinct responses over each region shows the value of using independent datasets, such as ET from MODIS and SMAP, and SIF from OCO-2, to characterize vegetation control on water and carbon cycle responses to hotter and drier conditions.

Chapter 4 is the first study to link the carbon and water cycles from space using data from MODIS, SMAP, and OCO-2. My findings help to fill a large knowledge gap in the earth system related to the coupled carbon and water cycle response. The results from this study demonstrate the opportunity to apply remotely sensed ET datasets through the lens of coupled carbon, water, and energy cycles. Future directions of this work, should focus on coupled response using *in situ* observations from each region over the same time frame to test the new hypotheses generated from

this study. Specifically, eddy covariance observations in these regions may help elucidate how vegetation control at higher-frequencies impacts the carbon and water cycle and can validate the inter-annual changes in GPP and transpiration. Due to data availability constraints, this study only focuses on a two-year window. However, to better understand and characterize vegetation response to stress, a long-term evaluation has the potential to better constrain model predictions. I plan to extend SIF and transpiration records to analyze how longer-term perturbations can help to shape the state-of-the-art understanding of at what point temperature and water availability deviations cause stress and/or vegetation mortality. Continued observational records from SMAP, OCO-2, and MODIS will enable opportunity. Furthermore, leveraging observations from GOSAT, GOME, and SMOS will facilitate an extended record of independent carbon and water cycle observations.

Overall, the work during my dissertation touched on all the spheres ET interacts with in the Earth System. In Chapter 2 I use the energy cycle to evaluate the roll of G in ET uncertainty and discuss this variables importance for ET modeling. Chapter 3 focuses on the water cycle and the relationship between soil moisture and ET. I use soil moisture from SMAP to impose water availability constraints in the PT-JPL ET algorithm and generate a new global ET dataset. Lastly, in Chapter 4 I link the carbon and water cycles from space using transpiration and SIF. In this study, I analyze regional coupling between the carbon and water cycles in responses to changes in soil moisture, precipitation, and temperature. Additionally, I characterize how vegetation responds to warmer and drier conditions to regulate the carbon and water cycles. I hope to continue research in ET, global hydrology, and earth system science. As I demonstrated in the previous chapters, ET is a variable not just to study water use, but a key climate variable with endless opportunities

to improve the present understanding of the earth system. Satellite-based observations of ET provide a unique measure to continue to explore and contribute to advancing earth system science.

5.2 Future Directions

Satellite-based ET science has contributed to advancing earth science. Specifically, RS ET datasets have helped benchmark modeling datasets, close the global water cycle from space, and measure the role of human intervention on the climate system through land and water management (Castle et al., 2016; Mueller et al., 2013; Rodell et al., 2015). Despite the mature nature of many RS ET algorithms, many areas exist to continue to fill knowledge gaps in the earth system with ET data. Fisher et al. (2017) list numerous topics related to ET with room for improvement including but not limited to: ET partitioning (Chapter 2 & 3), quantifying species and ecosystem water use and needs (Chapter 3), measuring vegetation response to stress (Chapter 4), land-atmosphere coupling, and linking the energy, carbon, and water cycles from space (Chapter 4). The work presented in this dissertation touches on some the limitations, but opportunity still exists to close these gaps and address limitations with ET observations, models, and analyses. Primarily, extended observational datasets in addition to new observations, further model development, and synergistic carbon and water cycle analyses are all still necessary to eliminate these gaps in knowledge.

5.2.1 Observational datasets

Both extended observational records and new observations will be needed to further improve ET-related science. Extended records of observations are needed for climate scale (10+years) studies. Such data will benefit identification of ecosystem and agricultural water use and need, in addition to identifying the impacts from shifts in climate on vegetation stress. Longer records from SMAP and MODIS will enable multi-year analyses to determine how much water

ecosystems use. These extended records will help identify at what point soil water availability limits ET and plant productivity. Chapter 3 and Chapter 4 point out how the current limited records of observations from SMAP and OCO-2 hinder applications to support drought identification and quantify how shifts in climate will impact the carbon and water cycles. Both MODIS and SMAP have met their planned mission lifetimes, however continued operational global coverage is expected and would facilitate this such analyses. Additionally, upcoming potential satellite missions such as Hyperspectral Infrared Imager (HyspIRI) will help to extend long-term ET datasets from MODIS at climate relevant scales (Lee et al., 2015). Such observations will fill the need for finer spatial resolution datasets and enable more applications of ET data (Allen et al., 2015). Global satellite observations have greatly advanced the scientific communities understanding of ET, however since satellite overpasses occur during mid-morning the scientific community has a limited understanding of the diurnal cycle of ET.

New observations from ECOSTRESS will provide the opportunity to study diurnal changes of ET. Varied satellite overpass times due to the space station's orbit will provide an opportunity to track how plants respond to hot days by measuring when plants shut down stomata to limit water loss. Over time, these measurements are needed to quantify how much plants transpire across the day and distinguish whether natural ecosystems and managed land respond differently to drought. Despite the fine spatial resolution data and varied temporal sampling, ECOSTRESS will not provide global coverage and the limited length of the missions will not support climate scale studies. Therefore, continued ground monitoring networks are required fill the void. The bulk of this dissertation focuses on space-based observations to support global analyses and modeling. However, both Chapter 2 and Chapter 3 demonstrate the value of *in situ* observations of energy and water fluxes to support model evaluation and refinement.

New observational datasets will be required to address ET partitioning. Currently, networks of eddy covariance provide long-term continuous records of ET (Baldocchi et al., 2001) and emerging networks such as SAPFLUXNET (Poyatos et al., 2016) will aid overcoming the challenge of how much soil evaporation, canopy transpiration, and canopy evaporation contributes to ET. Sapflow studies are often geared towards species-level analyses. SAPFLUXNET will provide stand scale observations more relevant in scale to support RS ET algorithms and LSM's. Additional observations of canopy interception and evaporation, especially in non-forested regions, will be needed to complete this task. These new observations come at an exciting time in RS ET algorithm development to evaluate our process level understanding of soil evaporation and canopy transpiration. To date limited evaluations have attempted to disentangle the appropriate means to partition ET (Talsma et al., *in review*). Leveraging current eddy covariance towers with dense networks of sapflow sensors and canopy storage observations creates a great opportunity to reduce the uncertainty in ET partitioning and guide model refinement. However, care should be taken to ensure sampling is distributed to assist both global applications. By doing this, observations will support quantifying biome and plant functional type variability while not overlooking representing the global distribution of climate zones and plant functional types. Other observational techniques have focused on isotopes to partition the water cycle and have been successful at identifying the source of canopy transpired water (Evaristo et al., 2015; McDonnell, 2017). Isotopes provide an under-utilized means to address such issues as ET partitioning and may prove fruitful in the coming years to provide a dataset independent from FLUXNET and SAPFLUXNET to diagnose RS ET modeling (McDonnell, 2017). Both efforts could go a long way towards refining RS ET algorithms and LSM development.

5.2.2 Remote sensing ET model refinement

Continued model development is needed to appropriately address ET partitioning and how plants respond to stressful conditions to regulate carbon uptake and water loss. Chapter 2 argues for synergistic efforts to minimize model differences in order to better evaluate mechanistic model response to environmental conditions. Currently, ET partitioning between soil evaporation, canopy transpiration and canopy interception is one area that shows large disagreement that can benefit from the work in Chapter 2. Chapter 3 provides global estimates of partitioning fractions (24% soil evaporation, 54% canopy transpiration, and 22% canopy evaporation) which fit within the range of model estimates (25% to 64 % canopy transpiration), but vary greatly compared to another ET dataset (7% soil evaporation, 80% canopy transpiration, 7% canopy interception) (Miralles et al., 2011b; Wang and Dickinson, 2012). Current analysis frameworks exist to apply ecosystem scale experiments to evaluate processes within vegetation models, but these types of studies have yet to be applied to RS ET algorithms with regard to partitioning ET (Medlyn et al., 2015). With new observation datasets becoming available from SAPFLUXNET, RS ET datasets and their partitioned components need to be scrutinized. Analyses should specifically focus on radiation partitioning methods between the canopy and soil surface, and the equations governing soil evaporation, canopy transpiration, and canopy interception. Improving partitioning will further reduce uncertainty in studies exploring how plants respond to regulate carbon uptake and water loss under stressful conditions.

To appropriately model how plants respond to stressful conditions, hard-wiring a link between plant control of carbon and water is necessary. Currently, the best performing ET models utilize the Priestley-Taylor formula to estimate ET. Despite the track record of this method to quantify ET, the Penman Monteith method provides a more direct avenue to model vegetation

control on the carbon and water cycles through canopy conductance. Many LSMs employ the Penman Monteith to model plant resistances' sensitivities to water availability, temperature, and the vapor pressure deficit. Since a large disparity exits across LSMs regarding the fraction that transpiration makes up of ET, improving plant sensitivity to soil water availability is an area of great need from the modeling community. In many LSMs, plants are overly sensitive to soil water availability and drought. Therefore, improving stomatal resistance parameterizations, including distinguishing to what degree and when soil moisture, temperature, and vapor pressure deficit impact plant regulation can establish a firm understanding of where and how tightly the carbon and water cycles are actually coupled. Previous RS ET algorithm efforts to provide surface conductance parameterizations have been hindered by gross underestimations of ET, especially transpiration (Miralles et al., 2015). Revisiting this model formulation has potential to address this area of deficiency. Current high performing RS ET datasets may prove useful to provide an independent method to evaluate these new parameterizations. Or as a means to study ecosystem scale responses. Establishing this direct link will help constrain the biosphere feedback in the earth system and reduce the uncertainty in future climate simulations.

5.2.3 Future ET analyses

Daily ecosystem physiological responses are important to appropriately model ET, but longer-term studies are needed to quantify ecosystem water use and need, and identify how vegetation stress impacts the carbon and water cycles. The work done to complete Chapter 3 and Chapter 4 facilitates future long-term analyses with the extension of observational records. Distinguishing ecosystem scale water use and water need helps to identify regions that may become vulnerable to more frequent periods of vegetation stress. In Chapter 4 I analyze how vegetation responds to regulate the carbon and water cycle in response to short-term climate

perturbations. Extending the SMAP, MODIS, and OCO-2 datasets will help to distinguish how long-term shifts in temperature and water availability impact vegetation vigor. These extended datasets and analyses will ultimately help constrain the uncertainty in the long-term feedbacks of carbon and water cycles (Friedlingstein et al., 2003). Specifically, distinguishing which areas show strong coupling across these cycles will help distinguish how our models stack up to the observational record (Fig. 5.1). Results from such studies also have the potential to identify ecosystem scale susceptibility to mortality. Higher spatial resolution datasets of ET and SIF analyzed in same manner as Chapter 4 would further their impact by identifying stand-level stress levels and help predict watershed scale responses.
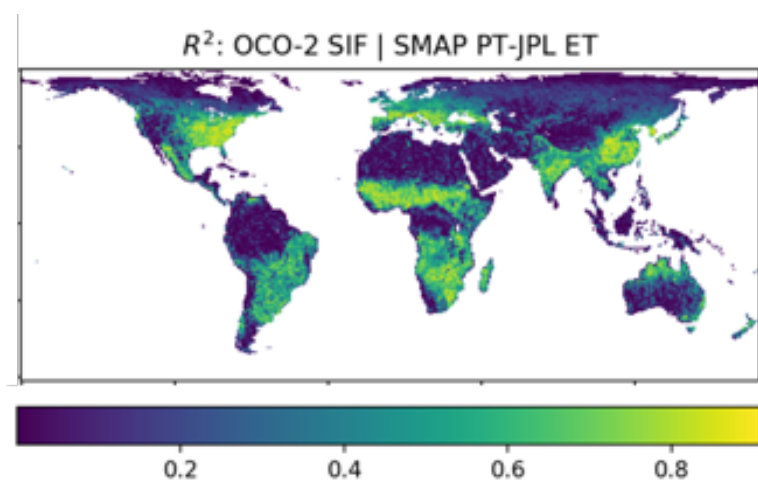
Figure 5.1 Correlation between SIF and canopy transpiration from PT-JPL modeled ET. Yellow areas indicate regions with tighter coupling between vegetation water loss and carbon uptake.

The need for finer spatial resolutions and more frequent data is driven by applications-based needs of ET datasets. Since ET is nonlinearly related to soil moisture, as demonstrated in Chapter 3, understanding how modeled ET varies across spatial resolutions is important to understand its impact on regional scale assessments. Already, successful attempts to downscale SMAP soil moisture to 1km using MODIS LST have shown to be successful and thus have great potential for RS ET (Colliander et al., 2017b). The SMAP repository provides nested soil moisture

observations across multiple spatial resolutions (3km, 9km, 36km). Preliminary analysis with the PT-JPL model reveals a difference in ET generated with different resolution soil moisture data. The areas of greatest difference occur over heterogeneous land cover and in regions with a gradient between wet and dry conditions (Figure 5.2). As RS ET algorithms move toward finer spatial resolutions, understanding how regional estimates of models vary across spatial scales is necessary to both accurately map ET while also providing accurate regional estimates. Further work to distinguish whether scaling relationships are required should focus on RS ET models that ingest soil moisture. The three months of fine-spatial resolution radar data from SMAP with finer resolution meteorological forcing datasets offers a path forward to complete such an analysis.
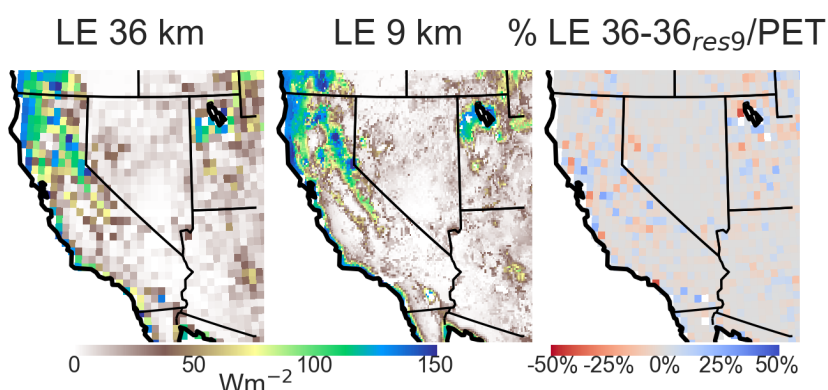
Figure 5.2 Modeled LE difference resulting from soil moisture at 9 and 36 km resolutions.

The work presented in my dissertation advances ET science and applies ET data in a novel way to link the carbon and water cycles. Working independently, I have developed the tools, techniques, and confidence necessary to take on any challenge related to earth system science. But, the work presented here is also the product from leaning on the expertise of advisors, colleagues, and friends. Often times, scientists get wrapped up in their own research and need to take a step back to discuss our work with colleagues to dial in the science questions that ultimately drive our work. Tools, techniques, and confidence provide a strong foundation to work on many projects moving forward, but the quality of the scientific questions ultimately determines the

impact. Questions about the earth are at the start of the end of the scientific method. Only when we have appropriate questions can we more effectively contribute to the greater understanding of the world as we know it. Moving forward I plan to work harder on identifying and refining these questions to ensure my work continues to advance earth system science.

Bibliography

AghaKouchak, A., Farahmand, A., Melton, F.S., Teixeira, J., Anderson, M.C., Wardlow, B.D., Hain, C.R., 2015. Remote sensing of drought: Progress, challenges and opportunities. Rev. Geophys. 53, 1–29. doi:10.1002/2014RG000456.Received

Alfieri, J.G., Kustas, W.P., Prueger, J.H., Hipps, L.E., Evett, S.R., Basara, J.B., Neale, C.M.U., French, A.N., Colaizzi, P., Agam, N., Cosh, M.H., Chavez, J.L., Howell, T.A., 2012. On the discrepancy between eddy covariance and lysimetry-based surface flux measurements under strongly advective conditions. Adv. Water Resour. 50, 62–78. doi:10.1016/j.advwatres.2012.07.008

Allen, R.G., Morton, C., Kamble, B., Kilic, A., Huntington, J., Thau, D., Gorelick, N., Erickson, T., Moore, R., Trezza, R., Ratcliffe, I., Robison, C., 2015. EEFlux: A Landsat-based Evapotranspiration mapping tool on the Google Earth Engine, in: 2015 ASABE / IA Irrigation Symposium: Emerging Technologies for Sustainable Irrigation - A Tribute to the Career of Terry Howell, Sr. Conference Proceedings. pp. 1–11. doi:10.13031/irrig.20152143511

Allen, R.G., Pereira, L.S., Raes, D., Smith, M., Ab, W., 1998. Allen_FAO1998 1–15. doi:10.1016/j.eja.2010.12.001

Allen, R.G., Tasumi, M., Morse, A., Trezza, R., Wright, J.L., Bastiaanssen, W., Kramber, W., Lorite, I., Robison, C.W., 2007a. Satellite-Based Energy Balance for Mapping Evapotranspiration with Internalized Calibration „ METRIC …— Model. J. Irrig. Drain. Eng. 133, 380–395.

Allen, R.G., Tasumi, M., Trezza, R., 2007b. Satellite-Based Energy Balance for Mapping Evapotranspiration with Internalized Calibration „ METRIC …— Model 380–395.

Amiro, B.D., 1998. Footprint climatologies for evapotranspiration in a boreal catchment. Agric. For. Meteorol. 90, 195–201. doi:10.1016/S0168-1923(97)00096-8

Anderson, M.C., Hain, C., Otkin, J., Zhan, X., Mo, K., Svoboda, M., Wardlow, B., Pimstein, A., 2013. An Intercomparison of Drought Indicators Based on Thermal Remote Sensing and NLDAS-2 Simulations with U.S. Drought Monitor Classifications. J. Hydrometeorol. 14, 1035–1056. doi:10.1175/JHM-D-12-0140.1

Anderson, M.C., Kustas, W.P., 2008. Mapping evapotranspiration and drought at local to continental scales using thermal remote sensing, in: International Geoscience and Remote Sensing Symposium (IGARSS). doi:10.1109/IGARSS.2008.4779671

Anderson, M.C., Kustas, W.P., Norman, J.M., Hain, C.R., Mecikalski, J.R., Schultz, L., González-Dugo, M.P., Cammalleri, C., D'Urso, G., Pimstein, A., Gao, F., 2011. Mapping daily evapotranspiration at field to continental scales using geostationary and polar orbiting satellite imagery. Hydrol. Earth Syst. Sci. 15, 223–239. doi:10.5194/hess-15-223-2011

Anderson, M.C., Norman, J.M., Mecikalski, J.R., Otkin, J.A., Kustas, W.P., 2007. A climatological study of evapotranspiration and moisture stress across the continental United States based on thermal remote sensing: 1. Model formulation. J. Geophys. Res. Atmos. 112. doi:10.1029/2006JD007506

Anderson, R.G., Canadell, J.G., Randerson, J.T., Jackson, R.B., Hungate, B. a, Baldocchi, D.D., Ban-Weiss, G. a, Bonan, G.B., Caldeira, K., Cao, L., Diffenbaugh, N.S., Gurney, K.R., Kueppers, L.M., Law, B.E., Luyssaert, S., O'Halloran, T.L., 2011. Biophysical considerations in forestry for climate protection. Front. Ecol. Environ. 9, 174–182. doi:10.1890/090179

Aragão, L.E.O.C., Malhi, Y., Roman-Cuesta, R.M., Saatchi, S., Anderson, L.O., Shimabukuro, Y.E., 2007. Spatial patterns and fire response of recent Amazonian droughts. Geophys. Res. Lett. 34, L07701. doi:10.1029/2006GL028946

Badgley, G., Fisher, J.B., Jiménez, C., Tu, K.P., Vinukollu, R., 2015. On Uncertainty in Global Terrestrial Evapotranspiration Estimates from Choice of Input Forcing Datasets*. J. Hydrometeorol. 16, 1449–1455. doi:10.1175/JHM-D-14-0040.1

Baldocchi, D., Falge, E., Gu, L., Olson, R., Hollinger, D., Running, S., Anthoni, P., Bernhofer, C., Davis, K., Evans, R., Fuentes, J., Goldstein, A., Katul, G., Law, B., Lee, X., Malhi, Y., Meyers, T., Munger, W., Oechel, W., Paw, U.K.T., Pilegaard, K., Schmid, H.P., Valentini, R., Verma, S., Vesala, T., Wilson, K., Wofsy, S., 2001. FLUXNET: A New Tool to Study the Temporal and Spatial Variability of Ecosystem-Scale Carbon Dioxide, Water Vapor, and Energy Flux Densities. Bull. Am. Meteorol. Soc. 82, 2415–2434. doi:10.1175/1520-0477(2001)082<2415:FANTTS>2.3.CO;2

Baldocchi, D., Valentini, R., Running, S., Oechel, W., Dahlman, R., 1996. Strategies for measuring and modelling carbon dioxide and water vapour fluxes over terrestrial ecosystems. Glob. Chang. Biol. 2, 159–168. doi:10.1111/j.1365-2486.1996.tb00069.x

Bastiaanssen, W.G.M., Menenti, M., Feddes, R. a., Holtslag, a. a. M., 1998. A remote sensing surface energy balance algorithm for land (SEBAL). 1. Formulation. J. Hydrol. 212–213, 198–212. doi:10.1016/S0022-1694(98)00253-4

Bennett, W.B., Wang, J., Bras, R.L., 2008. Estimation of Global Ground Heat Flux. J. Hydrometeorol. 9, 744–759. doi:10.1175/2008JHM940.1

Biederman, J.A., Scott, R.L., Bell, T.W., Bowling, D.R., Dore, S., Garatuza-Payan, J., Kolb, T.E., Krishnan, P., Krofcheck, D.J., Litvak, M.E., Maurer, G.E., Meyers, T.P., Oechel, W.C., Papuga, S.A., Ponce-Campos, G.E., Rodriguez, J.C., Smith, W.K., Vargas, R., Watts, C.J., Yepez, E.A., Goulden, M.L., 2017. CO2 exchange and evapotranspiration across dryland ecosystems of southwestern North America. Glob. Chang. Biol. 23, 4204–4221. doi:10.1111/gcb.13686

Biederman, J.A., Scott, R.L., Goulden, M.L., Vargas, R., Litvak, M.E., Kolb, T.E., Yepez, E.A., Oechel, W.C., Blanken, P.D., Bell, T.W., Garatuza-Payan, J., Maurer, G.E., Dore, S., Burns, S.P., 2016. Terrestrial carbon balance in a drier world: The effects of water

113

availability in southwestern North America. Glob. Chang. Biol. 22, 1867–1879. doi:10.1111/gcb.13222

Bowen, I.S., 1926. The ratio of heat losses by conduction and by evaporation from any water surface. Phys. Rev. 27, 779–787. doi:10.1103/PhysRev.27.779

Brienen, R.J.W., Phillips, O.L., Feldpausch, T.R., Gloor, E., Baker, T.R., Lloyd, J., Lopez-Gonzalez, G., Monteagudo-Mendoza, A., Malhi, Y., Lewis, S.L., Vásquez Martinez, R., Alexiades, M., Álvarez Dávila, E., Alvarez-Loayza, P., Andrade, A., Aragaõ, L.E.O.C., Araujo-Murakami, A., Arets, E.J.M.M., Arroyo, L., Aymard C., G.A., Bánki, O.S., Baraloto, C., Barroso, J., Bonal, D., Boot, R.G.A., Camargo, J.L.C., Castilho, C. V., Chama, V., Chao, K.J., Chave, J., Comiskey, J.A., Cornejo Valverde, F., Da Costa, L., De Oliveira, E.A., Di Fiore, A., Erwin, T.L., Fauset, S., Forsthofer, M., Galbraith, D.R., Grahame, E.S., Groot, N., Hérault, B., Higuchi, N., Honorio Coronado, E.N., Keeling, H., Killeen, T.J., Laurance, W.F., Laurance, S., Licona, J., Magnussen, W.E., Marimon, B.S., Marimon-Junior, B.H., Mendoza, C., Neill, D.A., Nogueira, E.M., Núñez, P., Pallqui Camacho, N.C., Parada, A., Pardo-Molina, G., Peacock, J., Penã-Claros, M., Pickavance, G.C., Pitman, N.C.A., Poorter, L., Prieto, A., Quesada, C.A., Ramírez, F., Ramírez-Angulo, H., Restrepo, Z., Roopsind, A., Rudas, A., Salomaõ, R.P., Schwarz, M., Silva, N., Silva-Espejo, J.E., Silveira, M., Stropp, J., Talbot, J., Ter Steege, H., Teran-Aguilar, J., Terborgh, J., Thomas-Caesar, R., Toledo, M., Torello-Raventos, M., Umetsu, R.K., Van Der Heijden, G.M.F., Van Der Hout, P., Guimarães Vieira, I.C., Vieira, S.A., Vilanova, E., Vos, V.A., Zagt, R.J., 2015. Long-term decline of the Amazon carbon sink. Nature 519, 344–348. doi:10.1038/nature14283

Brodzik, M.J., Billingsley, B., Haran, T., Raup, B., Savoie, M.H., 2012. EASE-Grid 2.0: Incremental but Significant Improvements for Earth-Gridded Data Sets. ISPRS Int. J. Geo-Information 1, 32–45. doi:10.3390/ijgi1010032

Burba, G.G., Verma, S.B., 2005. Seasonal and interannual variability in evapotranspiration of native tallgrass prairie and cultivated wheat ecosystems. Agric. For. Meteorol. 135, 190–201. doi:10.1016/j.agrformet.2005.11.017

Canadell, J., Jackson, R.B., Ehleringer, J.B., Mooney, H.A., Sala, O.E., Schulze, E.-D., 1996. Maximum rooting depth of vegetation types at the global scale. Oecologia 108, 583–595. doi:10.1007/BF00329030

Castle, S.L., Reager, J.T., Thomas, B.F., Purdy, A.J., Lo, M.H., Famiglietti, J.S., Tang, Q., 2016. Remote detection of water management impacts on evapotranspiration in the Colorado River Basin. Geophys. Res. Lett. 43, 5089–5097. doi:10.1002/2016GL068675

Chan, S.K., Bindlish, R., O'Neill, P.E., Njoku, E., Jackson, T., Colliander, A., Chen, F., Burgin, M., Dunbar, S., Piepmeier, J., Yueh, S., Entekhabi, D., Cosh, M.H., Caldwell, T., Walker, J., Wu, X., Berg, A., Rowlandson, T., Pacheco, A., McNairn, H., Thibeault, M., Martinez-Fernandez, J., Gonzalez-Zamora, A., Seyfried, M., Bosch, D., Starks, P., Goodrich, D., Prueger, J., Palecki, M., Small, E.E., Zreda, M., Calvet, J.C., Crow, W.T., Kerr, Y., 2016. Assessment of the SMAP Passive Soil Moisture Product. IEEE Trans. Geosci. Remote

Sens. 54, 4994–5007. doi:10.1109/TGRS.2016.2561938

Chen, B., Black, T.A., Coops, N.C., Hilker, T., Trofymow, J.A., Morgenstern, K., 2009. Assessing tower flux footprint climatology and scaling between remotely sensed and eddy covariance measurements. Boundary-Layer Meteorol. 130, 137–167. doi:10.1007/s10546-008-9339-1

Chen, T., Van Der Werf, G.R., De Jeu, R.A.M., Wang, G., Dolman, A.J., Werf, G.R., Jeu, R.A.M., Wang, G., Dolman, A.J., 2013. A global analysis of the impact of drought on net primary productivity. Hydrol. Earth Syst. Sci 17, 3885–3894. doi:10.5194/hess-17-3885-2013

Chen, Y., Morton, D.C., Andela, N., Van Der Werf, G.R., Giglio, L., Randerson, J.T., 2017. A pan-tropical cascade of fire driven by El Niño/Southern Oscillation. Nat. Clim. Chang. 7, 906–911. doi:10.1038/s41558-017-0014-8

Chen, Y., Xia, J., Liang, S., Feng, J., Fisher, J.B., Li, X., Li, X., Liu, S., Ma, Z., Miyata, A., Mu, Q., Sun, L., Tang, J., Wang, K., Wen, J., Xue, Y., Yu, G., Zha, T., Zhang, L., Zhang, Q., Zhao, T., Zhao, L., Yuan, W., 2014. Comparison of satellite-based evapotranspiration models over terrestrial ecosystems in China. Remote Sens. Environ. 140, 279–293. doi:10.1016/j.rse.2013.08.045

Choudhury, B.J., Idso, S.B., Reginato, R.J., 1987. Analysis of an empirical model for soil heat flux under a growing wheat crop for estimating evaporation by an infrared-temperature based energy balance equation. Agric. For. Meteorol. 39, 283–297. doi:10.1016/0168-1923(87)90021-9

Cleugh, H.A., Leuning, R., Mu, Q., Running, S.W., 2007. Regional evaporation estimates from flux tower and MODIS satellite data. Remote Sens. Environ. 106, 285–304. doi:10.1016/j.rse.2006.07.007

Clothier, B.E., Clawson, K.L., Pinter, P.J., Moran, M.S., Reginato, R.J., Jackson, R.D., 1986. Estimation of soil heat flux from net radiation during the growth of alfalfa. Agric. For. Meteorol. 37, 319–329. doi:10.1016/0168-1923(86)90069-9

Colliander, A., Cosh, M.H., Misra, S., Jackson, T.J., Crow, W.T., Chan, S., Bindlish, R., Chae, C., Holifield Collins, C., Yueh, S.H., 2017a. Validation and scaling of soil moisture in a semi-arid environment: SMAP validation experiment 2015 (SMAPVEX15). Remote Sens. Environ. 196, 101–112. doi:10.1016/j.rse.2017.04.022

Colliander, A., Fisher, J.B., Halverson, G., Merlin, O., Misra, S., Bindlish, R., Jackson, T.J., Yueh, S., 2017b. Spatial Downscaling of SMAP Soil Moisture Using MODIS Land Surface Temperature and NDVI During SMAPVEX15. IEEE Geosci. Remote Sens. Lett. doi:10.1109/LGRS.2017.2753203

Colliander, A., Jackson, T.J., Bindlish, R., Chan, S., Das, N., Kim, S.B., Cosh, M.H., Dunbar, R.S., Dang, L., Pashaian, L., Asanuma, J., Aida, K., Berg, A., Rowlandson, T., Bosch, D., Caldwell, T., Caylor, K., Goodrich, D., al Jassar, H., Lopez-Baeza, E., Martínez-Fernández,

J., González-Zamora, A., Livingston, S., McNairn, H., Pacheco, A., Moghaddam, M., Montzka, C., Notarnicola, C., Niedrist, G., Pellarin, T., Prueger, J., Pulliainen, J., Rautiainen, K., Ramos, J., Seyfried, M., Starks, P., Su, Z., Zeng, Y., van der Velde, R., Thibeault, M., Dorigo, W., Vreugdenhil, M., Walker, J.P., Wu, X., Monerris, A., O'Neill, P.E., Entekhabi, D., Njoku, E.G., Yueh, S., 2017. Validation of SMAP surface soil moisture products with core validation sites. Remote Sens. Environ. 191, 215–231. doi:10.1016/j.rse.2017.01.021

Daughtry, C.S.T., Kustas, W.P., Moran, M.S., Pinter, P.J., Jackson, R.D., Brown, P.W., Nichols, W.D., Gay, L.W., 1990. Spectral estimates of net radiation and soil heat flux. Remote Sens. Environ. 32, 111–124. doi:10.1016/0034-4257(90)90012-B

Dirmeyer, P.A., Gao, X., Zhao, M., Guo, Z., Oki, T., Hanasaki, N., 2006. GSWP-2: Multimodel analysis and implications for our perception of the land surface. Bull. Am. Meteorol. Soc. 87, 1381–1397. doi:10.1175/BAMS-87-10-1381

Dirmeyer, P.A., Guo, Z., Gao, X., 2004. Comparison, Validation, and Transferability of Eight Multiyear Global Soil Wetness Products. J. Hydrometeorol. 5, 1011–1033. doi:10.1175/JHM-388.1

Dirmeyer, P.A., Niyogi, D., De Noblet-Ducoudré, N., Dickinson, R.E., Snyder, P.K., 2010. Impacts of land use change on climate. Int. J. Climatol. 30, 1905–1907. doi:10.1002/joc.2157

Dolman, A.J., Miralles, D.G., de Jeu, R.A.M., 2014. Fifty years since Monteith's 1965 seminal paper: The emergence of global ecohydrology. Ecohydrology. doi:10.1002/eco.1505

Doughty, C.E., Goulden, M.L., 2009. Are tropical forests near a high temperature threshold? J. Geophys. Res. Biogeosciences 114. doi:10.1029/2007JG000632

Entekhabi, D., Njoku, E., O'Neill, P., Kellogg, K., Entin, J., 2011. The NASA Soil Moisture Active Passive (SMAP) mission formulation, in: International Geoscience and Remote Sensing Symposium (IGARSS). pp. 2302–2305. doi:10.1109/IGARSS.2011.6049669

Entekhabi, D., Njoku, E.G., O'Neill, P.E., Kellogg, K.H., Crow, W.T., Edelstein, W.N., Entin, J.K., Goodman, S.D., Jackson, T.J., Johnson, J., Kimball, J., Piepmeier, J.R., Koster, R.D., Martin, N., McDonald, K.C., Moghaddam, M., Moran, S., Reichle, R., Shi, J.C., Spencer, M.W., Thurman, S.W., Tsang, L., Van Zyl, J., 2010. The soil moisture active passive (SMAP) mission. Proc. IEEE 98, 704–716. doi:10.1109/JPROC.2010.2043918

Ershadi, A., McCabe, M.F., Evans, J.P., Chaney, N.W., Wood, E.F., 2014. Multi-site evaluation of terrestrial evaporation models using FLUXNET data. Agric. For. Meteorol. 187, 46–61. doi:10.1016/j.agrformet.2013.11.008

Evaristo, J., Jasechko, S., McDonnell, J.J., 2015. Global separation of plant transpiration from groundwater and streamflow. Nature 525, 91–94. doi:10.1038/nature14983

Falge, E., Baldocchi, D., Olson, R., Anthoni, P., Aubinet, M., Bernhofer, C., Burba, G., Ceulemans, R., Clement, R., Dolman, H., Granier, A., Gross, P., Gr??nwald, T., Hollinger, D., Jensen, N.O., Katul, G., Keronen, P., Kowalski, A., Ta Lai, C., Law, B.E., Meyers, T., Moncrieff, J., Moors, E., William Munger, J., Pilegaard, K., Rannik, ??llar, Rebmann, C., Suyker, A., Tenhunen, J., Tu, K., Verma, S., Vesala, T., Wilson, K., Wofsy, S., 2001a. Short communication: Gap filling strategies for long term energy flux data sets. Agric. For. Meteorol. 107, 71–77. doi:10.1016/S0168-1923(00)00235-5

Falge, E., Baldocchi, D., Olson, R., Anthoni, P., Aubinet, M., Bernhofer, C., Burba, G., Ceulemans, R., Clement, R., Dolman, H., Granier, A., Gross, P., Grünwald, T., Hollinger, D., Jensen, N.O., Katul, G., Keronen, P., Kowalski, A., Lai, C.T., Law, B.E., Meyers, T., Moncrieff, J., Moors, E., Munger, J.W., Pilegaard, K., Rannik, Ü., Rebmann, C., Suyker, A., Tenhunen, J., Tu, K., Verma, S., Vesala, T., Wilson, K., Wofsy, S., 2001b. Gap filling strategies for defensible annual sums of net ecosystem exchange. Agric. For. Meteorol. 107, 43–69. doi:10.1016/S0168-1923(00)00225-2

Famiglietti, J.S., Ryu, D., Berg, A.A., Rodell, M., Jackson, T.J., 2008. Field observations of soil moisture variability across scales. Water Resour. Res. 44. doi:10.1029/2006WR005804

Fan, Y., Miguez-Macho, G., Jobbágy, E.G., Jackson, R.B., Otero-Casal, C., 2017. Hydrologic regulation of plant rooting depth. Proc. Natl. Acad. Sci. 201712381. doi:10.1073/pnas.1712381114

Field, C.B., Randerson, J.T., Malmström, C.M., 1995. Global net primary production: Combining ecology and remote sensing. Remote Sens. Environ. 51, 74–88. doi:10.1016/0034-4257(94)00066-V

Fisher, J.B., Melton, F., Middleton, E., Hain, C., Anderson, M., Allen, R., McCabe, M.F., Hook, S., Baldocchi, D., Townsend, P.A., Kilic, A., Tu, K., Miralles, D.D., Perret, J., Lagouarde, J.-P., Waliser, D., Purdy, A.J., French, A., Schimel, D., Famiglietti, J.S., Stephens, G., Wood, E.F., 2017. The future of evapotranspiration: Global requirements for ecosystem functioning, carbon and climate feedbacks, agricultural management, and water resources. Water Resour. Res. 53, 2618–2626. doi:10.1002/2016WR020175

Fisher, J.B., Tu, K.P., Baldocchi, D.D., 2008. Global estimates of the land-atmosphere water flux based on monthly AVHRR and ISLSCP-II data, validated at 16 FLUXNET sites. Remote Sens. Environ. 112, 901–919. doi:10.1016/j.rse.2007.06.025

Fisher, J.B., Whittaker, R.J., Malhi, Y., 2011. ET come home: Potential evapotranspiration in geographical ecology. Glob. Ecol. Biogeogr. 20, 1–18. doi:10.1111/j.1466-8238.2010.00578.x

Fisher, R.A., Williams, M., da Costa, A.L., Malhi, Y., da Costa, R.F., Almeida, S., Meir, P., 2007. The response of an Eastern Amazonian rain forest to drought stress: Results and modelling analyses from a throughfall exclusion experiment. Glob. Chang. Biol. 13, 2361–2378. doi:10.1111/j.1365-2486.2007.01417.x

Foken, T., 2008. The energy balance closure problem: An overview. Ecol. Appl. 18, 1351–1367.

doi:10.1890/06-0922.1

Foken, T., Aubinet, M., Finnigan, J.J., Leclerc, M.Y., Mauder, M., Paw U, K.T., 2011. Results of a panel discussion about the energy balance closure correction for trace gases, in: Bulletin of the American Meteorological Society. doi:10.1175/2011BAMS3130.1

Frankenberg, C., Fisher, J.B., Worden, J., Badgley, G., Saatchi, S.S., Lee, J.E., Toon, G.C., Butz, A., Jung, M., Kuze, A., Yokota, T., 2011. New global observations of the terrestrial carbon cycle from GOSAT: Patterns of plant fluorescence with gross primary productivity. Geophys. Res. Lett. 38. doi:10.1029/2011GL048738

Frankenberg, C., O'Dell, C., Berry, J., Guanter, L., Joiner, J., Köhler, P., Pollock, R., Taylor, T.E., 2014. Prospects for chlorophyll fluorescence remote sensing from the Orbiting Carbon Observatory-2. Remote Sens. Environ. 147, 1–12. doi:10.1016/j.rse.2014.02.007

Friedlingstein, P., Cox, P., Betts, R., Bopp, L., von Bloh, W., Brovkin, V., Cadule, P., Doney, S., Eby, M., Fung, I., Bala, G., John, J., Jones, C., Joos, F., Kato, T., Kawamiya, M., Knorr, W., Lindsay, K., Matthews, H.D., Raddatz, T., Rayner, P., Reick, C., Roeckner, E., Schnitzler, K.-G., Schnur, R., Strassmann, K., Weaver, A.J., Yoshikawa, C., Zeng, N., 2006. Climate–Carbon Cycle Feedback Analysis: Results from the C 4 MIP Model Intercomparison. J. Clim. 19, 3337–3353. doi:10.1175/JCLI3800.1

Friedlingstein, P., Dufresne, J.-L.L., Cox, P.M., Rayner, P., 2003. How positive is the feedback between climate change and the carbon cycle? Tellus, Ser. B Chem. Phys. Meteorol. 55, 692–700. doi:10.1034/j.1600-0889.2003.01461.x

Gao, X., Dirmeyer, P. a., 2006. A Multimodel Analysis, Validation, and Transferability Study of Global Soil Wetness Products. J. Hydrometeorol. 7, 1218–1236. doi:10.1175/JHM551.1

Gedney, N., Cox, P.M., Betts, R.A., Boucher, O., Huntingford, C., Stott, P.A., 2006. Continental runoff: A quality-controlled global runoff data set (Reply). Nature. doi:10.1038/nature05481

Gelaro, R., McCarty, W., Suárez, M.J., Todling, R., Molod, A., Takacs, L., Randles, C.A., Darmenov, A., Bosilovich, M.G., Reichle, R., Wargan, K., Coy, L., Cullather, R., Draper, C., Akella, S., Buchard, V., Conaty, A., da Silva, A.M., Gu, W., Kim, G.K., Koster, R., Lucchesi, R., Merkova, D., Nielsen, J.E., Partyka, G., Pawson, S., Putman, W., Rienecker, M., Schubert, S.D., Sienkiewicz, M., Zhao, B., 2017. The modern-era retrospective analysis for research and applications, version 2 (MERRA-2). J. Clim. 30, 5419–5454. doi:10.1175/JCLI-D-16-0758.1

George H. Hargreaves, Zohrab A. Samani, 1985. Reference Crop Evapotranspiration from Temperature. Appl. Eng. Agric. 1, 96–99. doi:10.13031/2013.26773

Goulden, M.L., Anderson, R.G., Bales, R.C., Kelly, a. E., Meadows, M., Winston, G.C., 2012. Evapotranspiration along an elevation gradient in California's Sierra Nevada. J. Geophys. Res. 117, G03028. doi:10.1029/2012JG002027

Goulden, M.L., Bales, R.C., 2014. Mountain runoff vulnerability to increased evapotranspiration with vegetation expansion. Proc. Natl. Acad. Sci. 111, 14071–14075. doi:10.1073/pnas.1319316111

Goulden, M.L., Munger, W., Fan, S., Daube, B.C., Wofsy, S.C., 1996. Measurements of carbon sequestration by long-term eddy covariance: methods and a critical evaluation of accuracy. Glob. Chang. Biol. 2, 169–182. doi:10.1111/j.1365-2486.1996.tb00070.x

Granier, A., Reichstein, M., Bréda, N., Janssens, I.A., Falge, E., Ciais, P., Grünwald, T., Aubinet, M., Berbigier, P., Bernhofer, C., Buchmann, N., Facini, O., Grassi, G., Heinesch, B., Ilvesniemi, H., Keronen, P., Knohl, A., Köstner, B., Lagergren, F., Lindroth, A., Longdoz, B., Loustau, D., Mateus, J., Montagnani, L., Nys, C., Moors, E., Papale, D., Peiffer, M., Pilegaard, K., Pita, G., Pumpanen, J., Rambal, S., Rebmann, C., Rodrigues, A., Seufert, G., Tenhunen, J., Vesala, T., Wang, Q., 2007. Evidence for soil water control on carbon and water dynamics in European forests during the extremely dry year: 2003. Agric. For. Meteorol. 143, 123–145. doi:10.1016/j.agrformet.2006.12.004

Gregory, J.M., Jones, C.D., Cadule, P., Friedlingstein, P., 2009. Quantifying carbon cycle feedbacks. J. Clim. 22, 5232–5250. doi:10.1175/2009JCLI2949.1

Greve, P., Orlowsky, B., Mueller, B., Sheffield, J., Reichstein, M., Seneviratne, S.I., 2014. Global assessment of trends in wetting and drying over land. Nat. Geosci. 7, 716–721. doi:10.1038/NGEO2247

Greve, P., Seneviratne, S.I., 2015. Assessment of future changes in water availability and aridity. Geophys. Res. Lett. 42, 5493–5499. doi:10.1002/2015GL064127

Gu, L., Baldocchi, D.D., Wofsy, S.C., William Munger, J., Michalsky, J.J., Urbanski, S.P., Boden, T.A., 2003. Response of a deciduous forest to the Mount Pinatubo eruption: Enhanced photosynthesis. Science (80-.). 299, 2035–2038. doi:10.1126/science.1078366

Guanter, L., Zhang, Y., Jung, M., Joiner, J., Voigt, M., Berry, J.A., Frankenberg, C., Huete, A.R., Zarco-Tejada, P., Lee, J.-E., Moran, M.S., Ponce-Campos, G., Beer, C., Camps-Valls, G., Buchmann, N., Gianelle, D., Klumpp, K., Cescatti, A., Baker, J.M., Griffis, T.J., 2014. Global and time-resolved monitoring of crop photosynthesis with chlorophyll fluorescence. Proc. Natl. Acad. Sci. 111, E1327–E1333. doi:10.1073/pnas.1320008111

Hain, C.R., Mecikalski, J.R., Anderson, M.C., 2009. Retrieval of an Available Water-Based Soil Moisture Proxy from Thermal Infrared Remote Sensing. Part I: Methodology and Validation. J. Hydrometeorol. 10, 665–683. doi:10.1175/2008JHM1024.1

Holmes, J.W., 1984. Measuring evapotranspiration by hydrological methods. Agric. Water Manag. 8, 29–40. doi:10.1016/0378-3774(84)90044-1

Holmes, T.R.H., Owe, M., De Jeu, R.A.M., Kooi, H., 2008. Estimating the soil temperature profile from a single depth observation: A simple empirical heatflow solution. Water Resour. Res. 44. doi:10.1029/2007WR005994

119

Huete, A., Justice, C., 1999. Modis Vegetation Index Algorithm Theoretical Basis. Environ. Sci. 129. doi:10.1016/j.rse.2007.07.019

Huntington, T.G., 2006. Evidence for intensification of the global water cycle: Review and synthesis. J. Hydrol. doi:10.1016/j.jhydrol.2005.07.003

Idso, S.B., 1978. Mathematical models in plant physiology: A quantitative approach to problems in plant and crop physiology. Agric. Meteorol. doi:10.1016/0002-1571(78)90038-9

Jackson, R.B., Moore, L.A., Hoffmann, W.A., Pockman, W.T., Linder, C.R., 1999. Ecosystem rooting depth determined with caves and DNA. Proc. Natl. Acad. Sci. U. S. A. 96, 11387–92. doi:10.1073/pnas.96.20.11387

Jacobsen, A., Hansen, B.U., 1999. Estimation of the soil heat flux/net radiation ratio based on spectral vegetation indexes in high-latitude Arctic areas. Int. J. Remote Sens. 20, 445–461. doi:10.1080/014311699213532

Jarvis, P.G., Mcnaughton, K.G., 1986. Stomatal Control of Transpiration: Scaling Up from Leaf to Region. Adv. Ecol. Res. 15, 1–49. doi:10.1016/S0065-2504(08)60119-1

Jiménez, C., Prigent, C., Mueller, B., Seneviratne, S.I., McCabe, M.F., Wood, E.F., Rossow, W.B., Balsamo, G., Betts, A.K., Dirmeyer, P.A., Fisher, J.B., Jung, M., Kanamitsu, M., Reichle, R.H., Reichstein, M., Rodell, M., Sheffield, J., Tu, K., Wang, K., 2011. Global intercomparison of 12 land surface heat flux estimates. J. Geophys. Res. 116, 1–27. doi:10.1029/2010JD014545

Jin, Y., Randerson, J.T., Goulden, M.L., 2011. Continental-scale net radiation and evapotranspiration estimated using MODIS satellite observations. Remote Sens. Environ. 115, 2302–2319. doi:10.1016/j.rse.2011.04.031

Johnson, J.T., Mohammed, P.N., Piepmeier, J.R., Bringer, A., Aksoy, M., 2016. Soil Moisture Active Passive (SMAP) microwave radiometer radio-frequency interference (RFI) mitigation: Algorithm updates and performance assessment, in: International Geoscience and Remote Sensing Symposium (IGARSS). pp. 123–124. doi:10.1109/IGARSS.2016.7729022

Joiner, J., Yoshida, Y., Vasilkov, A.P., Yoshida, Y., Corp, L.A., Middleton, E.M., 2011. First observations of global and seasonal terrestrial chlorophyll fluorescence from space. Biogeosciences 8, 637–651. doi:10.5194/bg-8-637-2011

Jung, M., Reichstein, M., Ciais, P., Seneviratne, S.I., Sheffield, J., Goulden, M.L., Bonan, G., Cescatti, A., Chen, J., de Jeu, R., Dolman, A.J., Eugster, W., Gerten, D., Gianelle, D., Gobron, N., Heinke, J., Kimball, J., Law, B.E., Montagnani, L., Mu, Q., Mueller, B., Oleson, K., Papale, D., Richardson, A.D., Roupsard, O., Running, S., Tomelleri, E., Viovy, N., Weber, U., Williams, C., Wood, E., Zaehle, S., Zhang, K., 2010. Recent decline in the global land evapotranspiration trend due to limited moisture supply. Nature 467, 951–4. doi:10.1038/nature09396

Jung, M., Reichstein, M., Margolis, H.A., Cescatti, A., Richardson, A.D., Arain, M.A., Arneth, A., Bernhofer, C., Bonal, D., Chen, J., Gianelle, D., Gobron, N., Kiely, G., Kutsch, W., Lasslop, G., Law, B.E., Lindroth, A., Merbold, L., Montagnani, L., Moors, E.J., Papale, D., Sottocornola, M., Vaccari, F., Williams, C., 2011. Global patterns of land-atmosphere fluxes of carbon dioxide, latent heat, and sensible heat derived from eddy covariance, satellite, and meteorological observations. J. Geophys. Res. Biogeosciences 116. doi:10.1029/2010JG001566

JUSTICE, C.O., TOWNSHEND, J.R.G., HOLBEN, B.N., TUCKER, C.J., 1985. Analysis of the phenology of global vegetation using meteorological satellite data. Int. J. Remote Sens. 6, 1271–1318. doi:10.1080/01431168508948281

Kerr, Y.H., Al-Yaari, A., Rodriguez-Fernandez, N., Parrens, M., Molero, B., Leroux, D., Bircher, S., Mahmoodi, A., Mialon, A., Richaume, P., Delwart, S., Al Bitar, A., Pellarin, T., Bindlish, R., Jackson, T.J., Rüdiger, C., Waldteufel, P., Mecklenburg, S., Wigneron, J.P., 2016. Overview of SMOS performance in terms of global soil moisture monitoring after six years in operation. Remote Sens. Environ. 180, 40–63. doi:10.1016/j.rse.2016.02.042

Kerr, Y.H., Waldteufel, P., Wigneron, J.P., Martinuzzi, J.M., Font, J., Berger, M., 2001. Soil moisture retrieval from space: The Soil Moisture and Ocean Salinity (SMOS) mission. IEEE Trans. Geosci. Remote Sens. 39, 1729–1735. doi:10.1109/36.942551

Köhli, M., Schrön, M., Zreda, M., Schmidt, U., Dietrich, P., Zacharias, S., 2015. Footprint characteristics revised for field-scale soil moisture monitoring with cosmic-ray neutrons. Water Resour. Res. 51, 5772–5790. doi:10.1002/2015WR017169

Kustas, W.P., Daughtry, C.S.T., Van Oevelen, P.J., 1993. Analytical treatment of the relationships between soil heat flux/net radiation ratio and vegetation indices. Remote Sens. Environ. 46, 319–330. doi:10.1016/0034-4257(93)90052-Y

Kustas, W.P., Prueger, J.H., Hatfield, J.L., Ramalingam, K., Hipps, L.E., 2000. Variability in soil heat flux from a mesquite dune site. Agric. For. Meteorol. 103, 249–264. doi:10.1016/S0168-1923(00)00131-3

Lee, C.M., Cable, M.L., Hook, S.J., Green, R.O., Ustin, S.L., Mandl, D.J., Middleton, E.M., 2015. An introduction to the NASA Hyperspectral InfraRed Imager (HyspIRI) mission and preparatory activities. Remote Sens. Environ. 167, 6–19. doi:10.1016/j.rse.2015.06.012

Lee, J.-E., Frankenberg, C., van der Tol, C., Berry, J.A., Guanter, L., Boyce, C.K., Fisher, J.B., Morrow, E., Worden, J.R., Asefi, S., Badgley, G., Saatchi, S., 2013. Forest productivity and water stress in Amazonia: observations from GOSAT chlorophyll fluorescence. Proc. R. Soc. B Biol. Sci. 280, 20130171–20130171. doi:10.1098/rspb.2013.0171

Levine, P.A., Randerson, J.T., Swenson, S.C., Lawrence, D.M., 2016. Evaluating the strength of the land-atmosphere moisture feedback in Earth system models using satellite observations. Hydrol. Earth Syst. Sci. 20, 4837–4856. doi:10.5194/hess-20-4837-2016

Liu, J., Bowman, K.W., Schimel, D.S., Parazoo, N.C., Jiang, Z., Lee, M., Bloom, A.A., Wunch,

D., Frankenberg, C., Sun, Y., O'Dell, C.W., Gurney, K.R., Menemenlis, D., Gierach, M., Crisp, D., Eldering, A., 2017. Contrasting carbon cycle responses of the tropical continents to the 2015–2016 El Niño. Science (80-.). 358, eaam5690. doi:10.1126/science.aam5690

Lo, M.H., Famiglietti, J.S., 2013. Irrigation in California's Central Valley strengthens the southwestern U.S. water cycle. Geophys. Res. Lett. 40, 301–306. doi:10.1002/grl.50108

Loeb, N.G., Wielicki, B.A., Doelling, D.R., Smith, G.L., Keyes, D.F., Kato, S., Manalo-Smith, N., Wong, T., 2009. Toward optimal closure of the Earth's top-of-atmosphere radiation budget. J. Clim. 22, 748–766. doi:10.1175/2008JCLI2637.1

Long, D., Scanlon, B.R., Longuevergne, L., Sun, A.Y., Fernando, D.N., Save, H., 2013. GRACE satellite monitoring of large depletion in water storage in response to the 2011 drought in Texas. Geophys. Res. Lett. 40, 3395–3401. doi:10.1002/grl.50655

Malhi, Y., Gardner, T.A., Goldsmith, G.R., Silman, M.R., Zelazowski, P., 2014. Tropical Forests in the Anthropocene. Annu. Rev. Environ. Resour. 39, 125–159. doi:10.1146/annurev-environ-030713-155141

Martens, B., Miralles, D.G., Lievens, H., Van Der Schalie, R., De Jeu, R.A.M., Fernández-Prieto, D., Beck, H.E., Dorigo, W.A., Verhoest, N.E.C., 2017. GLEAM v3: Satellite-based land evaporation and root-zone soil moisture. Geosci. Model Dev. 10, 1903–1925. doi:10.5194/gmd-10-1903-2017

Mccabe, M.F., Ershadi, A., Jimenez, C., Miralles, D.G., Michel, D., Wood, E.F., 2016. The GEWEX LandFlux project: evaluation of model evaporation using tower-based and globally gridded forcing data. Geosci. Model Dev 9, 283–305. doi:10.5194/gmd-9-283-2016

McCabe, M.F., Ershadi, A., Jimenez, C., Miralles, D.G., Michel, D., Wood, E.F., 2016. The GEWEX LandFlux project: Evaluation of model evaporation using tower-based and globally gridded forcing data. Geosci. Model Dev. 9, 283–305. doi:10.5194/gmd-9-283-2016

McDonnell, J.J., 2017. Beyond the water balance. Nat. Geosci. doi:10.1038/ngeo2964

McDowell, N.G., 2011. Mechanisms Linking Drought, Hydraulics, Carbon Metabolism, and Vegetation Mortality. PLANT Physiol. 155, 1051–1059. doi:10.1104/pp.110.170704

Medlyn, B.E., Zaehle, S., De Kauwe, M.G., Walker, A.P., Dietze, M.C., Hanson, P.J., Hickler, T., Jain, A.K., Luo, Y., Parton, W., Prentice, I.C., Thornton, P.E., Wang, S., Wang, Y.P., Weng, E., Iversen, C.M., Mccarthy, H.R., Warren, J.M., Oren, R., Norby, R.J., 2015. Using ecosystem experiments to improve vegetation models. Nat. Clim. Chang. doi:10.1038/nclimate2621

Melton, F.S., Johnson, L.F., Lund, C.P., Pierce, L.L., Michaelis, A.R., Hiatt, S.H., Guzman, A., Adhikari, D.D., Purdy, A.J., Rosevelt, C., Votava, P., Trout, T.J., Temesgen, B., Frame, K., Sheffner, E.J., Nemani, R.R., 2012. Satellite irrigation management support with the

terrestrial observation and prediction system: A framework for integration of satellite and surface observations to support improvements in agricultural water resource management. IEEE J. Sel. Top. Appl. Earth Obs. Remote Sens. 5, 1709–1721. doi:10.1109/JSTARS.2012.2214474

Mercado, L.M., Bellouin, N., Sitch, S., Boucher, O., Huntingford, C., Wild, M., Cox, P.M., 2009. Impact of changes in diffuse radiation on the global land carbon sink. Nature 458, 1014–1017. doi:10.1038/nature07949

Michel, D., Jim??nez, C., Miralles, D.G., Jung, M., Hirschi, M., Ershadi, A., Martens, B., Mccabe, M.F., Fisher, J.B., Mu, Q., Seneviratne, S.I., Wood, E.F., Fern??ndez-Prieto, D., 2016. The WACMOS-ET project - Part 1: Tower-scale evaluation of four remote-sensing-based evapotranspiration algorithms. Hydrol. Earth Syst. Sci. 20, 803–822. doi:10.5194/hess-20-803-2016

Middleton, E.M., Cheng, Y. Ben, Hilker, T., Black, T.A., Krishnan, P., Coops, N.C., Huemmrich, K.F., 2009. Linking foliage spectral responses to canopy-level ecosystem photosynthetic light-use efficiency at a douglas-fir forest in canada. Can. J. Remote Sens. 35, 166–188. doi:10.5589/m09-008

Miralles, D.G., De Jeu, R.A.M., Gash, J.H., Holmes, T.R.H., Dolman, A.J., 2011a. Magnitude and variability of land evaporation and its components at the global scale. Hydrol. Earth Syst. Sci. 15, 967–981. doi:10.5194/hess-15-967-2011

Miralles, D.G., Holmes, T.R.H., De Jeu, R.A.M., Gash, J.H., Meesters, A.G.C.A., Dolman, A.J., 2011b. Global land-surface evaporation estimated from satellite-based observations. Hydrol. Earth Syst. Sci. 15, 453–469. doi:10.5194/hess-15-453-2011

Miralles, D.G., Jiménez, C., Jung, M., Michel, D., Ershadi, A., McCabe, M.F., Hirschi, M., Martens, B., Dolman, A.J., Fisher, J.B., Mu, Q., Seneviratne, S.I., Wood, E.F., Fernaìndez-Prieto, D., 2015. The WACMOS-ET project – Part 2: Evaluation of global terrestrial evaporation data sets. Hydrol. Earth Syst. Sci. Discuss. 12, 10651–10700. doi:10.5194/hessd-12-10651-2015

Miralles, D.G., Teuling, A.J., van Heerwaarden, C.C., Vilà-Guerau de Arellano, J., 2014. Mega-heatwave temperatures due to combined soil desiccation and atmospheric heat accumulation. Nat. Geosci. 7, 345–349. doi:10.1038/ngeo2141

Miralles, D.G., van den Berg, M.J., Gash, J.H., Parinussa, R.M., de Jeu, R.A.M., Beck, H.E., Holmes, T.R.H., Jimenez, C., Verhoest, N.E.C., Dorigo, W.A., Teuling, A.J., Dolman, A.J., 2014. El Nino-La Nina cycle and recent trends in continental evaporation. Nat. Clim. Chang. 4, 122–126. doi:Doi 10.1038/Nclimate2068

Miralles, D.G., Van Den Berg, M.J., Teuling, A.J., De Jeu, R.A.M., 2012. Soil moisture-temperature coupling: A multiscale observational analysis. Geophys. Res. Lett. 39. doi:10.1029/2012GL053703

Mohammed, P.N., Aksoy, M., Piepmeier, J.R., Johnson, J.T., Bringer, A., 2016. SMAP L-Band

Microwave Radiometer: RFI Mitigation Prelaunch Analysis and First Year On-Orbit Observations. IEEE Trans. Geosci. Remote Sens. 54, 6035–6047. doi:10.1109/TGRS.2016.2580459

Monteith, J.L., 1981. Evaporation and surface temperature. Q. J. R. Meteorol. Soc. 107, 1–27. doi:10.1002/qj.49710745102

Monteith, J.L.L., 1965. Evaporation and Environment. Symp. Soc. Exp. Biol. 19, 205–234. doi:10.1613/jair.301

Mu, Q., Zhao, M., Kimball, J.S., McDowell, N.G., Running, S.W., 2013. A remotely sensed global terrestrial drought severity index. Bull. Am. Meteorol. Soc. 94, 83–98. doi:10.1175/BAMS-D-11-00213.1

Mu, Q., Zhao, M., Running, S.W., 2011. Improvements to a MODIS global terrestrial evapotranspiration algorithm. Remote Sens. Environ. 115, 1781–1800. doi:10.1016/j.rse.2011.02.019

Mueller, B., Hirschi, M., Jimenez, C., Ciais, P., Dirmeyer, P.A., Dolman, A.J., Fisher, J.B., Jung, M., Ludwig, F., Maignan, F., Miralles, D.G., McCabe, M.F., Reichstein, M., Sheffield, J., Wang, K., Wood, E.F., Zhang, Y., Seneviratne, S.I., 2013. Benchmark products for land evapotranspiration: LandFlux-EVAL multi-data set synthesis. Hydrol. Earth Syst. Sci. 17, 3707–3720. doi:10.5194/hess-17-3707-2013

Nagler, P.L., Cleverly, J., Glenn, E., Lampkin, D., Huete, A., Wan, Z., 2005. Predicting riparian evapotranspiration from MODIS vegetation indices and meteorological data. Remote Sens. Environ. 94, 17–30. doi:10.1016/j.rse.2004.08.009

Nagler, P.L., Glenn, E.P., Nguyen, U., Scott, R.L., Doody, T., 2013. Estimating riparian and agricultural actual evapotranspiration by reference evapotranspiration and MODIS enhanced vegetation index. Remote Sens. 5, 3849–3871. doi:10.3390/rs5083849

Nemani, R.R., Keeling, C.D., Hashimoto, H., Jolly, W.M., Piper, S.C., Tucker, C.J., Myneni, R.B., Running, S.W., 2003. Climate-driven increases in global terrestrial net primary production from 1982 to 1999. Science 300, 1560–3. doi:10.1126/science.1082750

Nepstad, D.C., de Carvalho, C.R., Davidson, E.A., Jipp, P.H., Lefebvre, P.A., Negreiros, G.H., da Silva, E.D., Stone, T.A., Trumbore, S.E., Vieira, S., 1994. The role of deep roots in the hydrological and carbon cycles of Amazonian forests and pastures. Nature 372, 666–669. doi:10.1038/372666a0

Njoku, E.G., Entekhabi, D., 1996. Passive microwave remote sensing of soil moisture. J. Hydrol. doi:10.1016/0022-1694(95)02970-2

Njoku, E.G., Jackson, T.J., Lakshmi, V., Chan, T.K., Nghiem, S. V., 2003. Soil moisture retrieval from AMSR-E. IEEE Trans. Geosci. Remote Sens. 41, 215–228. doi:10.1109/TGRS.2002.808243

Novick, K.A., Ficklin, D.L., Stoy, P.C., Williams, C.A., Bohrer, G., Oishi, A.C., Papuga, S.A., Blanken, P.D., Noormets, A., Sulman, B.N., Scott, R.L., Wang, L., Phillips, R.P., 2016. The increasing importance of atmospheric demand for ecosystem water and carbon fluxes. Nat. Clim. Chang. 6, 1023–1027. doi:10.1038/nclimate3114

Oliva, R., Daganzo-Eusebio, E., Kerr, Y.H., Mecklenburg, S., Nieto, S., Richaume, P., Gruhier, C., 2012. SMOS radio frequency interference scenario: Status and actions taken to improve the RFI environment in the 1400-1427-MHZ passive band. IEEE Trans. Geosci. Remote Sens. 50, 1427–1439. doi:10.1109/TGRS.2012.2182775

Oliveira, P.H.F., Artaxo, P., Pires, C., De Lucca, S., Procópio, A., Holben, B., Schafer, J., Cardoso, L.F., Wofsy, S.C., Rocha, H.R., 2007. The effects of biomass burning aerosols and clouds on the CO2 flux in Amazonia, in: Tellus, Series B: Chemical and Physical Meteorology. pp. 338–349. doi:10.1111/j.1600-0889.2007.00270.x

Penman, H.L., 1948. Evaporation from open water, bare soils and grass. Proc. R. Soc. London. Ser. A. Math. Phys. 193, 120–145.

Penman, H.L., 1948. Natural Evaporation from Open Water, Bare Soil and Grass. Proc. R. Soc. A Math. Phys. Eng. Sci. 193, 120–145. doi:10.1098/rspa.1948.0037

Phillips, O., Aragão, L., Lewis, S., Fisher, J., Lloyd, J., Lopez-Gonzalez, G., Malhi, Y., Monteagudo, A., Peacock, J., Quesada, C., Heijden, G. Van Der, Almeida, S., 2009. Drought sensitivity of the Amazon carbon sink. IOP Conf. Ser. Earth Environ. Sci. 6, 42004. doi:10.1088/1755-1307/6/4/042004

Phillips, O.L., Aragao, L.E.O.C., Lewis, S.L., Fisher, J.B., Lloyd, J., Lopez-Gonzalez, G., Malhi, Y., Monteagudo, A., Peacock, J., Quesada, C.A., van der Heijden, G., Almeida, S., Amaral, I., Arroyo, L., Aymard, G., Baker, T.R., Banki, O., Blanc, L., Bonal, D., Brando, P., Chave, J., de Oliveira, A.C.A., Cardozo, N.D., Czimczik, C.I., Feldpausch, T.R., Freitas, M.A., Gloor, E., Higuchi, N., Jimenez, E., Lloyd, G., Meir, P., Mendoza, C., Morel, A., Neill, D.A., Nepstad, D., Patino, S., Penuela, M.C., Prieto, A., Ramirez, F., Schwarz, M., Silva, J., Silveira, M., Thomas, A.S., Steege, H. t., Stropp, J., Vasquez, R., Zelazowski, P., Davila, E.A., Andelman, S., Andrade, A., Chao, K.-J., Erwin, T., Di Fiore, A., C., E.H., Keeling, H., Killeen, T.J., Laurance, W.F., Cruz, A.P., Pitman, N.C.A., Vargas, P.N., Ramirez-Angulo, H., Rudas, A., Salamao, R., Silva, N., Terborgh, J., Torres-Lezama, A., 2009. Drought Sensitivity of the Amazon Rainforest. Science (80-.). 323, 1344–1347. doi:10.1126/science.1164033

Piepmeier, J.R., Johnson, J.T., Mohammed, P.N., Bradley, D., Ruf, C., Aksoy, M., Garcia, R., Hudson, D., Miles, L., Wong, M., 2014. Radio-Frequency Interference Mitigation for the Soil Moisture Active Passive Microwave Radiometer. Geosci. Remote Sensing, IEEE Trans. 52, 761–775. doi:10.1109/TGRS.2013.2281266

Polhamus, A., Fisher, J.B., Tu, K.P., 2013. What controls the error structure in evapotranspiration models? Agric. For. Meteorol. 169, 12–24. doi:10.1016/j.agrformet.2012.10.002

Poulter, B., Frank, D., Ciais, P., Myneni, R.B., Andela, N., Bi, J., Broquet, G., Canadell, J.G., Chevallier, F., Liu, Y.Y., Running, S.W., Sitch, S., van der Werf, G.R., 2014. Contribution of semi-arid ecosystems to interannual variability of the global carbon cycle. Nature 509, 600–603. doi:10.1038/nature13376

Poyatos, R., Granda, V., Molowny-Horas, R., Mencuccini, M., Steppe, K., Martínez-Vilalta, J., 2016. SAPFLUXNET: Towards a global database of sap flow measurements. Tree Physiol. 36, 1449–1455. doi:10.1093/treephys/tpw110

Priestley, C.H.B., & T.R.J., 1972. On the assessment of sruface heat flux and evaporation using large scale parameters. Mon. Weather Rev. 81–92.

Priestley, C., Taylor, R., 1972. On the assessment of surface heat flux and evaporation using large-scale parameters. Mon. Weather Rev. 81–92. doi:10.1175/1520-0493(1972)100<0081:OTAOSH>2.3.CO;2

Priestley, C.H.B., Physics, R.J.T.A., 1972. On the Assessment of Surface Heat Flux and Evaporation Using Large-Scale Parameters 81–92.

Purdy, A.J., Fisher, J.B., Goulden, M.L., Famiglietti, J.S., 2016. Ground heat flux: An analytical review of 6 models evaluated at 88 sites and globally. J. Geophys. Res. Biogeosciences 121, 3045–3059. doi:10.1002/2016JG003591

Reager, J.T., Gardner, A.S., Famiglietti, J.S., Wiese, D.N., Eicker, A., Lo, M.H., 2016. A decade of sea level rise slowed by climate-driven hydrology. Science (80-.). 351, 699–703. doi:10.1126/science.aad8386

Reginato, R.J., Jackson, R.D., Pinter, P.J., 1985. Evapotranspiration calculated from remote multispectral and ground station meteorological data. Remote Sens. Environ. 18, 75–89. doi:10.1016/0034-4257(85)90039-2

Rodell, M., Beaudoing, H.K., L'Ecuyer, T.S., Olson, W.S., Famiglietti, J.S., Houser, P.R., Adler, R., Bosilovich, M.G., Clayson, C.A., Chambers, D., Clark, E., Fetzer, E.J., Gao, X., Gu, G., Hilburn, K., Huffman, G.J., Lettenmaier, D.P., Liu, W.T., Robertson, F.R., Schlosser, C.A., Sheffield, J., Wood, E.F., 2015. The Observed State of the Water Cycle in the Early 21st Century. J. Clim. 150707115923006. doi:10.1175/JCLI-D-14-00555.1

Rodell, M., McWilliams, E.B., Famiglietti, J.S., Beaudoing, H.K., Nigro, J., 2011. Estimating evapotranspiration using an observation based terrestrial water budget. Hydrol. Process. 25, 4082–4092. doi:10.1002/hyp.8369

Roderick, M.L., Farquhar, G.D., Berry, S.L., Noble, I.R., 2001. On the direct effect of clouds and atmospheric particles on the productivity and structure of vegetation. Oecologia 129, 21–30. doi:10.1007/s004420100760

Ryu, D., Famiglietti, J.S., 2005. Characterization of footprint-scale surface soil moisture variability using Gaussian and beta distribution functions during the Southern Great Plains 1997 (SGP97) hydrology experiment. Water Resour. Res. 41, 1–13.

doi:10.1029/2004WR003835

Ryu, Y., Baldocchi, D.D., Black, T.A., Detto, M., Law, B.E., Leuning, R., Miyata, A., Reichstein, M., Vargas, R., Ammann, C., Beringer, J., Flanagan, L.B., Gu, L., Hutley, L.B., Kim, J., McCaughey, H., Moors, E.J., Rambal, S., Vesala, T., 2012. On the temporal upscaling of evapotranspiration from instantaneous remote sensing measurements to 8-day mean daily-sums. Agric. For. Meteorol. 152, 212–222. doi:10.1016/j.agrformet.2011.09.010

Santanello, J. a., Friedl, M. a., 2003. Diurnal Covariation in Soil Heat Flux and Net Radiation. J. Appl. Meteorol. 42, 851–862. doi:10.1175/1520-0450(2003)042<0851:DCISHF>2.0.CO;2

Scanlon, B.R., Tyler, S.W., Wierenga, P.J., 1997. Hydrologic issues in arid, unsaturated systems and implications for contaminant transport. Rev. Geophys. 35, 461–490. doi:10.1029/97RG01172

Schenk, H.J., Jackson, R.B., 2002. Rooting depths, lateral root spreads and belowground aboveground allometries of plants in water limited ecosystems. J. Ecol. 480–494. doi:10.1046/j.1365-2745.2002.00682.x

Schneider, U., Becker, A., Finger, P., Meyer-Christoffer, A., Rudolf, B., Ziese, M., 2015. GPCC Full Data Reanalysis Version 7.0 at 0.5°: Monthly Land-Surface Precipitation from Rain-Gauges built on GTS-based and Historic Data. Glob. Precip. Climatol. Cent. doi:10.5676/DWD_GPCC/FD_M_V6_050

Schneider, U., Becker, A., Finger, P., Meyer-Christoffer, A., Rudolf, B., Ziese, M., 2011. GPCC Monitoring Product: Near Real-Time Monthly Land-Surface Precipitation from Rain-Gauges based on SYNOP and CLIMAT data. [Data set]. doi:10.5676/DWD_GPCC/MP_M_V4_100

Schneider, U., Ziese, M., Meyer-Christoffer, A., Finger, P., Rustemeier, E., Becker, A., 2016. The new portfolio of global precipitation data products of the Global Precipitation Climatology Centre suitable to assess and quantify the global water cycle and resources. Proc. Int. Assoc. Hydrol. Sci. 374, 29–34. doi:10.5194/piahs-374-29-2016

Schwalm, C.R., Williams, C.A., Schaefer, K., Baldocchi, D., Black, T.A., Goldstein, A.H., Law, B.E., Oechel, W.C., Paw U, K.T., Scott, R.L., 2012. Reduction in carbon uptake during turn of the century drought in western North America. Nat. Geosci. doi:10.1038/ngeo1529

Seguin, B., Itier, B., 1983. Using midday surface temperature to estimate daily evaporation from satellite thermal IR data. Int. J. Remote Sens. 4, 371–383. doi:10.1080/01431168308948554

Senay, G.B., Leake, S., Nagler, P.L., Artan, G., Dickinson, J., Cordova, J.T., Glenn, E.P., 2011. Estimating basin scale evapotranspiration (ET) by water balance and remote sensing methods. Hydrol. Process. 25, 4037–4049. doi:10.1002/hyp.8379

Simard, M., Pinto, N., Fisher, J.B., Baccini, A., 2011. Mapping forest canopy height globally with spaceborne lidar. J. Geophys. Res. Biogeosciences 116. doi:10.1029/2011JG001708

Sorooshian, S., Li, J., Hsu, K.L., Gao, X., 2011. How significant is the impact of irrigation on the local hydroclimate in Californias Central Valley? Comparison of model results with ground and remote-sensing data. J. Geophys. Res. Atmos. 116. doi:10.1029/2010JD014775

Su, Z., 2002. The Surface Energy Balance System (SEBS) for estimation of turbulent heat fluxes. Hydrol. Earth Syst. Sci. 6, 85–100. doi:10.5194/hess-6-85-2002

Sun, Y., Fu, R., Dickinson, R., Joiner, J., Frankenberg, C., Gu, L., Xia, Y., Fernando, N., 2015. Drought onset mechanisms revealed by satellite solar-induced chlorophyll fluorescence: Insights from two contrasting extreme events. J. Geophys. Res. G Biogeosciences 120, 2427–2440. doi:10.1002/2015JG003150

Swann, A.L.S., Hoffman, F.M., Koven, C.D., Randerson, J.T., 2016. Plant responses to increasing CO_2 reduce estimates of climate impacts on drought severity. Proc. Natl. Acad. Sci. 113, 10019–10024. doi:10.1073/pnas.1604581113

Swann, A.L.S., Koven, C.D., 2017. A Direct Estimate of the Seasonal Cycle of Evapotranspiration over the Amazon Basin. J. Hydrometeorol. 18, 2173–2185. doi:10.1175/JHM-D-17-0004.1

Syed, T.H., Famiglietti, J.S., Chambers, D.P., Willis, J.K., Hilburn, K., 2010. Satellite-based global-ocean mass balance estimates of interannual variability and emerging trends in continental freshwater discharge. Proc. Natl. Acad. Sci. 107, 17916–17921. doi:10.1073/pnas.1003292107

Taylor, P.G., Cleveland, C.C., Wieder, W.R., Sullivan, B.W., Doughty, C.E., Dobrowski, S.Z., Townsend, A.R., 2017. Temperature and rainfall interact to control carbon cycling in tropical forests. Ecol. Lett. doi:10.1111/ele.12765

Taylor, R.J., 1972. On the Assessment of Surface Heat Flux and Evaporation Using Large-Scale Parameters. Mon. Weather Rev. 100, 81–92. doi:10.1175/1520-0493(1972)100<0081:OTAOSH>2.3.CO;2

Trenberth, K.E., Fasullo, J.T., Kiehl, J., 2009. Earth's global energy budget. Bull. Am. Meteorol. Soc. 90, 311–323. doi:10.1175/2008BAMS2634.1

Tucker, C.J., 1979. Red and photographic infrared linear combinations for monitoring vegetation. Remote Sens. Environ. 8, 127–150. doi:10.1016/0034-4257(79)90013-0

Twine, T.E.E., Kustas, W.P.P., Norman, J.M.M., Cook, D.R.R., Houser, P.R.R., Meyers, T.P.P., Prueger, J.H.H., Starks, P.J.J., Wesely, M.L.L., 2000. Correcting eddy-covariance flux underestimates over a grassland. Agric. For. Meteorol. 103, 279–300. doi:10.1016/S0168-1923(00)00123-4

van Diepen, C.A., Wolf, J., van Keulen, H., Rappoldt, C., 1989. WOFOST: a simulation model of crop production. Soil Use Manag. 5, 16–24. doi:10.1111/j.1475-2743.1989.tb00755.x

Vecchi, G.A., Wittenberg, A.T., 2010. El Ni??o and our future climate: Where do we stand?

Wiley Interdiscip. Rev. Chang. 1, 260–270. doi:10.1002/wcc.33

Vinukollu, R.K., Wood, E.F., Ferguson, C.R., Fisher, J.B., 2011. Global estimates of evapotranspiration for climate studies using multi-sensor remote sensing data: Evaluation of three process-based approaches. Remote Sens. Environ. 115, 801–823. doi:10.1016/j.rse.2010.11.006

Wada, Y., Reager, J.T., Chao, B.F., Wang, J., Lo, M.H., Song, C., Li, Y., Gardner, A.S., 2017. Recent Changes in Land Water Storage and its Contribution to Sea Level Variations. Surv. Geophys. doi:10.1007/s10712-016-9399-6

Wahr, J., Swenson, S., Zlotnicki, V., Velicogna, I., 2004. Time-variable gravity from GRACE: First results. Geophys. Res. Lett. 31. doi:10.1029/2004GL019779

Wang, K., Dickinson, R.E., 2012. A REVIEW OF GLOBAL TERRESTRIAL EVAPOTRANSPIRATION : OBSERVATION ,. J. Geophys. Res. Lett. doi:10.1029/2011RG000373.1.INTRODUCTION

Wild, M., Grieser, J., Schär, C., 2008. Combined surface solar brightening and increasing greenhouse effect support recent intensification of the global land-based hydrological cycle. Geophys. Res. Lett. 35. doi:10.1029/2008GL034842

Wilson, K., Goldstein, A., Falge, E., Aubinet, M., Baldocchi, D., Berbigier, P., Bernhofer, C., Ceulemans, R., Dolman, H., Field, C., Grelle, A., Ibrom, A., Law, B.., Kowalski, A., Meyers, T., Moncrieff, J., Monson, R., Oechel, W., Tenhunen, J., Valentini, R., Verma, S., 2002. Energy balance closure at FLUXNET sites. Agric. For. Meteorol. 113, 223–243. doi:10.1016/S0168-1923(02)00109-0

Wolf, S., Eugster, W., Ammann, C., Häni, M., Zielis, S., Hiller, R., Stieger, J., Imer, D., Merbold, L., Buchmann, N., 2013. Contrasting response of grassland versus forest carbon and water fluxes to spring drought in Switzerland. Environ. Res. Lett. 8. doi:10.1088/1748-9326/8/3/035007

Wolf, S., Keenan, T.F., Fisher, J.B., Baldocchi, D.D., Desai, A.R., Richardson, A.D., Scott, R.L., Law, B.E., Litvak, M.E., Brunsell, N.A., Peters, W., van der Laan-Luijkx, I.T., 2016. Warm spring reduced carbon cycle impact of the 2012 US summer drought. Proc. Natl. Acad. Sci. 113, 5880–5885. doi:10.1073/pnas.1519620113

Yang, Y., Guan, H., Batelaan, O., McVicar, T.R., Long, D., Piao, S., Liang, W., Liu, B., Jin, Z., Simmons, C.T., 2016. Contrasting responses of water use efficiency to drought across global terrestrial ecosystems. Sci. Rep. 6, 23284. doi:10.1038/srep23284

Zhang, Y., Xiao, X., Guanter, L., Zhou, S., Ciais, P., Joiner, J., Sitch, S., Wu, X., Nabel, J., Dong, J., Kato, E., Jain, A.K., Wiltshire, A., Stocker, B.D., 2016. Precipitation and carbon-water coupling jointly control the interannual variability of global land gross primary production. Sci. Rep. 6, 39748. doi:10.1038/srep39748

Zhao, M., Running, S.W., Zhao, M., Running, S.W., Samanta, A., Medlyn, B.E., Zhao, M.,

Running, S.W., Nemani, R.R., Samanta, A., Phillips, O.L., Jönsson, P., Eklundh, L., Clark, D.A., Piper, S.C., Keeling, C.D., Clark, D.B., Peng, S.B., Tjoelker, M.J., Oleksyn, J., Reich, P.B., Piao, S., Mahecha, M.D., Zheng, D., Prince, S., Wright, R., Beer, C., Atkin, O., Millar, H., Turnbull, M., Knapp, A.K., Smith, M.D., Nemani, R.R., Jung, M., Brando, P.M., Lewis, S.L., Brando, P.M., Phillips, O.L., Heijden, G.M.F. van der, Nepstad, D., Gobron, N., Belward, A., Pinty, B., Knorr, W., Barriopedro, D., Fischer, E.M., Luterbacher, J., Trigo, R.M., García-Herrera, R., 2010. Drought-induced reduction in global terrestrial net primary production from 2000 through 2009. Science 329, 940–3. doi:10.1126/science.1192666

Zreda, M., Desilets, D., Ferré, T.P.A., Scott, R.L., 2008. Measuring soil moisture content non-invasively at intermediate spatial scale using cosmic-ray neutrons. Geophys. Res. Lett. 35. doi:10.1029/2008GL035655

Zreda, M., Shuttleworth, W.J., Zeng, X., Zweck, C., Desilets, D., Franz, T., Rosolem, R., 2012. COSMOS: The cosmic-ray soil moisture observing system. Hydrol. Earth Syst. Sci. 16, 4079–4099. doi:10.5194/hess-16-4079-2012

Appendix

1. Ground Heat Flux
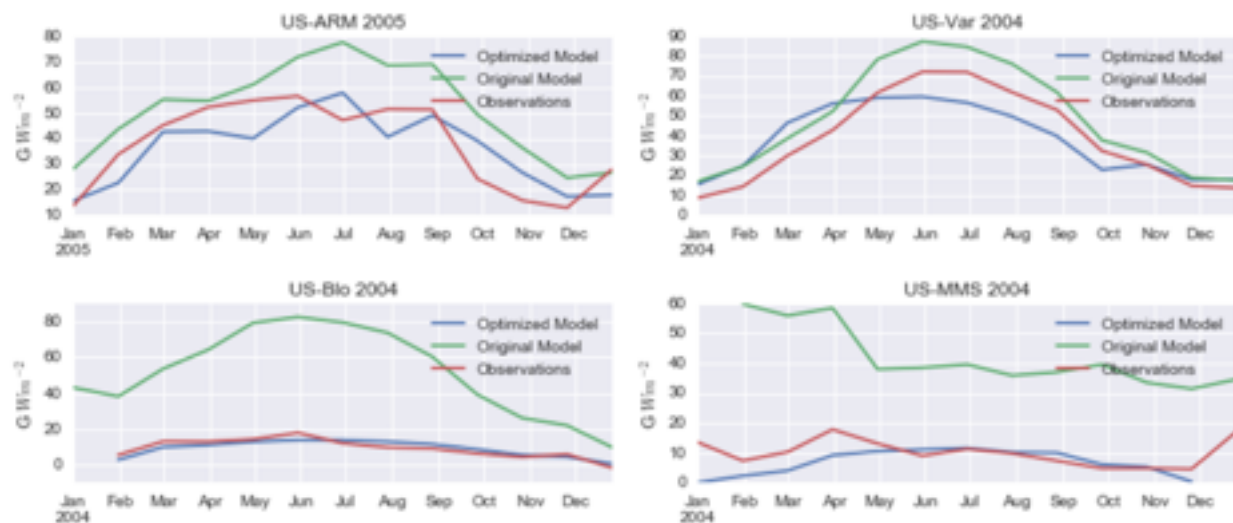
Figure A.1.1 Optimized model compared at 4 locations. US-ARM and US-Var short vegetation, US-Blo and US-MMS tall vegetation. Largest improvements are for taller canopies.

Table A.1.1 Observation towers used for this analysis. Site names, locations, land cover, climate, and time range used.

Site	Latitude	Longitude	PFT	Climate Code	Climate Description	Years : Days	Citation
AT-Neu	47.117	11.318	GRA	Cfb	Temperate	2002 : 321, 2003 : 260, 2004 : 291	Wohlfahrt G., Hammerle A., Haslwanter A., Bahn M., Tappeiner U., Cernusca A. (2008) Seasonal and inter-annual variability of the net ecosystem CO2 exchange of a temperate mountain grassland: effects of weather and management. Journal of Geophysical Research 113, D08110, doi:10.1029/2007JD009286.
AU-Fog	-12.542	131.307	WET	Aw	Tropical	2006 : 306, 2007 : 256	Jason Beringer (2013) Fogg Dam OzFlux tower site OzFlux: Australian and New Fogg Dam Zealand Flux Research and Monitoring hdl: 102.100.100/14233
AU-How	-12.494	131.152	WSA	Aw	Tropical	2001 : 223, 2002 : 365, 2003 : 365, 2004 : 366, 2005 : 365	Jason Beringer (2013) Howard Springs OzFlux tower site OzFlux: Australian and Howard Spr New Zealand Flux Research and Monitoring hdl: 102.100.100/14234
AU-Tum	-35.656	148.152	EBF	Cfb	Temperate	2001 : 313, 2002 : 365, 2003 : 365, 2004 : 298, 2005 : 365, 2006 : 121	Eva vanGorsel (2013) Tumbarumba OzFlux tower site OzFlux: Australian and New Tumbarumba Zealand Flux Research and Monitoring hdl: 102.100.100/14241
AU-Wac	-37.429	145.187	EBF	Cfb	Temperate	2006 : 365	Jason Beringer (2013) Wallaby Creek OzFlux tower site OzFlux: Australian and New Wallaby Ck Zealand Flux Research and Monitoring hdl: 102.100.100/14231
BE-Bra	51.309	4.521	MF	Cfb	Temperate	2000 : 357, 2001 : 360, 2004 : 342, 2005 : 241, 2006 : 287	I. A. Janssens; A. S. Kowalski; R. Ceulemans. 2001. Intercomparison of forest floor CO2 efflux estimates by eddy correlation and a chamber-ased emperical model.Agricultural and Forest Meteorology. 106, 61-69.
BE-Lon	50.552	4.745	CRO	Cfb	Temperate	2004 : 263, 2005 : 352,	Moureaux, C., Debacq, A., Bodson, B., Heinesch, B., Aubinet, M., 2006. Annual net ecosystem carbon exchange by

						2006 : 335	a sugar beet crop. Agricultural and Forest Meteorology 139, 25-39.
BE-Vie	50.306	5.997	MF	Cfb	Temperate	2000 : 344, 2001 : 352, 2002 : 335, 2003 : 338, 2004 : 240, 2005 : 349	Aubinet, M., Chermanne, B., Vandenhaute, M., Longdoz, B., Yernaux, M., Laitat, E., 2001. Long term carbon dioxide exchange above a mixed forest in the Belgian Ardennes. Agricultural and Forest Meteorology 108(4), 293-315.
BR-Sa3	-3.018	-54.971	EBF	Am	Tropical	2001 : 364, 2002 : 365, 2003 : 365	M. Keller; A. Alencar; G. P. Asner; B. Braswell; M. Bustamante; E. Davidson; T. Feldpausch; E. Fernandes; M. Goulden; P. Kabat; B. Kruijt; F. Luizao; S. Miller; D. Markewitz; A. D. Nobre; C. A. Nobre; N. Priante; H. da Rocha; P. S. Dias; C. von Randow; G. L. Vourlitis. 2004. Ecological research in the large-scale biosphere-atmosphere experiment in Amazonia: Early resultsEcological Applications. 14:4, S3-S16.
BW-Ma1	-19.916	23.56	WSA	BSh	Dry (arid and semi arid)	2000 : 362, 2001 : 304	Arneth et al., Biogeosciences, 3, 421–437, 2006; www.biogeosciences.net/3/421/2006/
CA-Mer	45.409	-75.519	WET	Dfb	Temperate-Continental with hot or warm summers	2000 : 279, 2001 : 270, 2002 : 328, 2003 : 267, 2004 : 266	Lafleur, P.M., N.T. Roulet, J.L. Bubier, T.R. Moore & S. Frolking, 2003. Interannual variability in the peatland-atmosphere carbon dioxide exchange at an ombrotrophic bog. Global Biogeochemical Cycles, 17(2), 5.1-5.13, 1036, doi:10.1029/2002GB001983.
CA-Qcu	49.267	-74.036	ENF	Dfc	Boreal	2002 : 338, 2003 : 365, 2004 : 331, 2005 : 360, 2006 : 305	Giasson, M.-A., Coursolle, C., Margolis, H.A. 2006. Ecosystem-level carbon fluxes from a boreal cutover in eastern Canada before and after scarification. Agric. Forest Meteorol. 140: 23-40; doi:10.1016/j.agrformet.2006.08.001.
CA-Qfo	49.693	-74.342	ENF	Dfc	Boreal	2004 : 321, 2005 : 359, 2006 : 350	Bergeron, O., Margolis, H.A., Black, T.A., Coursolle, C., Dunn, A.L., Barr, A.G., Wofsy, S.C. 2007. Comparison of CO2 fluxes over three boreal black spruce forests in Canada. Global Change Biol. 13: 89-107, doi:10.1111/j.1365-2486.2006.01281.x.

CH-Oe1	47.286	7.732	GRA	Cfb	Temperate	2004 : 361, 2005 : 365, 2006 : 344	Ammann C., Flechard C., Leifeld J., Neftel A., Fuhrer J., 2007. The carbon budget of newly established temperate grassland depends on management intensity. Agriculture Ecosystems and Environment 121, 5-20.
CH-Oe2	47.286	7.734	CRO	Cfb	Temperate	2005 : 321	W. L. Kutsch, Aubinet, M., Buchmann, N., Smith, P., Osborne, B., Eugster, W., Wattenbach, M., Schrumpf, M., Schulze, E. D., and Tomelleri, E., ÒThe net biome production of full crop rotations in EuropeÓ, Agriculture, Ecosystems & Environment, vol. 139, no. 3, pp. 336 - 345, 2010.
DE-Geb	51.1	10.914	CRO	Cfb	Temperate	2004 : 340, 2005 : 335, 2006 : 317	P. M. Anthoni; A. Knohl; C. Rebmann; A. Freibauer; M. Mund; W. Ziegler; O. Kolle; E. D. Schulze. 2004. Forest and agricultural land-use-dependent CO2 exchange in Thuringia, GermanyGlobal Change Biology. 10:12, 2005-2019
DE-Gri	50.95	13.512	GRA	Cfb	Temperate	2005 : 308, 2006 : 312	T.G. Gilmanov e,*, J.F. Soussana e, L. Aires a, V. Allard e, C. Ammann i, M. Balzarolo p, Z. Barcza q, C. Bernhofer o, C.L. Campbell c, A. Cernusca l, A. Cescatti k, J. Clifton-Brown b, .O.M. Dirks f, S. Dore p, W. Eugster j, J. Fuhrer i, C. Gimeno d, T. Gruenwald o, L. Haszpra q, A. Hensen f,g, A. Ibrom n, A.F.G. Jacobs h, M.B. Jones b, G. Lanigan b, T. Laurila s, A. ohila t, G.Manca k, B. Marcolla k, Z. Nagy r, K. Pilegaard m, K. Pinter r, C. Pio a, A. Raschi m, N. Rogiers u, M.J. Sanz d, P. Stefani m, M. Sutton c, Z. Tuba r,s, R. Valentini p, M.L. illiams b, G. Wohlfahrt l Partitioning European grassland net ecosystem CO2 exchange into gross primary productivity and ecosystem respiration using light response function analysis AGRICULTURE ECOSYSTEMS & ENVIRONMENT 121 (1-2): 93-120 JUN 2007
DE-Hai	51.079	10.452	DBF	Cfb	Temperate	2000 : 366, 2001 : 363, 2002 : 360, 2003 : 365, 2004 :	A. Knohl; E. D. Schulze; O. Kolle; N. Buchmann. 2003. Large carbon uptake by an unmanaged 250-year-old deciduous forest in Central GermanyAgricultural and Forest Meteorology. 118:3-4, 151-167.

						365, 2005 : 365, 2006 : 365	
DE-Kli	50.893	13.523	CRO	Cfb	Temperate	2005 : 271	P. Smith, Lanigan, G., Kutsch, W. L., Buchmann, N., Eugster, W., Aubinet, M., Ceschia, E., BŽziat, P., Yeluripati, J. B., and Osborne, B., Measurements necessary for assessing the net ecosystem carbon budget of croplandsÓ, Agriculture, Ecosystems & Environment, vol. 139, no. 3, pp. 302 - 315, 2010.
DE-Meh	51.275	10.656	GRA	Cfb	Temperate	2004 : 366, 2005 : 365, 2006 : 365	A. X. E. L. DON, Rebmann, C., KOLLE, O. L. A. F., SCHERER-LORENZEN, M. I. C. H. A. E. L., and SCHULZE, E. R. N. S. T. - D. E. T. L. E. F., Impact of afforestation-associated management changes on the carbon balance of grasslandÓ, Global Change Biology, vol. 15, no. 8, pp. 1990 - 2002, 2009.
DE-Tha	50.964	13.567	ENF	Cfb	Temperate	2000 : 363, 2001 : 365, 2002 : 358, 2003 : 357, 2004 : 297, 2005 : 364, 2006 : 362	T. Grünwald, Ch. Berhofer, 2007: A decade of carbon, water and energy flux measurements of an old spruce forest at the Anchor Station Tharandt. Tellus (2007), 59B, 387–396
DE-Wet	50.453	11.458	ENF	Cfb	Temperate	2002 : 341, 2003 : 331, 2004 : 356, 2005 : 347, 2006 : 338	P. M. Anthoni; A. Knohl; C. Rebmann; A. Freibauer; M. Mund; W. Ziegler; O. Kolle; E. D. Schulze. 2004. Forest and agricultural land-use-dependent CO2 exchange in Thuringia, GermanyGlobal Change Biology. 10:12, 2005-2019
DK-Fou	56.484	9.587	CRO	Cfb	Temperate	2005 : 292	W. Eugster, Moffat, A. M., Ceschia, E., Aubinet, M., Ammann, C., Osborne, B., Davis, P. A., Smith, P., Jacobs, C., and Moors, E., ÒManagement effects on European cropland respirationÓ, Agriculture, Ecosystems & Environment, vol. 139, no. 3, pp. 346 - 362, 2010.

DK-Sor	55.487	11.646	DBF	Cfb	Temperate	2004 : 352, 2005 : 310	K. Pilegaard; P. Hummelshoj; N. O. Jensen; Z. Chen. 2001. Two years of continuous CO2 eddy-flux measurements over a Danish beech forest. Agricultural and Forest Meteorology. 107:1, 29-41.
ES-ES1	39.346	-0.319	ENF	Csa	SubTropical-Mediterranean	2000 : 282, 2001 : 349, 2002 : 236, 2003 : 242, 2004 : 351, 2005 : 284	Sanz, M. J., A. Carrara, and C. Gimeno (2004), Effects of a dry and warm summer conditions on CO2 and energy fluxes from three Mediterranean ecosystems, Geophys. Res. Abstr., 6, 3239
ES-ES2	39.276	-0.315	CRO	Csa	SubTropical-Mediterranean	2004 : 233, 2005 : 362, 2006 : 296	E. J. Moors, Jacobs, C., Jans, W., Supit, I., Kutsch, W. L., Bernhofer, C., BŽziat, P., Buchmann, N., Carrara, A., and Ceschia, E., ÒVariability in carbon exchange of European croplandsÓ, Agriculture, Ecosystems & Environment, vol. 139, no. 3, pp. 325 - 335, 2010.
ES-LMa	39.942	-5.773	SAV	Csa	SubTropical-Mediterranean	2004 : 358, 2005 : 361, 2006 : 331	-
ES-VDA	42.152	1.449	GRA	Cfb	Temperate	2004 : 320, 2005 : 221, 2006 : 256	T.G. Gilmanov e,*, J.F. Soussana e, L. Aires a, V. Allard e, C. Ammann i, M. Balzarolo p, Z. Barcza q, C. Bernhofer o, C.L. Campbell c, A. Cernusca l, A. Cescatti k, J. Clifton-Brown b, .O.M. Dirks f, S. Dore p, W. Eugster j, J. Fuhrer i, C. Gimeno d, T. Gruenwald o, L. Haszpra q, A. Hensen f,g, A. Ibrom n, A.F.G. Jacobs h, M.B. Jones b, G. Lanigan b, T. Laurila s, A. ohila t, G.Manca k, B. Marcolla k, Z. Nagy r, K. Pilegaard m, K. Pinter r, C. Pio a, A. Raschi m, N. Rogiers u, M.J. Sanz d, P. Stefani m, M. Sutton c, Z. Tuba r,s, R. Valentini p, M.L. illiams b, G. Wohlfahrt l Partitioning European grassland net ecosystem CO2 exchange into gross primary productivity and ecosystem respiration using light response function analysis AGRICULTURE ECOSYSTEMS & ENVIRONMENT 121 (1-2): 93-120 JUN 2007

FI-Hyy	61.847	24.295	ENF	Dfc	Boreal	2005 : 365, 2006 : 365	U. Rannik; N. Altimir; J. Raittila; T. Suni; A. Gaman; T. Hussein; T. Holtta; H. Lassila; M. Latokartano; A. Lauri; A. Natsheh; T. Petaja; R. Sorjamaa; H. Yla-Mella; P. Keronen; F. Berninger; T. Vesala; P. Hari; M. Kulmala. 2002. Fluxes of carbon dioxide and water vapour over Scots pine forest and clearingAgricultural and Forest Meteorology. 111:3, 187-202.
FI-Sod	67.362	26.638	ENF	Dfc	Boreal	2001 : 365, 2002 : 273, 2003 : 365, 2004 : 361, 2005 : 365	J. Rinne; J. P. Tuovinen; T. Laurila; H. Hakola; M. Aurela; H. Hypen. 2000. Measurements of hydrocarbon fluxes by a gradient method above a northern boreal forestAgricultural and Forest Meteorology. 102:1, 25-37.
FR-Gri	48.844	1.952	CRO	Cfb	Temperate	2005 : 350, 2006 : 334	Loubet B., Laville P., Lehuger S., Larmanou E., FlŽchard C., Mascher N., GŽnermont S., Roche R., Ferrara R.M., Stella P., Personne E., Durand B., Decuq C., Flura D., Masson S., Fanucci O., Rampon J.N., Siemens J., Kindler R., Gabrielle B., Schrumpf M., Cellier P., 2011. Carbon, nitrogen and Greenhouse gases budgets over a four years crop rotation in northern France. Plant and Soil, 343, 1/2, 109Ð137
FR-Hes	48.674	7.065	DBF	Cfb	Temperate	2001 : 365, 2002 : 365, 2003 : 365, 2004 : 366, 2005 : 365, 2006 : 365	A. Granier; E. Ceschia; C. Damesin; E. Dufrene; D. Epron; P. Gross; S. Lebaube; V. Le Dantec; N. Le Goff; D. Lemoine; E. Lucot; J. M. Ottorini; J. Y. Pontailler; B. Saugier. 2000. The carbon balance of a young Beech forestFunctional Ecology. 14:3, 312-325.
FR-LBr	44.717	-0.769	ENF	Cfb	Temperate	2003 : 339, 2004 : 366, 2005 : 365, 2006 : 365	Berbigier P., Bonnefond J.M., Mellmann P., 2001. CO2 and water vapour fluxes for 2 years above Euroflux forest site. Agricultural and Forest Meteorology, 108 (3), 183-197.

FR-Lq1	45.644	2.737	GRA	Cfb	Temperate	2004 : 366, 2005 : 365	T.G. Gilmanov e,*, J.F. Soussana e, L. Aires a, V. Allard e, C. Ammann i, M. Balzarolo p, Z. Barcza q, C. Bernhofer o, C.L. Campbell c, A. Cernusca l, A. Cescatti k, J. Clifton-Brown b, .O.M. Dirks f, S. Dore p, W. Eugster j, J. Fuhrer i, C. Gimeno d, T. Gruenwald o, L. Haszpra q, A. Hensen f,g, A. Ibrom n, A.F.G. Jacobs h, M.B. Jones b, G. Lanigan b, T. Laurila s, A. ohila t, G.Manca k, B. Marcolla k, Z. Nagy r, K. Pilegaard m, K. Pinter r, C. Pio a, A. Raschi m, N. Rogiers u, M.J. Sanz d, P. Stefani m, M. Sutton c, Z. Tuba r,s, R. Valentini p, M.L. illiams b, G. Wohlfahrt l Partitioning European grassland net ecosystem CO2 exchange into gross primary productivity and ecosystem respiration using light response function analysis AGRICULTURE ECOSYSTEMS & ENVIRONMENT 121 (1-2): 93-120 JUN 2007
FR-Lq2	45.639	2.737	GRA	Cfb	Temperate	2004 : 366, 2005 : 365	T.G. Gilmanov e,*, J.F. Soussana e, L. Aires a, V. Allard e, C. Ammann i, M. Balzarolo p, Z. Barcza q, C. Bernhofer o, C.L. Campbell c, A. Cernusca l, A. Cescatti k, J. Clifton-Brown b, .O.M. Dirks f, S. Dore p, W. Eugster j, J. Fuhrer i, C. Gimeno d, T. Gruenwald o, L. Haszpra q, A. Hensen f,g, A. Ibrom n, A.F.G. Jacobs h, M.B. Jones b, G. Lanigan b, T. Laurila s, A. ohila t, G.Manca k, B. Marcolla k, Z. Nagy r, K. Pilegaard m, K. Pinter r, C. Pio a, A. Raschi m, N. Rogiers u, M.J. Sanz d, P. Stefani m, M. Sutton c, Z. Tuba r,s, R. Valentini p, M.L. illiams b, G. Wohlfahrt l Partitioning European grassland net ecosystem CO2 exchange into gross primary productivity and ecosystem respiration using light response function analysis AGRICULTURE ECOSYSTEMS & ENVIRONMENT 121 (1-2): 93-120 JUN 2007
FR-Pue	43.741	3.596	EBF	Csa	SubTropical-Mediterranean	2006 : 365	J. P. Lhomme; A. Rocheteau; J. M. Ourcival; S. Rambal. 2001. Non-steady-state modelling of water transfer in a Mediterranean evergreen canopyAgricultural and Forest Meteorology. 108:1, 67-83.

HU-Bug	46.691	19.601	GRA	Cfb	Temperate	2003 : 318, 2004 : 320, 2005 : 336, 2006 : 364	Z. Nagy, Barcza, Z., Horvath, L., Balogh, J., Hagy—, A., Kaposztas, N., Grosz, B., and Machon, A., Atmospheric Greenhouse Gases: The Hungarian PerspectiveGrasslands. Dordrecht: Springer Netherlands, 2010, pp. 91 - 119.
HU-Mat	47.847	19.726	GRA	Cfb	Temperate	2004 : 317, 2005 : 284, 2006 : 318	Z. Nagy, Barcza, Z., Horvath, L., Balogh, J., Hagy—, A., Kaposztas, N., Grosz, B., and Machon, A., Atmospheric Greenhouse Gases: The Hungarian PerspectiveGrasslands. Dordrecht: Springer Netherlands, 2010, pp. 91 - 119.
IE-Ca1	52.859	-6.918	CRO	Cfb	Temperate	2004 : 351, 2005 : 323, 2006 : 363	T.G. Gilmanov e,*, J.F. Soussana e, L. Aires a, V. Allard e, C. Ammann i, M. Balzarolo p, Z. Barcza q, C. Bernhofer o, C.L. Campbell c, A. Cernusca l, A. Cescatti k, J. Clifton-Brown b, .O.M. Dirks f, S. Dore p, W. Eugster j, J. Fuhrer i, C. Gimeno d, T. Gruenwald o, L. Haszpra q, A. Hensen f,g, A. Ibrom n, A.F.G. Jacobs h, M.B. Jones b, G. Lanigan b, T. Laurila s, A. ohila t, G.Manca k, B. Marcolla k, Z. Nagy r, K. Pilegaard m, K. Pinter r, C. Pio a, A. Raschi m, N. Rogiers u, M.J. Sanz d, P. Stefani m, M. Sutton c, Z. Tuba r,s, R. Valentini p, M.L. illiams b, G. Wohlfahrt l Partitioning European grassland net ecosystem CO2 exchange into gross primary productivity and ecosystem respiration using light response function analysis AGRICULTURE ECOSYSTEMS & ENVIRONMENT 121 (1-2): 93-120 JUN 2007
IE-Dri	51.987	-8.752	GRA	Cfb	Temperate	2003 : 365, 2004 : 364, 2005 : 328	C. MOUREAUX, Bodson, B., and Aubinet, M., ÒMesure des flux de CO2 et bilan carbonŽ de grandes cultures : Etat de la question et mŽthodologieÓ, Biotechnologie, Agronomie, SociŽtŽ et Environnement (BASE), vol. 12, no. 3, pp. 303-315, 2008
IT-Amp	41.904	13.605	GRA	Cfa	SubTropical-Mediterranea n	2003 : 365, 2004 : 366, 2005 : 324, 2006 : 352	T. GILMANOV, SOUSSANA, J., Aires, L., ALLARD, V., AMMANN, C., BALZAROLO, M., Barcza, Z., Bernhofer, C., CAMPBELL, C., and CERNUSCA, A., ÒPartitioning European grassland net ecosystem CO2 exchange into

							gross primary productivity and ecosystem respiration using light response function analysisÓ, Agriculture, Ecosystems & Environment, vol. 121, no. 1-2, pp. 93 - 120, 2007.
IT-BCi	40.524	14.957	CRO	Csa	SubTropical-Mediterranean	2005 : 330, 2006 : 324	M. Reichstein; A. Rey; A. Freibauer; J. Tenhunen; R. Valentini; J. Banza; P. Casals; Y. F. Cheng; J. M. Grunzweig; J. Irvine; R. Joffre; B. E. Law; D. Loustau; F. Miglietta; W. Oechel; J. M. Ourcival; J. S. Pereira; A. Peressotti; F. Ponti; Y. Qi; S. Rambal; M. Rayment; J. Rom. 2003. Modeling temporal and large-scale spatial variability of soil respiration from soil water availability, temperature and vegetation productivity indicesGlobal Biogeochemical Cycles. 17:4.
IT-Col	41.849	13.588	DBF	Cfa	SubTropical-Mediterranean	2000 : 308, 2001 : 303, 2005 : 301	T. Chiti, Papale, D., Smith, P., Dalmonech, D., Matteucci, G., Yeluripati, J., Rodeghiero, M., and Valentini, R., ÒPredicting changes in soil organic carbon in mediterranean and alpine forests during the Kyoto Protocol commitment periods using the CENTURY modelÓ, Soil Use and Management, vol. 26, no. 4, pp. 475 - 484, 2010.
IT-Cpz	41.705	12.376	EBF	Csa	SubTropical-Mediterranean	2001 : 351, 2003 : 365, 2004 : 366, 2005 : 354, 2006 : 324	Garbulsky M. F, Penuelas J., Papale D., Filella I. (2008). Remote estimation of carbon dioxide uptake by a Mediterranean forest, Global Change Biology (14) 2860-2867
IT-Lav	45.955	11.281	ENF	Cfb	Temperate	2004 : 239, 2006 : 249	P. Smith, Lanigan, G., Kutsch, W. L., Buchmann, N., Eugster, W., Aubinet, M., Ceschia, E., BŽziat, P., Yeluripati, J. B., and Osborne, B., ÒMeasurements necessary for assessing the net ecosystem carbon budget of croplandsÓ, Agriculture, Ecosystems & Environment, vol. 139, no. 3, pp. 302 - 315, 2010.
IT-Lec	43.305	11.271	EBF	Cfa	SubTropical-Mediterranean	2006 : 365	-
IT-LMa	45.581	7.155	GRA	Cfb	Temperate	2003 : 363, 2004 : 321	-

IT-MBo	46.016	11.047	GRA	Cfb	Temperate	2005 : 365, 2006 : 365	Marcolla B., Cescatti A. 2005. Experimental analysis of flux footprint for varying stability conditions in an alpine meadow. Agricoltural and Forest Meteorology 135: 291-301
IT-Non	44.69	11.089	DBF	Cfa	SubTropical-Mediterranean	2001 : 333, 2002 : 356, 2003 : 230, 2006 : 264	-
IT-PT1	45.201	9.061	DBF	Cfa	SubTropical-Mediterranean	2003 : 323, 2004 : 365	Migliavacca, M.; Meroni, M.; Manca, G.; Matteucci, G.; Montagnani, L.; Grassi G.; Zenone, T.; Teobaldelli, M.; Goded, I.; Colombo, R. and Seufert, G. (2009).Seasonal and interannual patterns of carbon and water fluxes of a poplar plantation in Northern Italy. Agricultural and Forest Meteorology. 149 (9), 1460-1476
IT-Ren	46.588	11.435	ENF	Dfb	Temperate	2000 : 339, 2001 : 285, 2002 : 347, 2005 : 365	Marcolla B., Cescatti A., Montagnani L., Manca G., Kerschbaumer G., Minerbi S., 2005. Importance of advection in the atmospheric CO2 exchanges of an alpine forest. Agricultural and Forest Meteorology. 130:193-206.
IT-Ro1	42.408	11.93	DBF	Csa	SubTropical-Mediterranean	2001 : 326, 2002 : 357, 2003 : 344, 2004 : 310, 2005 : 287, 2006 : 324	Rey, A. et al. Annual variation in soil respiration and its components in a coppice oak forest in central italy. Global Change Biology 9, 851-866 (2002).
IT-Ro2	42.39	11.921	DBF	Csa	SubTropical-Mediterranean	2002 : 365, 2003 : 365, 2004 : 365, 2005 : 350, 2006 : 346	Tedeschi et al., 2006. Soil respiration in a Mediterranean oak forest at different developmental stages after coppicing. Global Change Biology, Volume 12, Issue 1: 110-121
NL-Ca1	51.971	4.927	GRA	Cfb	Temperate	2003 : 351, 2004 : 358, 2005 : 360, 2006 : 365	B. Gioli, Miglietta, F., DEMARTINO, B., HUTJES, R., DOLMAN, H., Lindroth, A., SCHUMACHER, M., SANZ, M., MANCA, G., and PERESSOTTI, A., Comparison between tower and aircraft-based eddy covariance fluxes in five European regions, Agricultural

							and Forest Meteorology, vol. 127, no. 1-2, pp. 1 - 16, 2004.
NL-Loo	52.168	5.744	ENF	Cfb	Temperate	2000 : 360, 2002 : 363, 2003 : 365, 2004 : 366, 2005 : 364, 2006 : 365	J. D. Tenhunen, Valentini, R., Kšstner, B., Zimmermann, R., and Granier, A., ÒVariation in forest gas exchange at landscape to continental scalesÓ, Annales des Sciences Foresti res, vol. 55, no. 1-2, pp. 1 - 11, 1998.
PL-wet	52.762	16.309	WET	Cfb	Temperate	2004 : 248	M. LUND, LAFLEUR, P., ROULET, N., LINDROTH, A., CHRISTENSEN, T., AURELA, M., CHOJNICKI, B., Flanagan, L. B., HUMPHREYS, E., Laurila, T., OECHEL, W.C. , OLEJNIK, J. Z., RINNE, J., SCHUBERT, P., and NILSSON, M., Variability in exchange of CO2 across 12 northern peatland and tundra sites, Global Change Biology, p. no - no, 2009.
PT-Mi2	38.477	-8.025	GRA	Csa	SubTropical-Mediterranean	2005 : 352, 2006 : 349	T. GILMANOV, SOUSSANA, J., Aires, L., ALLARD, V., AMMANN, C., BALZAROLO, M., Barcza, Z., Bernhofer, C., CAMPBELL, C., and CERNUSCA, A., ÒPartitioning European grassland net ecosystem CO2 exchange into gross primary productivity and ecosystem respiration using light response function analysisÓ, Agriculture, Ecosystems & Environment, vol. 121, no. 1-2, pp. 93 - 120, 2007.
RU-Fyo	56.462	32.924	ENF	Dfb	Temperate-Continental with hot or warm summers	2000 : 366, 2001 : 365, 2002 : 352, 2003 : 354, 2004 : 356	C. MOUREAUX, Bodson, B., and Aubinet, M., "Mesure des flux de CO2 et bilan carboné de grandes cultures : Etat de la question et méthodologie", Biotechnologie, Agronomie, Société et Environnement (BASE), vol. 12, no. 3, pp. 303-315, 2008.
RU-Zot	60.801	89.351	ENF	Dfc	Boreal	2002 : 248, 2003 : 317, 2004 : 225	S. Tanja, Berninger, F., Vesala, T., Markkanen, T., Hari, P., Makela, A., Ilvesniemi, H., Hanninen, H., Nikinmaa, E., Huttula, T., Laurila, T., AURELA, M. I. K. A., Grelle, A., LINDROTH, A. N. D. E. R. S., ARNETH, A. L. M. U. T., Shibistova, O., and Lloyd, J.,

							ÒAir temperature triggers the recovery of evergreen boreal forest photosynthesis in springÓ, Global Change Biology, vol. 9, no. 10, pp. 1410 - 1426, 2003.
SE-Nor	60.086	17.48	ENF	Dfb	Temperate-Continental with hot or warm summers	2005 : 346	A. Lindroth; A. Grelle; A. S. Moren. 1998. Long-term measurements of boreal forest carbon balance reveal large temperature sensitivityGlobal Change Biology. 4:4, 443-450.
SE-Sk1	60.125	17.918	ENF	Dfb	Temperate-Continental with hot or warm summers	2005 : 323	-
UK-AMo	55.792	-3.239	WET	Cfb	Temperate	2005 : 360	Soussana, J. F., et al. (2007), Full accounting of the greenhouse gas (CO2, N2O, CH4) budget of nine European grassland sites, Agric. Ecosyst. Environ., 121, 121Ð134.
UK-EBu	55.866	-3.206	GRA	Cfb	Temperate	2004 : 348	-
UK-ESa	55.907	-2.859	CRO	Cfb	Temperate	2004 : 248, 2005 : 324	-
UK-Gri	56.607	-3.798	ENF	Cfc	Temperate	2000 : 346, 2001 : 334, 2005 : 357, 2006 : 358	Rebmann, C., et al. (2005), Quality analysis applied on eddy covariance measurements at complex forest sites using footprint modelling, Theor. Appl. Climatol., 80, 121Ð141, doi:10.1007/s00704-004-0095-y.
UK-Ham	51.154	-0.858	DBF	Cfb	Temperate	2004 : 314, 2005 : 283	-
US-ARM	36.606	-97.489	CRO	Cfa	SubTropical-Mediterranean	2003 : 353, 2004 : 279, 2005 : 310	Fischer, M.L, Billesbach, D.P., Riley, W.J, Berry, J.A., and M.S. Torn. 2007. Spatiotemporal Variations in Growing Season Exchanges of CO2, H2O, and Sensible Heat in Agricultural Fields of the Southern Great Plains. Earth Interactions, 11, 1-21
US-Aud	31.591	-110.51	GRA	BSk	Dry (arid and semi arid)	2003 : 362, 2004 : 357, 2005 : 360, 2006 : 361	P. KRISHNAN, Meyers, T. P., Scott, R. L., Kennedy, L., and Heuer, M., "Energy exchange and evapotranspiration over two temperate semi-arid grasslands in North America", Agricultural and Forest Meteorology, vol. 153, pp. 31 - 44, 2012.

US-Bkg	44.345	-96.836	GRA	Dfa	Temperate-Continental with hot or warm summers	2005 : 362, 2006 : 364	T. G. Gilmanov; L. L. Tieszen; B. K. Wylie; et al.. 2005. Integration of CO2 flux and remotely-sensed data for primary production and ecosystem respiration analyses in the Northern Great Plains: potential for quantitative spatial extrapolationGlobal Ecology and Biogeography. 14:3 May, 271-292.
US-Blo	38.895	-120.633	ENF	Csa	SubTropical-Mediterranean	2000 : 362, 2001 : 353, 2002 : 359, 2003 : 352, 2004 : 352, 2005 : 342	A. H. Goldstein; N. E. Hultman; J. M. Fracheboud; M. R. Bauer; J. A. Panek; M. Xu; Y. Qi; A. B. Guenther; W. Baugh. 2000. Effects of climate variability on the carbon dioxide, water, and sensible heat fluxes above a ponderosa pine plantation in the Sierra Nevada (CA). Agricultural and Forest Meteorology. 101:2-3, 113-129.
US-Bo1	40.006	-88.29	CRO	Dfa	Temperate-Continental with hot or warm summers	2001 : 286, 2002 : 363, 2003 : 359, 2004 : 342, 2005 : 351, 2006 : 328	Tilden P. Meyers a,?, Steven E. Hollinger An assessment of storage terms in the surface energy balance of maize and soybean. Agricultural and Forest Meteorology 125 (2004) 105Ð115
US-FPe	48.308	-105.102	GRA	BSk	Dry (arid and semi arid)	2000 : 360, 2001 : 356, 2002 : 365, 2003 : 365, 2004 : 353, 2005 : 350, 2006 : 340	J. E. Horn and Schulz, K., ÒIdentification of a general light use efficiency model for gross primary productionÓ, Biogeosciences, vol. 8, no. 4, pp. 999 - 1021, 2011.
US-Goo	34.255	-89.873	GRA	Cfa	SubTropical-Mediterranean	2002 : 239, 2003 : 206, 2004 : 342, 2005 : 337, 2006 : 314	D. Y. HOLLINGER, OLLINGER, S. V., Richardson, A. D., MEYERS, T. P., DAIL, D. B., MARTIN, M. E., SCOTT, N. A., ARKEBAUER, T. J., Baldocchi, D. D., CLARK, K. L., Curtis, P. S., DAVIS, K. J., DESAI, A. R., Dragoni, D., GOULDEN, M. L., Gu, L., Katul, G. G., PALLARDY, S. G., Paw U, K. T., Schmid, H. P., Stoy, P. C., SUYKER, A. E., and VERMA, S. B., ÒAlbedo estimates for land surface models and support for a new paradigm based on foliage nitrogen concentrationÓ, Global Change

							Biology, vol. 16, no. 2, pp. 696 - 710, 2010.
US-Ho1	45.204	-68.74	ENF	Dfb	Temperate-Continental with hot or warm summers	2003 : 365, 2004 : 366	A. D. Richardson, Anderson, R. S., Arain, A. M., BARR, A. L. A. N. G., Bohrer, G., Chen, G., Chen, J. M., Ciais, P., Davis, K. J., Desai, A. R., Dietze, M. C., Dragoni, D., Garrity, S. R., Gough, C. M., Grant, R., Hollinger, D. Y., MARGOLIS, H. A. N. K. A., McCaughey, H., Migliavacca, M., Monson, R. K., Munger, W. J., Poulter, B., Raczka, B. M., Ricciuto, D. M., Sahoo, A. K., SCHAEFER, K. E. V. I. N., Tian, H., Vargas, R., Verbeeck, H., Xiao, J., and Xue, Y., ÒTerrestrial biosphere models need better representation of vegetation phenology: results from the North American Carbon Program Site SynthesisÓ, Global Change Biology, vol. 18, no. 2, pp. 566 - 584, 2011.
US-Los	46.083	-89.979	CSH	Dfb	Temperate-Continental with hot or warm summers	2001 : 353, 2002 : 260, 2003 : 357, 2004 : 287, 2005 : 330	Sulman, B.N., Desai, A.R., Cook, B.D., Saliendra, N., and Mackay, D.S., 2009. Contrasting carbon dioxide fluxes between a drying shrub wetland in Northern Wisconsin, USA, and nearby forests. Biogeosciences, 6: 1115-1126, doi:10.5194/bg-6-1115-2009.
US-MMS	39.323	-86.413	DBF	Cfa	SubTropical-Mediterranean	2002 : 365, 2003 : 365, 2004 : 366	D. Dragoni, Schmid, H. P., WAYSON, C. R. A. I. G. A., POTTER, H. E. N. R. Y., GRIMMOND, S. U. S. A. N. C. B., and RANDOLPH, J. A. M. E. S. C., ÒEvidence of increased net ecosystem productivity associated with a longer vegetated season in a deciduous forest in south-central Indiana, USAÓ, Global Change Biology, vol. 17, no. 2, pp. 886 - 897, 2011.
US-MOz	38.744	-92.2	DBF	Cfa	SubTropical-Mediterranean	2005 : 365, 2006 : 365	Gu et al., 2006: "Direct and indirect effects of atmospheric conditions and soil moisture on surface energy partitioning revealed by a prolonged drought at a temperate forest site", Journal of Geophysical Research, Vol. 111, D16102, doi:10.1029/2006JD007161.

US-Ne1	41.165	-96.477	CRO	Dfa	Temperate-Continental with hot or warm summers	2002 : 365, 2003 : 365, 2004 : 366	A. E. Suyker; S. B. Verma; G. G. Burba; T. J. Arkebauer; D. T. Walters; K. G. Hubbard. 2004. Growing season carbon dioxide exchange in irrigated and rainfed maize Agricultural and Forest Meteorology. 124:1-2, 1-13.
US-Ne2	41.165	-96.47	CRO	Dfa	Temperate-Continental with hot or warm summers	2002 : 365, 2003 : 365, 2004 : 366	Andrew E. Suyker; Shashi B. Verma; George G. Burba; Timothy J. Arkebauer. 2005. Gross primary production and ecosystem respiration of irrigated maize and irrigated soybean during a growing seasonAgricultural and Forest Meteorology. 131, 180-190.
US-Ne3	41.18	-96.44	CRO	Dfa	Temperate-Continental with hot or warm summers	2002 : 365, 2003 : 365, 2004 : 366	A. E. Suyker; S. B. Verma; G. G. Burba; T. J. Arkebauer; D. T. Walters; K. G. Hubbard. 2004. Growing season carbon dioxide exchange in irrigated and rainfed maizeAgricultural and Forest Meteorology. 124:1-2, 1-13.
US-Oho	41.555	-83.844	DBF	Dfa	Temperate-Continental with hot or warm summers	2004 : 328, 2005 : 337	Noormets, A, McNulty, SG, DeForest, JL, Sun, G, Li, Q, Chen, J. 2008. Drought during canopy development has lasting effect on annual carbon balance in a deciduous temperate forest. New Phytologist 179: 818-828.
US-SP1	29.738	-82.219	ENF	Cfa	SubTropical-Mediterranean	2005 : 333	H. L. Gholz; D. N. Guerin; W. P. Cropper. 1999. Phenology and productivity of saw palmetto (Serenoa repens) in a north Florida slash pine plantationCanadian Journal of Forest Research-Revue Canadienne De Recherche Forestiere. 29:8, 1248-1253.
US-SP2	29.765	-82.245	ENF	Cfa	SubTropical-Mediterranean	2000 : 340, 2001 : 322, 2002 : 341, 2003 : 339, 2004 : 340	K. L. Clark; H. L. Gholz; J. B. Moncrieff; F. Cropley; H. W. Loescher. 1999. Environmental controls over net exchanges of carbon dioxide from contrasting Florida ecosystemsEcological Applications. 9:3, 936.
US-SP3	29.755	-82.163	ENF	Cfa	SubTropical-Mediterranean	2000 : 343, 2001 : 362, 2002 : 362, 2003 : 342, 2004 : 366	H. L. Gholz; D. N. Guerin; W. P. Cropper. 1999. Phenology and productivity of saw palmetto (Serenoa repens) in a north Florida slash pine plantationCanadian Journal of Forest Research-Revue Canadienne De Recherche Forestiere. 29:8, 1248-1253.

US-Syv	46.242	-89.348	MF	Dfb	Temperate-Continental with hot or warm summers	2003 : 353, 2004 : 340, 2005 : 311	Desai, A.R., Bolstad, P.V., Cook, B.D., Davis, K.J., and Carey, E.V., 2005. Comparing net ecosystem exchange of carbon dioxide between an old-growth and mature forest in the upper midwest, USA. Ag. For. Met. 128(1-2): 33-55 (doi: 10.1016/j.agrformet.2004.09.005)
US-Ton	38.432	-120.966	WSA	Csa	SubTropical-Mediterranean	2002 : 365, 2003 : 365, 2004 : 365, 2005 : 365, 2006 : 365	Ma, S., Baldocchi, D.D., Xu, L., & Hehn, T. (2007). Inter-annual variability in carbon dioxide exchange of an oak/grass savanna and open grassland in California. Agricultural and Forest Meteorology, 147, 157-171
US-Var	38.413	-120.951	GRA	Csa	SubTropical-Mediterranean	2002 : 359, 2003 : 365, 2004 : 366, 2005 : 321, 2006 : 365	Ma, S., Baldocchi, D.D., Xu, L., & Hehn, T. (2007). Inter-annual variability in carbon dioxide exchange of an oak/grass savanna and open grassland in California. Agricultural and Forest Meteorology, 147, 157-171
US-WCr	45.806	-90.08	DBF	Dfb	Temperate-Continental with hot or warm summers	2000 : 361, 2001 : 317, 2002 : 341, 2003 : 344, 2004 : 310, 2005 : 353, 2006 : 311	B. D. Cook;K. J. Davis;W. G. Wang;A. Desai;B. W. Berger;R. M. Teclaw;J. G. Martin;P. V. Bolstad;P. S. Bakwin;C. X. Yi;W. Heilman. 2004. Carbon exchange and venting anomalies in an upland deciduous forest in northern Wisconsin, USA, Agricultural and Forest Meteorology, 126:3-4. 271-295

2. SMAP Evapotranspiration

In situ soil properties

Soil properties were extracted from the USDA Web Soil Survey. I subset soil properties from the USDA Web Soil Survey tool for each eddy-covariance tower. The soil data explorer provides physical soil property reports on percentages of sand, silt, and clay. The soil properties enable using look-up-tables to determine the soil porosity and soil permanent wilting point. These data are used to force the model for each in situ location.

Table A.2.1 Soil texture properties extracted from the USDA Web Soil Survey for each EC tower.

Site	Sand	Silt	Clay
'SCZO-P301'	67	22	11
'SCT-DesertChaparral'	71	17	22
'SCT-CoastalSage'	68	19	13
'SCT-Grass'	26	29	45
'SCZO-Soaproot'	66	19	15
'US-UMB'	91	7	2
'US-MMS'	6	77	17
'US-Ho1'	6	77	17
'US-Me2'	35	50	15
'US-Ro1'	9	66	25
'US-Wkg'	63	26	11
'US-Ton'	27	54	19
'US-Moz'	7	78	15
'US-GLE'**	NA	NA	NA
***DATA NOT AVAILABLE: SMAP L4 SOIL PROPERTIES USED*			

We use the Soil-texture-triangle to obtain the soil texture from the sand, silt, and clay fractions. The texture is used to look up model coefficients to calculate field capacity and wilting point based on data from Clapp and Hornberger (1976). Field capacity is calculated as:

$$\theta_{fc} = \phi \cdot \left(\frac{|\psi_{ae}|}{340} \right)^{1/b} \tag{1}$$

where θ_{fc} is the soil field capacity [cm/cm], ϕ is the porosity, ψ_{ae} is the air entry tension in (cm) and b is the moisture characteristic curve parameter. The soil permanent wilting point is calculated as:

$$\theta_{pwp} = \phi \cdot \left(\frac{|\psi_{ae}|}{15,000} \right)^{1/b} \tag{2}$$

where θ_{pwp} is the soil permanent wilting point [cm/cm]. A complete table of the soil texture

parameters for the Eq. 1 and Eq. 2 are available in Table 2 of Clapp and Hornberger (1976).

Table A.2.2 Soil properties calculated from Clapp and Hornberger (1976) using soil survey data
from the USDA. Soil texture, porosity, field capacity, and wilting point for each validation site.

Site	Soil Texture	Porosity	Field Capacity	Wilting Point
'SCZO-P301'	Sandy Loam	0.435	0.182	0.055
'SCT-DesertChaparral'	Sandy Clay Loam	0.420	0.250	0.112
'SCT-CoastalSage'	Sandy Loam	0.435	0.182	0.055
'SCT-Grass'	Clay	0.482	0.366	0.224[+]
'SCZO-Soaproot'	Sandy Loam	0.435	0.182	0.055
'US-UMB'	Sand	0.395	0.091	0.017
'US-MMS'	Silt Loam	0.485	0.313	0.101
'US-Ho1'	Silt Loam	0.485	0.313	0.101
'US-Me2'	Loam	0.451	0.258	0.088
'US-Ro1'	Silt Loam	0.485	0.313	0.101
'US-Wkg'	Sandy Loam	0.435	0.182	0.055
'US-Ton'	Silt Loam	0.485	0.313	0.101
'US-Moz'	Silt Loam	0.485	0.313	0.101
'US-GLE'*	NA	NA	NA	NA
** No site survey data available, data values presented are from SMAP L4 data. [+] Coversation with site PI indicated this is too high of wilting point for study region. The next soil class was used "Sandy Loam".				

3. Vegetation Stress
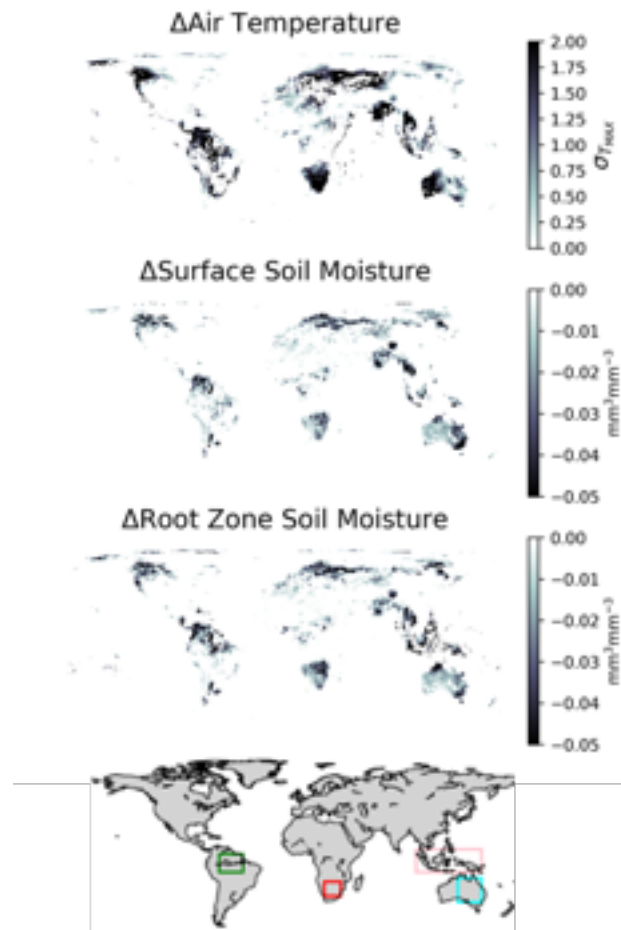
Focus area identification

Figure A.3.1 Focus region identification using temperature (top), surface soil moisture (2nd from top), root zone soil moisture (2nd from bottom).
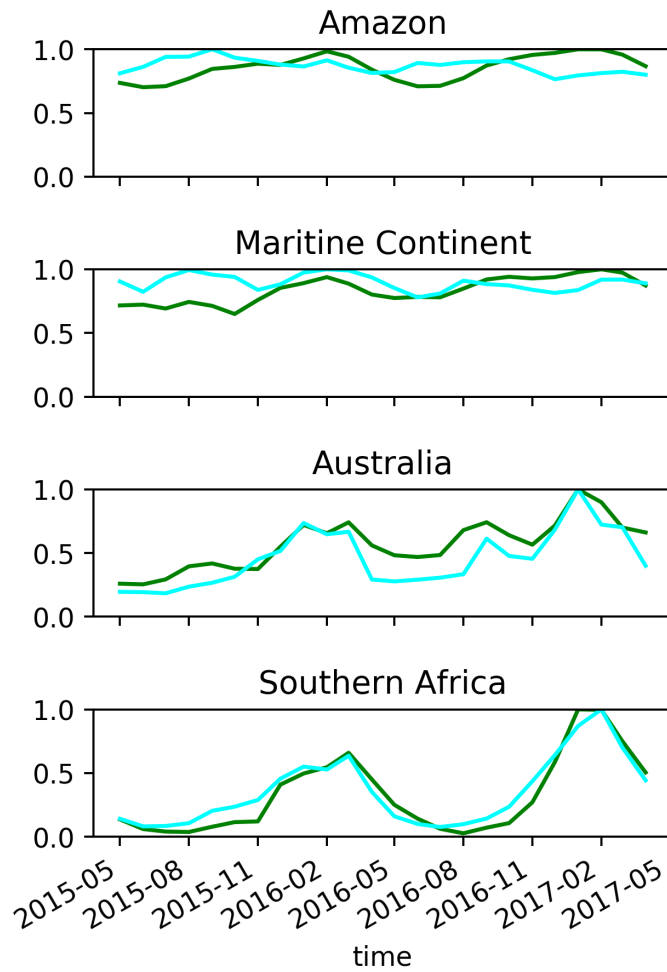
Figure A 3.2 Normalized SIF and Transpiration across each study region. SIF (green) is shows changes similar in magnitude relative to the seasonal cycle of transpiration (cyan).